Advancements in Modeling Self-Consistent Core-Collapse Supernovae with CHIMERA

A Dissertation Presented for the
Doctor of Philosophy Degree
The University of Tennessee, Knoxville

Merek Austin Chertkow

August 2012

Dedication

I lovingly dedicated this dissertation to my sister Blair, who has always been my counselor on the ways and truths of life; to my brother Adam, who will always be the builder to my architect; my mother Rhonda, who has taught me the truest meaning of love; and to my father Merek, thank you for your name, I hope I've made you proud.

Acknowledgments

The work composing my thesis and dissertation is certainly not a product of my efforts alone, but rather, of a closely knit group of highly skilled people, all pushing towards an understanding of supernovae at, what we lovingly refer to as, the bleeding edge of computational astrophysics.

When I began working on my Ph.D., I knew very little about working with supercomputers and numerical programs with architectures as large as CHIMERA's. Therefore, for for their guidance and extreme patience in helping mentor me throughout the years, I want to give special thanks to Dr. Bronson Messer and Dr. Reuben Budiardja. In addition, were it not for the comradeship and debates on the principles of physics with Dr. Suzanne Parete-Koon, I would have had a serious lack of people to complain to and bounce silly ideas off of.

I want to acknowledge the years of guidance and help from Dr. Eric Lentz and Dr. Steve Bruenn, without whom my thesis simply could not have existed. A great thanks to Dr. Bruenn for all of his insightful answers to my sometimes seemingly strange questions and inquiries about the physics and applications of our code. Thanks to Dr. Lentz for his mini-physics lessons that became one-man seminar lectures – I've learned so very much.

And finally, I want to express the depth of my gratitude towards Dr. William Raph Hix for being the kind of mentor and advisor every graduate student should be fortunate enough to have. His methods of stewardship with my research project has helped me become a resolved and independent researcher. His guidance has meant the world to me on both a professional and friendship level.

Finally, the simulations described herein were conducted at the Oak Ridge Leadership Computing Facility at ORNL and at the National Institute for Computational Sciences. This work was supported in part by NSF grants NSF-AST-0653376, NSF-PHY-0855315, NSF-OCI-0749242, NSF-OCI-0749204 & NASA grant 07-ATFP07-0011. MAC and WRH acknowledge support from the Office of Nuclear Physics, US Department of Energy, and from the Office of Advanced Scientific Computing Research, US Department of Energy.

Abstract

Using a sophisticated program named CHIMERA, we perform numerical simulations of the end of a massive star's life when its core can no longer support itself through electron degeneracy pressure. After a violent collapse to super-nuclear densities, the core releases its binding energy (10^{53} ergs) in the form of neutrinos. Simulations have shown that a small fraction of these neutrinos' energy is deposited into the matter above the forming neutron star, which drives a delayed explosion. Throughout this process, the oxygen and lighter elements that had composed the star's outer-core and envelope experience shock-driven explosive nucleosynthesis, forming newly synthesized heavy elements up to the iron and nickel At later times in the ejecta, other processes, such as the νp-process and possibly the r-process, create elements heavier than iron, which are required to match galactic and solar abundance studies. To follow these nuclear kinetics accurately and to more judiciously model reality, CHIMERA requires an efficient nuclear reaction network of approximately 150 to 300 species.

I will discuss my efforts in generalizing CHIMERA's 14-species nuclear reaction network to enable us to more accurately follow the proton-to-nucleon fraction within a complex hydrodynamic flow and the nuclear production and nuclear energy generation rates that results. I will discuss how these improvements have enabled the study of the lower mass limit of core-collapse supernovae. I will discuss the development of our post-processing scheme to extract detailed nucleosynthesis from our state-of-the-art multi-dimensional CHIMERA runs.

Contents

List of Tables

List of Figures

Chapter 1

Introduction

The final stage of stellar evolution for certain massive stars marks a unique class of phenomena in the observable universe known as core-collapse supernovae (CCSNe). Modern investigations attempting to understand these events have found that within a mass range from approximately 8 to perhaps 25 solar masses ($M_\odot$), CCSNe occur when a star's highly degenerate core grows too massive to support itself against gravitational collapse.

Core contraction takes place primarily due to the loss of electron pressure as electrons are captured onto nuclei and conditions proceed to ultrahigh densities (3×10^{14} g/cm^3), in excess of the densities of nucleons in the nucleus of an atom. Once the core reaches this incompressible super-nuclear density, the collapse halts as a newly formed proto-neutron star (PNS) acts like a piston and launches a pressure wave, which steepens into a shock wave, into the outer stellar core.

After core bounce, a neutrino outburst of all three flavors (electron, muon, and tau) releases the binding energy ($\sim3\times10^{53}$ ergs) of the newly formed PNS over a $\sim$10 second period. Although SNe are known to be wonderfully bright, only $\sim$ 0.01 % of the total neutrino energy is converted into photons (10^{49} ergs from recombination after the shock heating of the envelope and the decay of ^{56}Ni) and $< 10\%$ is converted into kinetic energy (10^{49} ergs) of the ejected matter. At these energy scales, supernovae are among the brightest and most energetic events in the universe.

As discussed in more detail in Chapter 2, after core collapse, the outbound shock wave is sapped of its energy through neutrino losses and from the dissociation of heavy elements within the core. Eventually the shock wave stalls into a standing accretion shock where the "explosion" process is temporarily halted*. Bethe & Wilson (1985) and Wilson (1985) first demonstrated that energy in the form of neutrinos emerging from the PNS can be deposited behind the shock and potentially revive it. As discussed in Chapter 3, current computer simulations attempt to self-consistently† describe how neutrino energy deposition, aided by the convection of neutrino-heated material below the stalled shock, eventually re-energizes the stalled shock and drives the explosion towards completion. This re-heating process accelerates as instabilities increase the size of the heating region until enough matter is energized to turn the collapse around and make the stellar envelope gravitationally unbound — thus creating a supernova.

Obtaining an accurate understanding of how supernovae occur requires calculating the forces, dynamics, and interactions across many fields of physics including; nuclear physics, particle physics, general relativity, and extreme magnetic fields. Modern computational models are the only way to explore and integrate the necessary complexity of this range of topics – as there can be no analytical solution. From an astrophysical point of view, a better understanding of CCSNe evolution will help us understand the direct link between a progenitor star and its remnant – a neutron star (NS) or a black hole (BH). Modern multi-dimensional supernovae models have proven to be useful for studying gravitational-wave signatures (Yakunin et al., 2010),

*Theories of the neutrino heating mechanism extend back to Colgate & White (1966).
†Self-consistency requires obtaining successful explosions without parameterized methods.

neutrino signals (Lund et al., 2010), and the determination of the stellar mass limit for black hole formation. CCSNe are one of the few sources by which newly synthesized elements are dispersed throughout the cosmos.

In addition, there is now an indisputable connection between peculiar "Type Ic" CCSNe, also known as "hypernovae", and long, soft gamma-ray bursts (Matheson et al., 2003; Galama et al., 1998). Like other types of CCNSe, there phenomena occur under a common umbrella of massive stellar core-collapse. A "first-principles" understanding of long, soft gamma-ray bursts must begin with an understanding of stellar core-collapse and the physics involved in CCSNe for both "ordinary" (Type II, Ib, ordinary Ic) supernovae and hypernovae. Thus, our work is the first stage in a longer-term effort to simulate, from progenitor to burst, hypernovae and long, soft gamma-ray bursts.

1.1 Our CCSNe Simulation Code, CHIMERA

Without question, CCSNe are complex, multi-dimensional events; and years of development have shown that the codes developed to model CCSNe must follow suit. A joint group consisting of scientists and students at Oak Ridge National Laboratory and The University of Tennessee, Knoxville (ORNL/UTK), in strong collaboration with Florida Atlantic University (FAU) and North Carolina State University (NCSU), have built a tightly coupled radiation hydrodynamic code called CHIMERA. The primary modules of the code are designed to evolve the stellar gas hydrodynamics, compute the neutrino transport, and solve the thermonuclear kinetics. These three "heads" are augmented by a sophisticated equation of state for nuclear matter and a self-gravity solver capable of an approximation to general-relativistic gravity. A more detailed description of CHIMERA is contained in Chapter 3.1.

Within the past 6 years, the CHIMERA team has become successful in generating self-consistent (i.e. non-parameterized) core-collapse explosions of 12, 15, 20, and 25 $M_\odot$ stars. General features of our recent two-dimensional simulations have been reported in Messer et al. (2007), Bruenn et al. (2010), and Chertkow et al. (2011). We currently have a suite of 2D full-physics production runs, which were initiated in February of 2012, and are progressing towards explosion energies. I give a status report of these runs in Chapter 5.5.

1.2 Nucleosynthesis with CHIMERA

Regardless of the initial mass, a prime motivation for modeling realistic CCSNe abundances is to reconstruct observables for the purpose of understanding the origin of the elements. The isotopic abundances are not the only product of a nuclear network, since thermonuclear energy generation can have a local effect upon the hydrodynamic model and should be directly related to the physical processes causing the explosion (Hix et al., 2007; Fröhlich et al., 2006). Evolution of the nuclear composition of the stellar matter can employ a hierarchy of methods. At low temperatures, a complete thermonuclear reaction network is required. During silicon burning the nuclear evolution is dominated by large groups of nuclei in mutual chemical equilibrium (Bodansky et al., 1968) – a condition referred to as quasi-statistical equilibrium (QSE), and a precursor to global nuclear statistical equilibrium (NSE). In NSE, the populations of the entire chain of light to heavy isotopes, obey chemical equilibrium; with heavy nuclei being built through the fusion of lighter elements and then being destroyed by way of photo-disintegrations. NSE applies under rapidly changing explosive conditions for temperatures in excess of 6 GK, though under the more slowly varying conditions of late stellar evolution, NSE may be achieved at temperatures as low as 3 GK. CHIMERA takes advantage of this hierarchy of approximations to provide the required physical fidelity at minimum computational cost.

As will be discuss more thoroughly in Chapter 4, accurately calculating complete and incomplete silicon burning is computationally expensive due to the large number of nuclear reactions involved. For conditions not in NSE, CHIMERA typically evolves nuclear compositions using a thermonuclear reaction network of 14-species alpha-chain (from ^{4}He to ^{60}Zn) (hereafter an “alpha-network”) with the XNet code of Hix & Thielemann (1999). The approximation of 14 species, although useful, does not include many of the reaction channels important for the production of iron, including electron- and neutrino-capture reactions that determine the neutron-richness (or “neutronization”) of the matter. As a feedback mechanism, the neutronization strongly determines which isotopes dominate the composition and how the composition evolves as a whole.

In lieu of a larger, more realistic network, it is currently common to study detailed nucleosynthesis of the ejecta by way of post-processing. In CHIMERA, several thousand massless, passive tracer particles, are evolved enabling us follow a Lagrangian perspective of bulk matter properties throughout the evolution of a supernova event. The tracer particles also allow us to explore multi-dimensional effects that stem from anisotropies, instabilities, and mixing. For example, in Chapter 5.6, I describe investigations of gravitational wave (GW) signal calculations using the tracer particles from our 15 $M_{\odot}$. In doing so, we have decomposed the GW signal geographically and determined which phenomena contribute to the various components of the waveforms. Specifically, using the tracers, we have identified an additional GW source of the prompt signal (previously attributed solely to prompt convection) due to the deflecting of in-falling matter through the shock (Yakunin et al., 2010).

The CHIMERA team has an ambitious agenda of running 2D and 3D models to examine the effects of progenitor mass, rotation rate, and micro-physics input on the supernovae mechanism (see Chapter 5.5 for the current status of these studies). Although these runs are subject to developmental improvements over the next few years, it must be stressed that the analyses of these runs will be incomplete without detailed calculations of the nucleosynthesis. As part of this dissertation, I have developed the tools necessary to undertake such analysis, and will present preliminary analysis of existing models in Chapter 5.

1.3 Nuclear Networks

While many supernova modeling groups continue to use either an alpha-network ("α-network") or a simpler "flashing" scheme[‡], I will describe in Chapter 4.1 my efforts towards efficiently evolving a larger set of species that will enable improved energy generation rates along with more accurate abundance calculations, which affect the level of neutronization. To this end, I have extended CHIMERA's ability to advect and track an arbitrary number of species. One example of this extention is a network of 150-species, which has been used in the first simulation of iron-core collapse supernovae to employ a realistic reaction network. I will describe this work in Chapter 4.1.

Since nucleosynthesis calculations are computationally expensive, there is a strong motivation to take advantage of modern supercomputer resources and applications. These applications include MPI and OpenMP software libraries, and the latest advancements in system architectures, such as *graphical processor units* (GPUs) for matrix or vector calculations. These advancements allow for an increase in the size of

[‡]Flashing schemes have a predefined composition based on density, temperature, and electron fraction

the nuclear network. In this dissertation I will describe my efforts to harness OpenMP (see Chapter 4.1).

With a self-consistent, multi-dimensional code, using a nuclear network extended beyond 14-species, and having tracer-laden models, CHIMERA is well suited to simulate the lower mass limit (between $\sim 8\ M_{\odot}$ and $10\ M_{\odot}$) of core-collapse supernovae wherein the core is composed, not of iron, but of oxygen, neon, and magnesium (ONeMg). As this star evolves, before reaching neon ignition, a rapid electron capture process begins causing the core to collapse — thus providing the name an *electron capture supernova* (ECSN). Interest in ECSNe lies in understanding their contribution to the rate of supernovae and especially for the search for the source of heavy, r-process elements from Zn to Zr. We describe our initial efforts towards evolving an ECSN in Chapter 6.

Were it not for their explosive deaths, the oxygen, silicon, and iron made during a star's life and death would not escape the star's gravitational pull to populate the universe as building blocks for other structures such as stars, planets, and ultimately, living organisms. The knowledge we obtain from supernovae ultimately leads to an understanding of our origins and the abundances of nuclear species that are found throughout the cosmos. But most importantly, we study supernovae because they are so stunningly bright, yet simply beyond our reach.

1.4 Thesis Workflow

CHIMERA is a large project with many collaborators. More than a decade of development and 100 million CPU hours have been spent in attempting to answer the central question, "How and why do supernovae occur?" Adding the capabilities utilized in my project has required delving deeply into CHIMERA's works. This thesis is a relatively small, yet significant, part in the larger project that makes up our studies. To show the connections between the various components of this thesis, Figure 1.1 depicts the relationship CHIMERA has to a generalized progenitor generator, the thermonuclear kinetics solver (XNet) Hix & Thielemann (1999), and the *tracer particle reader*. These components will be introduced and discussed in the forthcoming chapters. This schematic also shows the work-flow of how the CHIMERA team produces detailed post-processed nucleosynthesis results (of thousands of nuclear species) and their subsequent analysis. The numbered circles follow the sequence of events starting with the production of a progenitor, which is fed into CHIMERA. At stage number 2, CHIMERA, using the XNet "head", evolves a model with the limited alpha-network for the sake of computational efficiency. Stage number 3 is the beginning of the post-processing phase in which the Tracer Reader creates thermodynamics profiles to be post-processed by XNet, this time, using a more comprehensive nuclear network of thousands of nuclear species. At stage 5, XNet feeds these new results ("tso files") back into the Tracer Reader, this time acting as a data manager, to produces snap-shots of every tracer at specific time intervals.

As shown in the green boxes of Figure 1.1, this thesis is the result of developments on (1) improvements to the progenitor generator (for ONeMg-core models), (2) making improvements within CHIMERA to handle a generalized network fed to it by the XNet module, and (3) the development of the Tracer Reader as a necessary tool in the chain of producing nucleosyntheisis results by way of post-processing with XNet. The circles "P" indicates "intermediate" results in the context of nucleosynthesis studies of ejecta. Outside of this context, the study of explosion mechanisms is reliant upon the "Model Results" which come directly out of CHIMERA.

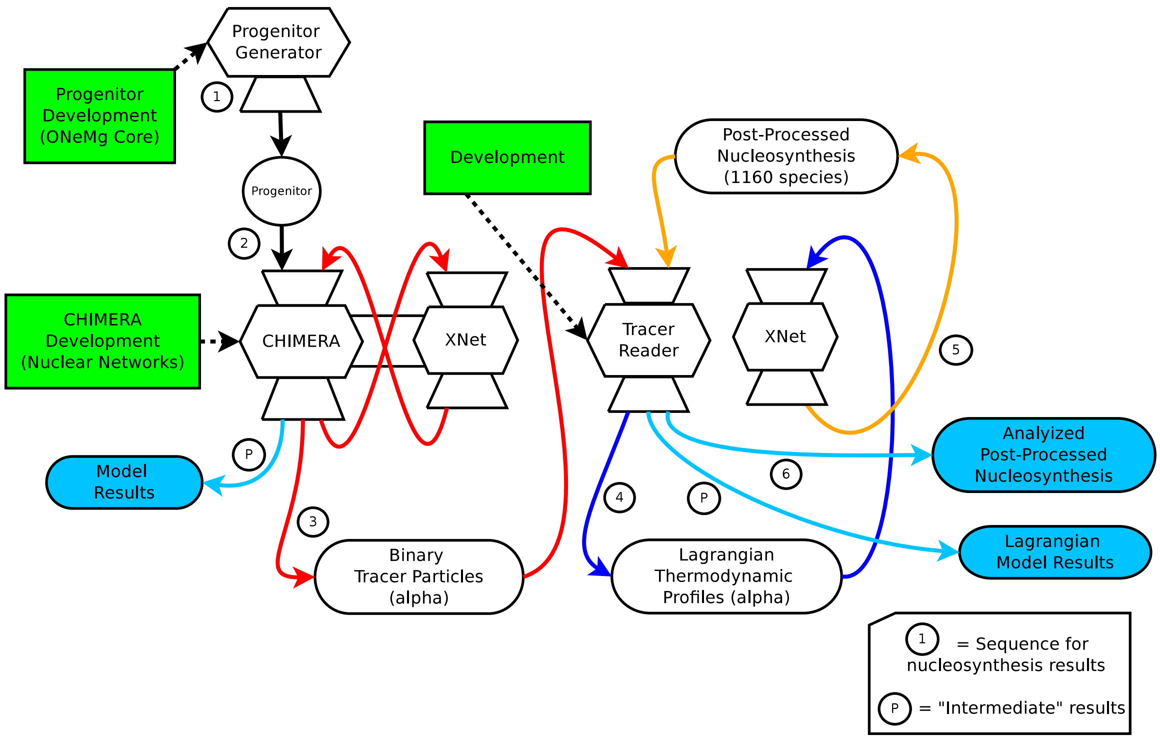

Figure 1.1: A simple schematic of the process of generating advanced nucleosynthesis burning results in relation to this thesis project showing the relationship CHIMERA has to the thermonuclear reaction network XNet, the progenitor generator, and the tracer reader module.

Chapter 2

The Death of Massive Stars

The supernovae community is concerned with the investigating the connection, proposed by Baade & Zwicky (1934), between massive stars, extremely bright explosion within galaxies (supernovae), and the birth of neutron stars (NS) and black holes (BH). Since these supernovae occur across intergalactic distances, we are restricted to observing the spectra and lightcures of SNe as well as building estimates of mass from luminosities and Doppler-shifted radial velocities of ejected masses after explosions.

Observationally, supernovae are classified (and sub-classified) into two categories or Types: The first is Type I (Ia,Ib, and Ic) and Type II (IIb,IIn,II-L, and II-P), all of which are derived from light curve measurements and spectroscopic observations of characteristic wavelengths. Type I supernovae exhibit no hydrogen lines. Type-Ia (the only non-core-collapse type) are distinguished by their characteristic Si II $\lambda 6355$ absorption line. The spectra of Type Ib SNe contain He $\lambda 5876$ absorption lines while those of Type Ic SNe contain neither He nor Si. Type-II progenitors retained their hydrogen envelopes and thus have a strong Hα absorption line. The Types IIb, IIL, and IIP are determined by the size of their outer hydrogen envelope and are distinguished by the unique shape of their light curves. Type IIn are caused by strong interaction with the circumstellar environment. Although the standard classification of "Types" is well motivated observationally, it is encumbered by mixing mechanisms across Type-numbers.

In short, every Type, excluding a Type-Ia, results from the collapsing core of a massive star. The mechanism for Type Ia is a thermonuclear reaction runaway within a carbon-oxygen white dwarf (WD). This runaway is energetic enough to completely disrupt its structure in a matter of seconds (Hoyle & Fowler, 1960). Because the Type-Ia mechanism is highly dependent upon specific conditions notably the approach to the Chandrasekhar mass, their absolute lightcurves are very nearly the same and scalable by way of empirical corrections to be used as standard candles for cosmic distance scale measurements.

The core-collapse mechanism occurs when a star's core (1) becomes gravitationally unstable through dissociation of iron nuclei and electron capture, (2) collapses, and (3) becomes a neutrino bomb driving off outer layers of the dying star while experiencing explosive nucleosynthesis. These *core-collapse supernova* take place in stars with masses of between approximately 8 and 25 $M_\odot$. The variables governing the mechanism for supernovae are (1) initial mass, which determines a star's lifetime on the main sequence (this can be modified by a mass donating companion in a binary system); and (2) initial elemental composition, which determines how much mass is lost throughout its lifetime as stellar wind. Beyond $\sim 25-40$ $M_\odot$, stars may evolve directly to black holes without going supernova. In extreme cases, around 140 to 260 $M_\odot$ are believed to be recently discovered *pair-instability supernovae* such as 2007bi (Kasen et al., 2011), which shows signs of experiencing a combination of both explosion mechanisms.

2.1 Non-Explosive Stellar Thermonuclear Burning

As a very massive star slowly contracts under its own gravity, it undergoes compression induced heating. Under proper density, temperature, and composition conditions, this heating can drive fusion reactions forward towards heavier element production providing a thermal-feedback to the star's evolution. Through the slow progression of gravitational contraction, progressive burning stages create a stellar core with a quasi-onion-like structure of heavy elements in the core and progressively lighter elements in the envelope. This process continues until the fuel is exhausted and nuclear burning ceases. The stability of a massive star throughout its lifetime occurs through a competition of gravitation contraction and pressure generated from the release of binding energy through stages of nuclear burning from hydrogen to helium, on to carbon, neon, oxygen, silicon, and eventually iron – including for a lesser degree the intermediate isotopes along the way.

The number of burning stages, and the star's ultimate fate, depend primarily on the star's initial mass and initial composition. The first ash formed is helium, created from the fusion of hydrogen via the pp-chain (proton-proton chain) or CNO (carbon-nitrogen-oxygen) cycle. The proton-proton chain is a three stage hydrogen fusion process that results in ^{3}He, which can then proceed through four temperature dependent branches, all of which result in producing ^{4}He. The CNO cycle is a catalytic cycle the net effect of which is four protons fusing using carbon, nitrogen, and oxygen isotopes as intermediaries to produce ^{4}He. At higher temperatures, helium fuses via the triple-alpha-process to become carbon. For low mass stars, carbon and oxygen, or even helium (in the lowest mass regime), may represent the limit of available fuel. Instabilities in the burning shell on the surface of the carbon-oxygen core can drive off the stellar envelope. Stripped of the envelope, the core will simply radiate heat back into the universe as a white dwarf and no further internal event will occur. Isolated stars below an approximate mass of $8M_{\odot}$ are energetically uneventful compared to supernovae. Just above this mass range, stars can produce ONeMg cores which may undergo rapid electron-capture-induced collapse, as described in the next section.

For stars greater than $\sim$10 $M_{\odot}$ the fusion cycle continues and, at high enough temperatures, it will approach a silicon burning stage. During this stage, the element production tends toward the iron-peak nuclei (elements from chromium to nickel) via a long chain of competitions between photo-disintegration and light particle captures in a temperature range of 3 to 4 GK (see Arnett, 1996), gradually reaching an equilibrium, termed *nuclear statistical equilibrium* (NSE). As the nuclei are rapidly created and destroyed, the ones with the higher binding energy per nucleon are favored, leading to a greater abundance within the iron-peak species. The progress towards this equilibrium begins with three small nuclei groups in local nuclear equilibrium known as *quasi-statistical equilibrium* (QSE) (Bodansky et al., 1968; Woosley et al., 1973). These groups are (1) a hydrogen-helium group, (2) a group centered around silicon, and (3) a group of nuclear species around iron and nickel. The membership of these QSE groups are weakly dependent on temperature and density and strongly dependent on the neutronization (set by β–decays). In QSE, the neutronization determines which isotopes of the iron-group dominate the composition and how long the groups are separated (Hix & Thielemann, 1996).

If and when the star is able to synthesize iron in the core, the self-sustaining fusion will stop since the fusion of iron, having the highest binding energy per nucleon, is an endothermic process. This marks the final stages of non-explosive nucleosynthesis and we refer to this iron-core the star as a "progenitor" that is primed to become a supernova.

2.2 The Core-Collapse Phase

With continued compression, the electron chemical potential in the core rises, accelerating the capture of electrons by protons and heavy nuclei, creating an even more neutron-rich environment. For iron-core stars, the loss of electron pressure causes the inner core to collapse homologously in a matter of hundreds of milliseconds to super-nuclear densities in excess of $3{\times}10^{14}\,\mathrm{g/cm^3}$. The collapse of the core is enhanced by two additional mechanisms which help accelerate the process: (1) the neutrinos that are initially produced within the core freely escape to carry their energy outside of the star; and (2) as the core compresses the temperature rises and creates photons with enough energy to endothermically photo-dissociate the iron nuclei into alpha particles and further decrease the core pressure (Hillebrandt, 1986). These two factors cause the iron core to become gravitationally unstable as it approaches its Chandrasekhar mass of approximately $\sim 1.1M_{\odot}$ (Yahil, 1983)). The stellar core is now a proto-neutron star (PNS) with a low entropy of about $\sim 1.4\,\mathrm{k_B}$/baryon and a radius of approximately 50 km.

2.3 The Bounce and Stalled Shock Accretion Phase

With the inner core having collapses subsonically to form a PNS, the matter above in supersonic free-fall is only halted once it slams into the incompressible core, which, acting like a springboard as the PNS relaxes from its super-nuclear density state, sends a sound wave back into the outer core. As the sound wave travels outward and passes into less dense material, it eventually steepens into a supersonic shock traveling at several thousand kilometers per second (Bethe, 1996).

This *bounce-shock* was once thought to provide the kinetic energy required to turn enough inward-falling matter into ejecta to complete the SN explosion.

However, the *prompt shock mechanism* failed to drive an explosion once more realistic nuclear equations of state were used (Burrows & Lattimer, 1985; Scheck et al., 2006). Instead, modern radiation-hydrodynamic simulations now show that the expanding shock wave is robbed of its momentum by both the loss of neutrinos and the dissociation of the in-falling matter at a price of almost 9 MeV per nucleon (equalling 10^{52} ergs/$M_{\odot}$) (Bruenn, 1985). At this rate, the shock eventually stalls to become a standing accretion shock with strong velocity discontinuities as its outward momentum becomes completely sapped at a radius between 100-200 km.

2.4 The Neutrino-Heating Explosion Mechanism

A supernova is, in essence, a neutrino explosion, powered by the gravitational binding energy ($E_b \sim G M_{ns}^2 / R_{ns}$) of a collapsed star. As charged-current (e.g. e^-/e^+ captures) and neutral-current (e.g. e^-/e^+ annihilation) processes occur within the dense nuclear matter of the PNS, the binding energy, approximately 10^{53} ergs, is released in the form of neutrinos of all flavors (electron, muon, and tau) (Bethe, 1996). During the later stages of core collapse, when densities become greater than 10^{11} g/cm^3, the neutrino diffusion time becomes longer than the characteristic time of the collapse, and the neutrinos become trapped in the local matter (Arnett, 1977). After bounce, a rapid deleptonization process occurs when the shock expands and reaches a low enough density that the mean free path of the trapped neutrinos becomes larger than the star's diameter resulting in a "breakout burst" of neutrinos.

While a prodigious amount of neutrino energy emerges from the PNS, the neutrinos are weakly coupled to the material directly below the shock, where the neutrino heating is very sensitive to the electron neutrino and anti-neutrino luminosities, spectra (often characterized by the the root mean square (rms) of the energies), and angular distributions in the region behind the shock (Burrows & Goshy, 1993; Janka & Müller, 1996; Messer et al., 1998; Mezzacappa et al., 1998, 2001; Janka, 2001).

The one-dimensional CCSNe models of Wilson (1985) and Bethe & Wilson (1985) demonstrated that energy in the form of neutrinos emerging from the PNS can be deposited behind the shock and revive it. Though the *delayed neutrino heating mechanism* began to take intellectual hold, improved one-dimensional models often failed to produce explosions because there was not enough energy transfered from the neutrinos to rejuvenate the kinetic energy of the shock (Bruenn, 1985; Wilson & Mayle, 1993; Bruenn et al., 2001).

In the mid 1990s, it was found that by breaking spherical symmetry with convection, modelers could greatly enhanced the neutrino's energy deposition behind the stalled shock. This convection either enhanced neutrino luminosity, due to fluid instabilities within the proto-neutron star (Wilson & Mayle, 1993; Keil et al., 1996), or enhanced the neutrino heating, due to large scale convection behind the shock (Herant et al., 1994; Burrows et al., 1995). However, those models employed grey (spectrally averaged) neutrino transport, and therefore questions remained.

The neutrino heating mechanism was aided by the multi-dimensional models of Blondin et al. (2003), where it was found that non-spherical perturbations lead to the growth of a *standing accretion shock instability* (SASI) that widened the radial extent of the neutrino heating region behind the stalled shock. The widening of the heating region aided by neutrino driven convection increases the likelihood that approximately 1% (10^{51} ergs) of the total neutrino energy will be deposited to help revive the SNe explosion (Janka et al., 2004). Simulations have found neutrino heating is aided and can sufficiently revive the stalled shock to drive the explosion to completion if low-order SASI models are permitted. The successful explosion of Bruenn et al. (2006)

and Marek et al. (2008) is contrasted by the ray-by-ray models of Buras et al. (2003), which did not produce explosions because full development of instabilities in the stalled accretion shock were inhibited by a constrained computational domain of 90° in latitude. Simulations which exhibit the SASI are found to have strong bipolar explosions which may be the underlying mechanism for generating neutron star kicks and the polarization of supernova light (Blondin & Mezzacappa, 2007).

Since the neutrinos dominate the energy of core-collapse supernovae, correctly calculating the neutrino interaction rates and neutrino transport are vital to obtaining self-consistent, realistic explosions. This heating depends sensitively on the neutrino luminosities, spectra, and angular distribution within the heating region (see Mezzacappa, 2004, for a review). The neutrino re-heating mechanism remains the leading explosion mechanism candidate for CCSNe (Bruenn et al., 2010). Although all flavors of neutrinos are emitted from the core, the electron neutrino and electron anti-neutrino are the primary source of the shock revival since they can interact with matter by neutral- *and* charged-current weak interactions.

2.5 Explosive Burning and the Ejecta

To meaningfully understand CCSNe, models must reproduce the many available observations, implying we must understand their nuclear evolution and how the supernova shock wave can alter and eject the layered structure of the star. The matter that ultimately becomes ejecta consists largely of the original oxygen layer from stellar nulcear burning and above. This will require a revisiting of silicon burning and other burning stages during the explosion. Before ejection, this matter undergoes explosive nucleosynthesis due to the passage of the shock wave.

Simulations have shown that as the bounce shock wave passes back up through the core into the silicon and oxygen layers, it reverses the in-falling matter and heats it beyond $\sim$5 GK, where explosive silicon burning ensues (Arnett, 1969). For sufficiently high temperatures, photo-dissociation of nuclei into light particles (such as protons, neutrons, and α-particles) occurs, creating an environment dominated by nuclear statistical equilibrium, which synthesizes nuclei up to the iron-peak species. Freeze-out occurs when reactions cease due to declining temperatures. Three outcomes are possible for explosive silicon burning: (1) when all the fuel is burnt, "*normal freeze-out*" occurs; (2) when all the alpha-particle are not re-constituted into heavy nuclei "*α-rich freeze-out*" occurs, and (3) when expansion occurs fast enough to cool and prohibit further reactions before the fuel is exhausted "*incomplete burning*" occurs (Woosley et al., 1973).

Normal freeze-out occurs under explosive conditions when the peak temperatures exceed 5 GK at high densities within the inner core. The result is similar to hydrostatic burning where all available silicon and sulfur burns through to the iron peak group. As the matter cools, the light nuclei recombine into iron and nickel nuclei (Woosley et al., 1973).

α-rich freeze-out occurs for peak temperatures greater than 5 GK, but at lower densities as the ejecta expands outward. The source of α-rich freeze-out is the instability of Beryllium-8 which frequently decays in 7×10^{-17} seconds before it can capture an additional α-particle. This slows the recombination of helium, leaving an excess of He (and free nucleons) excess when freeze-out occurs at low densities. At late times, a fraction of these α-particles capture onto heavier nuclei, altering the abundance pattern (see Woosley & Weaver, 1995; Thielemann et al., 1996; Limongi & Chieffi, 2003).

Incomplete silicon burning results for temperatures lower than 5 GK. This generally occurs above the innermost helium, iron, and nickel dominated regions, where insufficient shock heating leaves a significant fraction of mass that does not reach NSE. The results of incomplete silicon burning are the α isotopes; ^{40}Ca, ^{36}Ar, ^{32}S, ^{28}Si (Hix & Thielemann, 1999). Above this, the unaltered outer portion of the oxygen shell as well as the helium and hydrogen envelopes are also ejected, assuming they were not driven off by stellar winds. This matter will escape as part of the ejecta to contribue to the ongoing chemical evolution of the galaxy.

The ratio of protons-to-nucleons, (also known as "electron fraction", Y_e, neutron-richness, or neutronization) has a strong influence on the products of explosive nucleosynthesis in the innermost ejecta. Despite the expected importance of neutrinos to the core collapse mechanism, models of the nucleosynthesis have largely ignored this important effect. Recently, Fröhlich et al. (2006b) have found that strong neutrino fluxes play a significant role in modifying the abundance patters in the early proton-rich ejecta. They have termed this process the "νp-process", the result of strong neutrino fluxes creating proton-rich ejecta. In this process, anti-neutrino absorptions in the proton-rich environment produce neutrons that are immediately captured by neutron-deficient nuclei.

After a supernova explosion, the matter of the progenitor star is divided into matter that has been gravitationally bound, forming a remnant, and matter that is scattered back into the cosmos from where it came. The states, or properties, of the remnant and ejecta both say something about the history and processes that occurred during the CCSN. By the end of the explosion, approximately 90% of the star's mass is ejected into the surrounding medium. CCSNe are observed to produce about 0.1 $M_\odot$ of ^{56}Ni, whereas thermonuclear supernovae produce about $0.5-1.0$ $M_\odot$ of ^{56}Ni. This nickel then beta decays to cobalt and onto iron providing the decaying feature of CCSNe lightcurves. The ejecta is observed to have typical velocities of approximately 5,000 km/s for Type II SN and 10,000 km/s for Type Ia. Since CCSNe are so rare (about every century or so), and brief, we often use observations of ejecta to reverse engineer the beginnings of a progenitor star's death.

Chapter 3

Modeling Core Collapse Supernovae

There are many scientifically interesting aspects to core-collapse supernovae, but unraveling exactly how the explosion occurs remains a fundamentally unsolved question in supernovae theory. The computational SN community has compiled a list of physical ingredients required to describe and produce self-consistent SN simulations; hydrodynamics (e.g., turbulent flows and fluid instabilities), thermodynamics, nuclear physics (e.g., finite-temperature equation of state of neutron star matter), particle physics (e.g., neutrino-matter interactions), and general relativity (Janka, 2012). Evidence has accumulated indicating that multi-dimensional effects play a necessary role in the CCSN explosion mechanism. On the observational side, spectropolarimetry, the large average pulsar velocities, and the morphology of highly resolved images of SN 1987A all suggest that anisotropy develops very early in the explosion (Arnett et al., 1987; McCray, 1993).

On the theoretical side, analysis of immediate post-bounce core profiles of simulations show that a variety of fluid instabilities are present and are essential in driving the explosion mechanism (Buras et al., 2006). In particular, multi-dimensional numerical simulations have shown that convective overturn in the neutrino-heated region, behind the stalled shock, is important for the success of the neutrino-driven mechanism. Convection helps transport hot gas from the neutrino-heating region directly to the shock, while down-ows simultaneously carry cold, accreted matter to the layer of strongest neutrino heating, where a part of this gas readily absorbs more energy from the proto-neutron star.

Such models must consider (1) neutrino transport, (2) fluid instabilities, (3) rotation, (4) magnetic fields, together with proper treatments of (5) the nuclear equation of state, (6) nuclear burning, (7) general relativity, (8) neutrino-matter interactions at sufficient physical fidelity to capture the essential ingredients of the explosion. Points (2), (3), and (4) constrain analysis to multi-dimensional simulations, which have only been developed within the past two decades.

Including features (1)-(8) in simulations, in their full complexity, is not simply computationally expensive, it is beyond the capability of existing supercomputers. To create complete 3D models will require exa-scale computing (10^{18} floating point operations per second) and beyond. Ideally, neutrino transport would be implemented with full multidimensional Boltzmann transport, but solving the full multi-D Boltzmann equations is expensive even on exascale platforms (Bruenn et al., 2006; Messer et al., 2007; Sumiyoshi & Yamada, 2012). On current peta-scale (10^{15} floating point operations per second) platforms, lesser approximations of neutrino transport must be employed, notably *multi-group flux limited diffusion* (MGFLD) and *multi-group variable Eddington tensor factor* (MGVETF). While preserving the neutrino energy specular dependence, these methods make simplifying assumptions about the transition from diffusive transport to free-streaming.

Simulations have also revealed that a non-radial, low-mode standing accretion shock instability (SASI) may also grow, given time, via the propagation of sound waves (Blondin & Mezzacappa, 2006). This low-mode distortion of the shock may be at the root of some of the above-mentioned SN observables. Adequate multi-dimensional treatments of significant components such as point (1) have only been developed within the last few years.

More recently, Bruenn et al. (2006) and Marek et al. (2008) have produced simulations with successful neutrino-driven explosions using multi-group ray-by-ray models. These models perform independent calculations of the spectrally resolved radiation transport along each radial direction, thus capturing much of the transport realism. As a further compromise between accuracy and computational intensity, some groups employ the "ray-by-ray-plus" approximation (Buras et al., 2006) for neutrino transport, whereby the lateral effects of neutrinos such as lateral pressure gradients (in optically thick conditions), neutrino advection, and velocity corrections are taken into account, but neutrino transport is performed only in the radial direction.

Once fully realistic 3-dimensional models are an industry standard, it would not be surprising to discover unconsidered contributions which will require additional computational power. One known example, yet to be realistically implemented alongside realistic neutrino transport, is the role of magnetohydrodynamics (MHD), which may strongly affect the morphology and the evolution of the supernova explosions. Many computational issues caused by the limitation of incorporated physics, dimensionality, wall-clock time, and other forced approximations are gradually being resolved throughout the supernova community as more sophisticated simulations are combined with faster computers.

3.1 Modeling with CHIMERA

The ORNL/UTK group, in strong collaboration with Florida Atlantic University and NC State University, have built a tightly coupled radiation hydrodynamic code called CHIMERA. The code's primary modules are designed to evolve the stellar gas hydrodynamics (VH1), compute the "ray-by-ray-plus" neutrino transport (MGFLD-TRANS), and solve the thermonuclear kinetics (XNet) (Messer et al., 2010). These three "heads" are augmented by a sophisticated equation of state for nuclear matter (e.g. Lattimer & Swesty, 1991) and a self-gravity solver capable of an approximation to general-relativistic gravity. The addition of a prescription for nuclear burning to a multidimensional ray-by-ray radiation hydrodynamics scheme allows much of the known physics in the problem to be completely addressed. The simulation results provide reasonable physical fidelity (i.e. enough to determine the nature and many of the consequences of the explosion mechanism) at a tractable cost on current peta-scale architectures. A more general description of CHIMERA and general features of our recent two-dimensional simulations have been reported in Messer et al. (2007), Bruenn et al. (2010), and Chertkow et al. (2011).

To date, no three-dimensional models to date have included all of the following: (1) multi-frequency neutrino transport, (2) convection and other fluid instabilities, (3) rotation, and (4) nuclear burning. Our code, CHIMERA, has been developed with these notions in mind, and we have run several short duration, lower resolution tests (see Figure 3.1). The first production 3D model with a resolution of approximately 3° in latitude and longitude should start shortly.

CHIMERA uses a variety of equations of states (EoS) depending on the thermodynamic and nuclear conditions. An equation of state describes the relationships between thermodynamic variables characterizing a medium, for example, pressure as

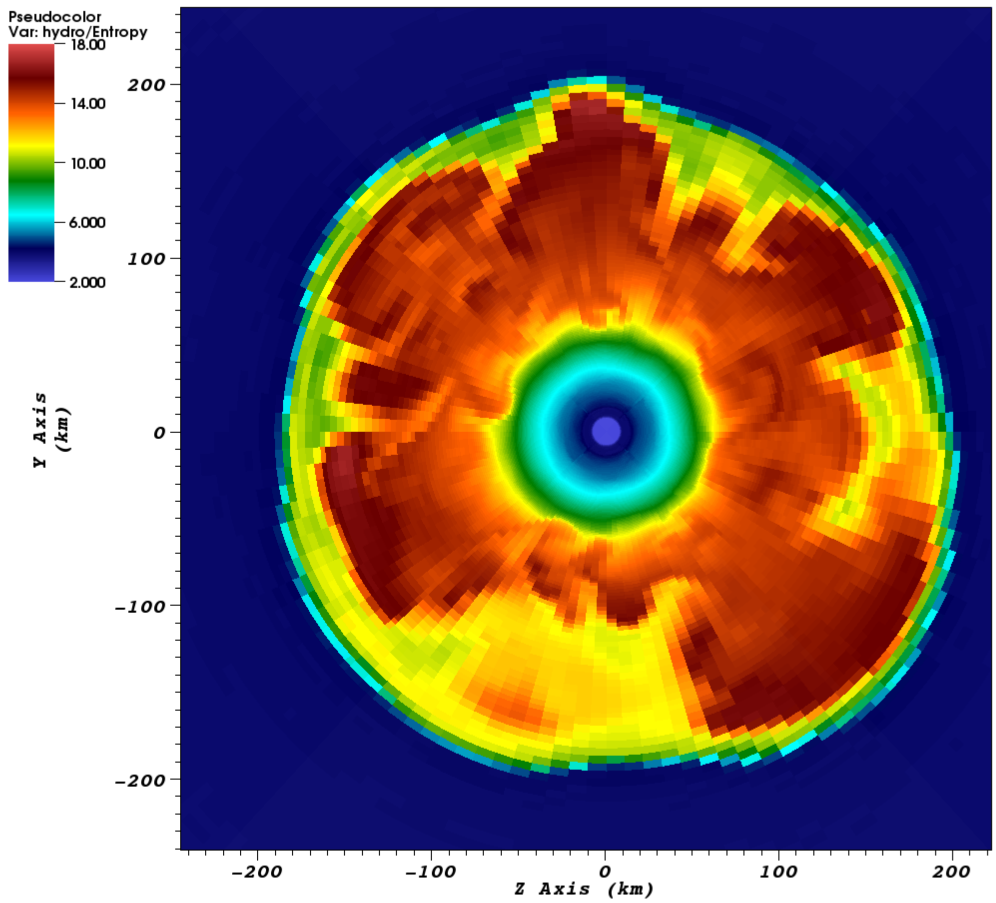

Figure 3.1: CHIMERA's 3D test run in preparation for full production models. Image is an entropy slice through center at 125 ms after core bounce of our 3D pilot run on 2 Eulerian "Ying-Yang" grids.

a function of temperature and density. Studies show that the EoS affects the stellar structure; the hydrodynamics; the core bounce; the propagation of the shock wave; the reaction rates and chemical compositions through the determination of temperature; and the formation of the proto-neutron star (Sumiyoshi et al., 2004). Proper EoS treatment is vital to obtain simulations which mirror astronomical observations. An electron-positron EoS, with arbitrary degeneracy and degree of relativity, spans the entire density-temperature regime of interest. Currently in CHIMERA, for regions in NSE (assumed to occur when temperatures exceed 5.5 GK), two equations of state are used to describe the matter; (1) the EoS of Lattimer & Swesty (1991), which is based on the compressible liquid drop model, is used to describe conditions where densities exceed 1.7×10^8 g/cm^3; (2) the modified EoS of (Baron et al., 1985), which is used when the density is below 1.7×10^8 g/cm^3 .

For non-NSE regions the EoS includes a nuclear component consisting of an ideal gas of the 14-species α-network (^{4}He to ^{60}Zn) plus free protons, neutrons, and an additional iron-like nucleus to preserve the electron fraction. The composition is evolved by XNet, the thermonuclear reaction network (Hix & Thielemann, 1995) operating on the 14-species α-network. Data for these reactions is drawn from the REACLIB compilations (Rauscher & Thielemann, 2000).

3.2 Building a CHIMERA Progenitor

In order to model the evolution of a star from core-collapse to a completed explosions, the supernovae modeling community must acquire stellar models from the research groups that evolve gaseous clouds into evolved stellar objects.

Since each group involved in such simulations work with different formats and at different resolutions, for our purposes, we must “transcribe” these models into a format compatible with CHIMERA. This is a detailed process where we (1) read the data from the original progenitor file; (2) remove or fix data discontinuities; (3) assign a network of species from the progenitor's composition, or, where such data is missing, use the Y_e to build a list of representative species to be contained in the CHIMERA simulation from the mass table of G. Audi & Wapstra (2003); and finally, (4) re-grid the original model to fit CHIMERA's radial indexing;

The progenitor infrastructure for CHIMERA was built based on experience with the $12 - 25M_{\odot}$ iron-core progenitors of Woosley & Heger (2007). Because these iron core progenitors have a flat density gradient, relative to the lighter ONeMg-core models of Nomoto (1987) (see Figure 6.1), our original progenitor generator used a re-gridding technique based on uniform changes in mass as a function of radius. To adapt to the differences posed by an ONeMg-core progenitor, we were required to change our zoning construction scheme to be based on monotonically decreasing density in an attempt to produce constant scaling in matter density ($d\rho/\rho$) for a user specified number of zones.

Chapter 4

Calculating Detailed Nucleosynthesis

Until recently, due to the frequent failure of more realistic models, 1D and 2D simulations of CCSN nucleosynthesis required parameterization, using arbitrary thermal energy bombs (Thielemann et al., 1996; Nagataki et al., 1998b) or kinetic energy pistons (Woosley & Weaver, 1995; Rauscher et al., 2002) to replace the central engine. In these parameterized models, thermal energy or momentum is artificially injected into the outer core to engender the required kinetic energy to generate an explosion that matches observations and a parameterized quantity of ejected matter. Such models have been the mainstay of supernova nucleosynthesis modeling (Woosley & Weaver, 1995; Thielemann et al., 1996; Nagataki et al., 1998b; Rauscher et al., 2002; Limongi & Chieffi, 2003), serving as input to calculations of galactic chemical evolution. These highly parameterized models do not adequately take into account the effects of neutrino interactions, convection, and other important features within a supernova's central engine that drives explosions.

Attempts have been made to pin the observations to the underlying mechanism(s) by using multi-group neutrino transport in spherical symmetry to focus on the role neutrinos play on the neutronization in the outer part of the heating region (see Liebendörfer et al., 2002; Rampp & Janka, 2002; Burrows et al., 2004). The modern developments in multi-dimensional, multi-group neutrino powered explosions are beginning to make progress by allowing us to quantitatively study the inner regions and total composition of core collapse supernovae in a self-consistent fashion — a prohibition in the thermal bomb or piston mechanisms.

In order to enhance the self-consistency of these models, a powerful supplement would be to directly consider the impact on nucleosynthesis in multi-dimensional hydrodynamics of networks larger than the canonical 14-species alpha-chains. Still, alpha-networks continue to be the mainstay (due to computational restraints). The aspherical models of Nagataki et al. (1998b) and Maeda et al. (2002) show a larger fraction of the ejecta experiencing α-rich freeze-out than their spherical equivalent, but they do not evolve the composition within the hydrodynamic simulations. Kifonidis et al. (2003) were the first to consider the effects on the nucleosynthesis of the multi-dimensional neutrino-driven convective overturn in the core, and, by abandoning the use of a thermal bomb or piston, they improved the fidelity of shock revival by using an adjustable neutrino "lightbulb", effectively making the shock revival neutrino-driven. By tracking the neutronization and using parameterized neutrino luminosities and spectra, coupled to an alpha-network, Kifonidis et al. (2003) showed higher ejecta velocities for heavy elements like ^{56}Ni than previous models (Hachisu et al., 1990; Müller et al., 1991; Herant & Benz, 1991). Unfortunately, the simulations of Kifonidis et al. (2003) seem to over-produce the neutron-rich iron group elements based on predictions of galactic chemical evolutions (Hammer et al., 2010), perhaps a result of their grey neutrino transport.

Prior to the use of multi-group flux limited diffusion, grey transport multi-dimensional simulations fell well outside the neutronization limits required to produce ejecta that match galactic chemical evolution calculations and relatively neutron-poor terrestrial iron and neighboring elements (Trimble, 1991), and modelers were forced to invoke the fallback of matter onto the neutron star to account for the discrepancy (Herant et al., 1994; Janka & Müller, 1996). Fortunately, recent neutrino powered explosions using multi-group transport show a decrease in neutronization. Pruet et al. (2005) and Fröhlich et al. (2006a) showed the nucleosynthesis products from models incorporating multi-group transport were qualitatively different from both of the parameterized nucleosynthesis models (thermal bombs and pistons) and the grey transport models.

Their studies of the inner-most layers of core-collapse supernovae reveal that neutrino interactions strongly influence the electron fraction, which plays a dominate role in the nucleosynthesis within the iron-peak species. Fröhlich et al. show that the innermost ejected layers are made proton-rich ($Y_e > 0.5$) by neutrino interactions resulting in SN ejecta that agrees much better with the abundance constraints from galactic evolution and solar abundances. This finding is at odds with the prediction of previous models, all of which neglect this important piece of physics. The decreased neutronization removes the overproduction of neutron-rich iron and nickel isotopes commonly seen in parameterized bomb and piston models (Woosley & Weaver, 1995; Thielemann et al., 1996). The simulations of Pruet et al. and Frölich et al. also show enhanced production of Sc, Cu, and Zn, elements which observations of metal-poor stars (see, Cayrel et al. (2004); Gratton & Sneden (1991)) suggest are $3 - 10$ times more abundant than previous models predicted. Finally, a significant neutrino driven flow to proton-rich nuclei above $A > 64$ is seen, suggesting that the innermost ejecta of core-collapse supernovae may be the production site of the light p-process nuclei (Fröhlich et al., 2006b). Neutrino captures by protons generates a small abundance of neutrons, which, via (n,p) reactions that accelerate slow beta-decays, may potentially explain the existence of elements like strontium in otherwise metal-poor stars (Fröhlich et al., 2006b). These investigations further promote the importance of multi-dimensional effects and neutrino interactions.

For our part, we are motivated to drive numerical simulations of nucleosynthesis results towards direct observational constraints, and we seek to extend existing supernova models to examine their nucleosynthesis in a self-consistent fashion. By accurately modeling the observed ejecta, we intend to understand the conditions deep in the interior of supernovae and how these conditions lead to the elements that make up ourselves and our world.

In order to reduce computational costs due to calculations of nuclear reactions, many models (for example, Marek et al. (2008)) use a simple "flashing" scheme where "oxygen" is converted to "silicon" and then "silicon" is instantly converted into "nickel" in NSE conditions when a zone reaches parameterized critical temperatures. More sophisticated models link 14 alpha-special in a network from ^{4}He to ^{60}Zn. The flashing approach is certainly a poor approximation and, unfortunately, even alpha-networks are only useful for acquiring general properties of a supernova explosion (Timmes et al., 2000). An alpha-network does not include the effects that electrons and neutrinos have on neutronization (Hix & Thielemann, 1996), so they can only provide appropriate burning timescales and cannot resolve the detailed supernova nucleosynthesis required to match the observations of astronomical and terrestrial compositions. Detailed nucleosynthesis modeling generates reliable thermonuclear energy generation rates and produces detailed evolution of abundances (Hix & Thielemann, 1995), however it requires evolving a minimum of 150 nuclear isotopes and thousands of reactions during the most computationally expensive burning phases. As I will show, a simple replacement of the 14-species network with 150 isotopes in the fully-implicit backward-Euler integration scheme represents a several hundred-fold increase in the computational cost of the reaction network.

4.1 Extending Thermonuclear Reaction Networks Towards Realism

In attempting to understand and simulate the mechanism of supernova explosions, comparison of model calculations with observations often relies upon detailed knowledge of the abundances of nuclear species. In lieu of a larger, more realistic, yet computationally expensive, network, we are currently studying detailed nucleosynthesis of the ejecta by way of post-processing. A fundamental limitation in post-processing nucleosynthesis (see Chapter 5.4) is the lack of feedback from energy generation rates, which in turn determines the thermodynamic evolution that drives further nucleosynthesis. By using post-processing methods, we are unable to follow the feedback these changes have on subsequent nuclear evolution as well as the encompassing hydrodynamic flows, leading to systematic differences in the final explosion products. Despite this, post-processing is the current standard for producing detailed nucleosynthesis results. Significant advancements are in sight as computational recourses continue to grow and better schemes are found to study the impact nucleosynthesis has on core-collapse models.

Pruet et al. (2005, 2006) and Fröhlich et al. (2006b) have studied the inner ejecta layers, showing that neutrino-powered explosions (using spectral neutrino transport) result in decreased neutronization, and that the electron fraction has a dominate effect on nucleosynthesis. Unfortunately, an alpha-network is unable to follow the proper neutronization as can be seen in Figure 4.1, which demonstrates the alpha-network's inability to represent the full range of abundance values for the given temperature and density profile even though the Y_e is 0.5. Figure 4.1 contains the full abundance pattern of hundreds of nuclear species at a density of 6.272×10^5 g/cm^3 and a temperature of 4.706 GK during the post-processing network calculations. It is important to note that three of the four most abundant species in this figure — protons, ^{54}Fe, and ^{58}Ni — are not members of an alpha-network, which is represented by the alpha symbols along the diagonal. It is also clear that the alpha-network does not span the entire regime of interest, whereas a 150 isotope network (represented by the nuclei within the area surrounded by the white dashed line) is much more inclusive of the significant species and allows for the creation of more neutron-rich species.

The nearly prohibitive nature of accurately calculating complete and incomplete silicon burning comes from the large number of nuclear reactions involved. Therefore, for conditions not in NSE, it is standard in CHIMERA to use a 14-species alpha-network to evolve the composition. As detailed in Timmes & Woosley (2000), since the implicit solution of a nuclear reaction network is, at its heart, the solution of a matrix equation, the computational cost grows non-linearly with the number of nuclei included in the calculation. A simple replacement of the 14 species network with 150 isotopes in the fully-implicit backward-Euler integration scheme represents at least a hundred-fold increase in the computational cost.

Post-processing nucleosynthesis requires the temporal evolution of bulk matter quantities, which we currently provide using a tracer particle method (described in detail in Chapter 5). Although post-processing is a viable scheme, we can only obtain accurate nuclear kinetics by evolving a network that allows for realistic nuclear reactions within our simulation's thermodynamic environments. For this reason,

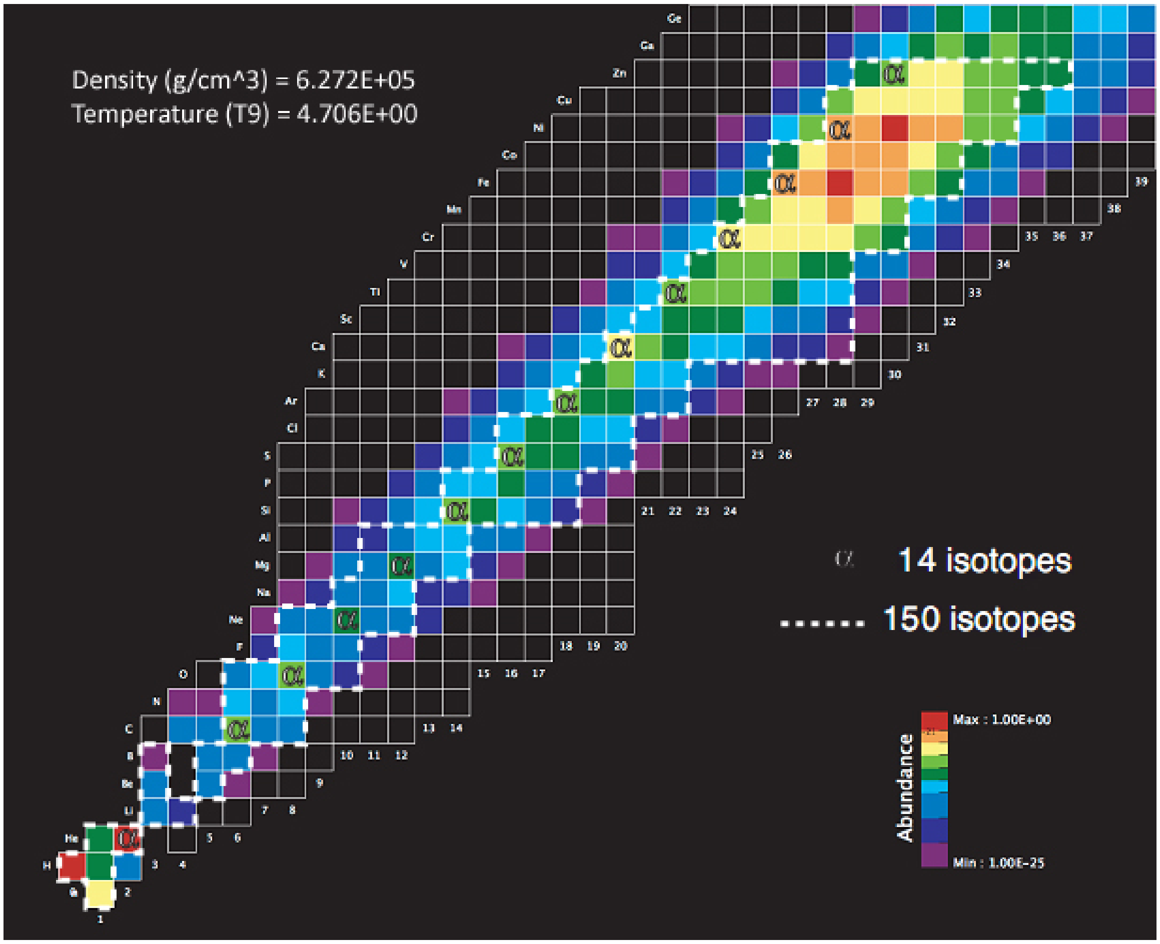

Figure 4.1: Mass Fractions during a post-processing nucleosynthesis calculation. It is important to note that the three most abundant species in this figure (Lingerfelt (2007)) — protons, ^{54}Fe, and ^{58}Ni — are not members of an alpha-network, which is represented by the alpha symbols along the diagonal. It is also clear that the alpha-network does not span the entire regime of interest, whereas a 150 isotope network (represented by the nuclei within the area surrounded by the white dashed line) is much more inclusive of the significant species and allows for the creation of more neutron-rich species.

we seek to overcome the need for post-processing by using a large network within CHIMERA. Canonically, for a iron core progenitor, a lower limit of roughly 150 species is required to satisfy this constraint (see Figure 4.1). Recent development has shown that up to 350 species may be required to accurately evolve an $8 - 10\ M_{\odot}$ ONeMg core model (see Chapter 6 and Figure 6.5). For these reasons, it is clear that an alpha-network does not provide sufficient realism within our runs and we must improve CHIMERA's link to its nuclear kinetic module, XNet, allowing it to handle a larger network capable of representing the majority of reactions involved. Until computational resources become unconstrained and large networks become a efficient standard practice, post-processing nucleosynthesis techniques, such as the ones outlined in this dissertation, will continue to be required for future, detailed investigations of non-energy generation phases like the r-process or p-process.

4.2 Results and Challenges of a Large Network

One major component of this thesis project was to improve CHIMERA's ability to handle a nuclear network larger than the canonical 14-species alpha-chain ("alpha-network") for the purpose of improving the nucleosynthesis and energy generation results. With an expanded network, our ultimate goal is to alleviate the need for post-processing results by solving comprehensive nuclear kinetics. Beyond producing more accurate compositions and energy-generation rates, a comprehensive network would facilitate the testing of post-processing approximations and help us understand the importance of mixing. To this end, we have successfully integrated a generalized nuclear network, which we have tested with 14, 16, 18, 20, and 150 species network. Below, I highlight the results of my simulation tests between an alpha-network and a 150-isotope network using the iron core $15M_{\odot}$ model of Woosley & Heger (2007) in spherical symmetry (1D).

Despite the failure of 1D core-collapse models are unable to explode, due to a lack of energy transfer through multi-dimensional effects, CHIMERA's large nuclear networks can still be tested for consistency and convergence since 1D models allows us to reach evolution times where nuclear burning becomes significant. As shown in Figure 4.2, I have evolved network tests for the 150-isotope run out to 490 ms from the start of collapse and correspondingly, an alpha-network to 600 ms (off the scale) from the start of collapse. By plotting the the evolution of the shock, the gain radius, and the boundary between the NSE and non-NSE regions, we can see that the models evolve in a very similar fashion, although very small differences are evident – this helps to insure errors in the network implementation do not cause the simulation to deviate in unexpected ways. The nuclear energy generation is not expected to have a "dramatic" global effect on the hydrodynamics during collapse, though it can play a role in the local environment and affect the ultimate fate of the star's composition.

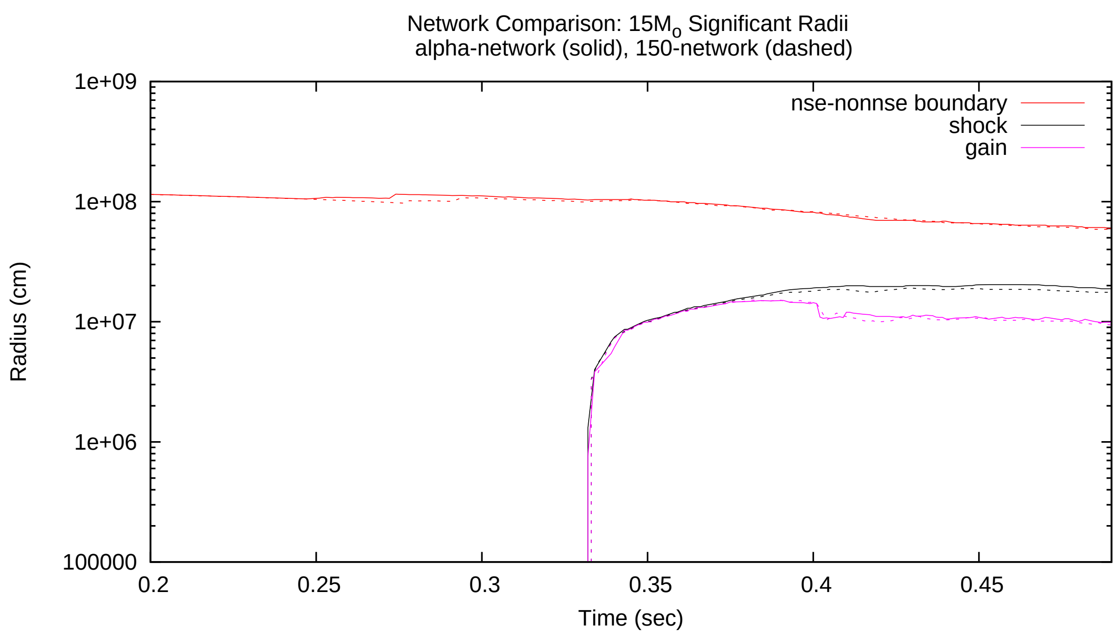

Figure 4.2: 1D testing of a 15 $M_\odot$ model using an alpha-network (solid) and a large-network (dashed). By showing the evolution of the shock, the non-NSE boundary, and the gain radius it can be seen that these changes between two networks does not severely change the evolution of significant radii of the models throughout their respective runs.

Figure 4.3 illustrates two 15 $M_\odot$ radial composition profiles of the nuclear species found in an alpha-network with compositions above 10^{-3} using an alpha-network (solid lines) and a large-network (dashed lines) within CHIMERA. While the alpha-network reproduces the general abundance patterns, there are many examples where it simply does not represent the composition accurately. More importantly, small changes in the co-evolution are evident. Since the only difference between the two runs is their nuclear reaction networks, our any change in hydrodynamic or thermodynamic profiles must be driven by deviations in their neutronization and nuclear energy generation rates. Figure 4.4 contains the composition of all species above a mass fraction of 10^{-2} for a 1D 15 $M_\odot$ model at 238 ms post-bounce of a run with a 150 species nuclear network. As an example in comparing the alpha-network to the large network, one can see that the abundance of ^{56}Ni in the alpha-nework from Figure 4.3 is more accurately represented by ^{54}Fe, ^{56}Ni, and ^{55}Co in the large network.

Our tests show the time required to run the 150-species network takes approximately 2.9 (44 hours/15 hours) times longer than evolving a 14-species alpha-network for the same number of cycles (see Figure 4.5). The total runtime is the wall-clock time required to evolve a designated simulation time. At a simulation time of ∼350 ms from collapse, the models have reached almost 100 ms post-bounce, and the shock is approaching the oxygen-rich portion of the progenitor. Our current runs show the alpha-network consumes approximately 5% of the total runtime; meaning the cost of the large, 150-isotope network is approximately 38.6 times more than an alpha-network — when extensive silicon and oxygen burning ensues in the shock, we expect this number to become moderately higher.

It is clear that our goal of implementing and running a 150 (or larger) isotope network is challenging to achieve, with current supercomputer architecture and limited allocation resources, unless other measures can be taken to improve the

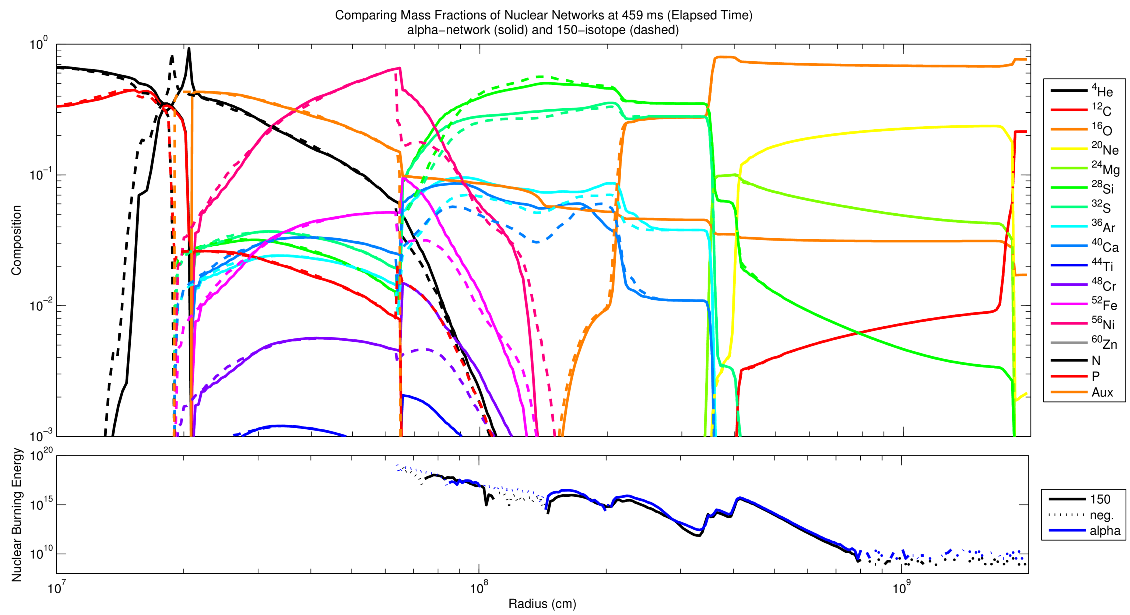

Figure 4.3: The composition of a 1D 15 $M_\odot$ model at 238 ms post-bounce for an alpha-network (solid) and a 150-isotope network (dashed). This radial composition profile example shows significant nuclear species highlighting the difference between the two networks. Most significant is the difference in abundances of ^{56}Ni between the two runs. The alpha-network is able to use components of the auxiliary ("aux") nucleus to artificially over-produce ^{56}Ni in lieu of non-alpha isotopes as can be seen in Figure 4.4

efficiency of our calculations. I have found that by utilizing a shared-memory parallel-programming API (application programming interface) called OpenMP, we can accelerate the time spent in solving the nuclear network calculations. Earlier tests with post-processing problems in XNet had indicated that by using 4-threads we could expect up to a factor of 3.5 improvement in the cost of nuclear burning times. But as shown in Figure 4.6, by utilizing the Cray's node architecture, where each physical node is organized into two 8-core non-uniform memory access (NUMA) nodes, and spreading the OpenMP threads across NUMA domains, we can obtain performance improvements in accessing memory. In Figure 4.6, we can see that by utilizing both NUMA domains, on each node, using 4- and 8-threads can drive the cost below 10%

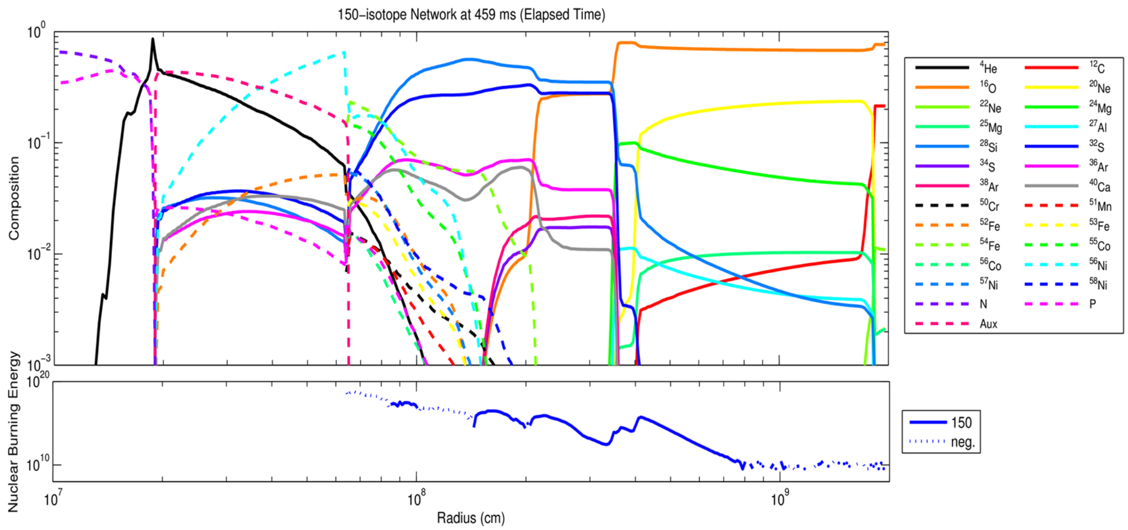

Figure 4.4: The composition of species above a mass fraction of 10^{-2} for a 1D 15 $M_\odot$ model at 238 ms post-bounce of a run with a 150 species nuclear network. As an example in comparing the alpha-network to the large network, one can see that the abundance of ^{56}Ni in the alpha-nework from Figure 4.3 is more accurately represented by ^{54}Fe, ^{56}Ni, and ^{55}Co in the large network.

of the 1-threaded run, which represents a factor of approximately 6.4 in network cost, which translates to an decrease in total wallclock by a factor of approximately 2 over the 1-threaded run (see Appendix 7). Although this improvement would seemingly remove the computational cost of a large network, when nuclear calculations are not being performed, we still incur the cost of the processors (i.e. computational time), meaning this scheme is still not affordable until a larger portion of CHIMERA utilizes OpenMP.

Given that our current 2D alpha-network runs take approximately 4 to 12 months to run to completion, using a larger 150-sotope network would require approximately 12 to 36 months to evolve. Although creating these simulations would not be an insurmountable task, it certainly does not facilitate a practical timetable for obtaining for creating useful science. If no other options were available, we would undertake this task as a milestone production run, but, as will be discussed in Section 4.2, we

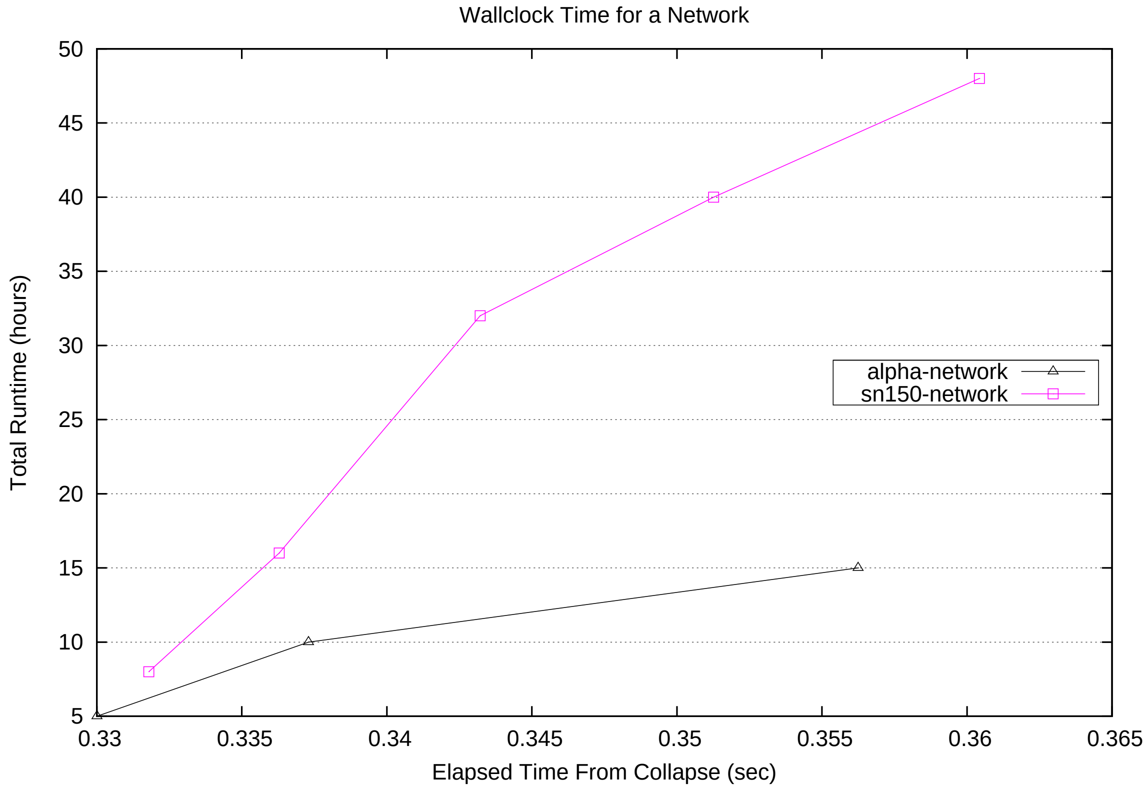

Figure 4.5: The timing difference between a small and large nuclear network. The large network takes approximately three times longer than the alpha network run to reach the same point of total elapsed time of approximately 350 ms from collapse (~ 100 ms post-bounce).

are working on utilizing better physics approximations (QSE conditions), modern supercomputer architecture (memory and cpu distributions), very modern hardware (GPUs), and software (OpenMP) to improve the cost of calculating realistic networks within our code. All of this work builds upon the use of a larger network in CHIMERA, which, as has already been described, I have implemented as part of this thesis.

By taking advantage of the physical conditions of QSE, nuclear burning can utilize an effective reduction of the number of reactions required to accurately solve the nuclear calculations. During silicon burning, nuclear evolution is dominated by large groups of nuclei in mutual chemical equilibrium — a condition referred to as quasi-statistical equilibrium (QSE), which is a precursor to global nuclear statistical equilibrium (NSE), where the entire chain of light to heavy isotopes, again through mutual chemical equilibrium, are created (by way of nuclear reactions) and destroyed (by way of photo-disintegration). In CHIMERA, the transition to NSE occurs when temperatures are in excess of 5.5 GK. An adaptive QSE-network has been developed in-house (Parete-Koon et al., 2008) and will be installed within CHIMERA in the forthcoming years to accelerate nuclear burning at temperatures just below the NSE threshold.

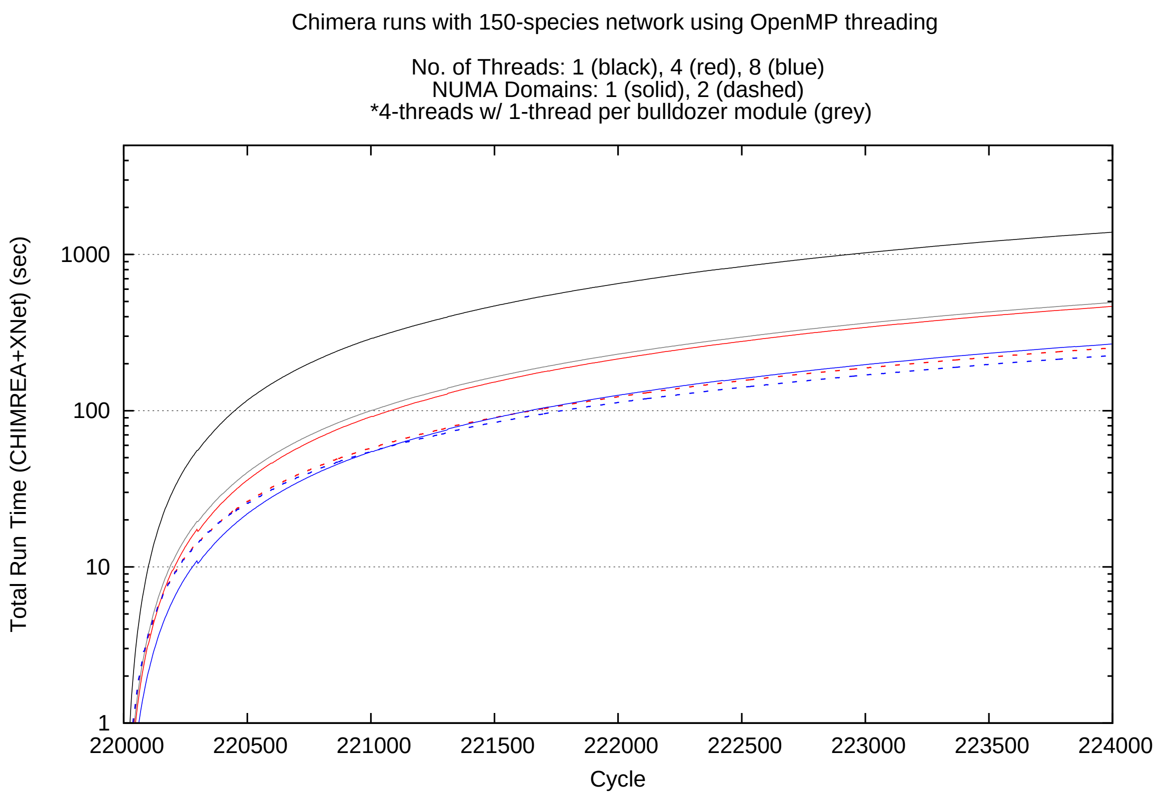

Figure 4.6: The growth in total runtime of a large network within CHIMERA using OpenMP. Although using 8-threads is faster than using 4-threads, we see the execution time depends strongly on how fast we can get operands from memory by distributing the threads across paired compute nodes, which have shared-access to memory. The trend of these values comes from the growth of the runtime.

Now that CHIMERA can handle any generalized network from XNet, our simulations can include many of the reaction channels that were prohibited from playing a role in the production of iron while using an alpha-network (Hix & Thielemann, 1996). More work is needed towards reducing the time required to evolve advanced networks into a manageable time frames. The best candidate for this improvement is also the most expensive constraint: silicon burning, which is responsible for the production of a wide range of nuclei with atomic numbers from 28 to 70. With this proof-of-principle now complete for the generalized network, we are able to begin expanding CHIMERA towards exploring the evolution of progenitor stars outside of our group's canonical $12 - 25\ M_{\odot}$ regime.

The CHIMERA team continues to improve supernova simulations with ongoing developments. While the νp-process cannot be studied with an alpha-network alone, I describe our initial studies of this process using a post-processing technique as described in Chapter 5.4. Although our current simulations are already fully self-consistent, the use of a more complete nuclear network will further improve the realism of our simulations and improve out understanding of the supernovae explosion.

Chapter 5

The Passive Tracer Particle Method

With unlimited computation resources, supernovae models would include all necessary physical processes required to obtain realistic radiation hydrodynamics simulations with realistic nuclear kinetics included. We are, however, limited by reality; the desire for a finite graduate student tenure, and current high performance computational architectures, which force us to adopt more limited approximations. Experience has taught us that by reducing the nuclear network to a chain of 14-alpha species, the computational cost can be greatly reduced while maintaining a useful level of adequate realism. Unfortunately, adequacy for explosions is not the same as adequacy for producing the full range of CCSNe observables, which requires a minimum of several hundred nuclear flux channels for isotope productions — of which a 14-species alpha-network is simply incomplete.

When using a limited network, within a simulation, the best means of probing more complete nucleosynthesis is through post-processing Lagragian tracer particles (also known as “tracers” or “particles”) that follow parcels of matter through a hydrodynamic flow. CHIMERA uses a passive tracer particle method, whose architecture within CHIMERA was developed by Lee (2008). This chapter focuses on my use of these tracers to produce thermodynamic profiles (for post-processing); my development of particle analysis tools; my preliminary, proof-of-principle post-processing results from our 2009 2D-CHIMERA simulations; and the status of our state-of-the-art 2012 simulations (also in 2D) — for which our particle analysis tools will be begin to produce a plethora of scientific results.

Our implementation of tracer particles is motivated by the the griding technique of CHIMERA and the dimensionality of our runs. In the context of calculating nuclear burning within a supernovae's hydrodynamic flow, a choice must be made for the type of grid one will use to reference events. The obvious choice would seem to be an Eulerian grid based on fixed points in space from which positions and velocities could be references. However, an Eulerian grid struggles to follow the temporal evolution of individual parcels of matter as hydrodynamic flows become increasingly complex and diverge from an initial symmetric configuration. If one chooses to focus on the behavior of a parcel of mass, one can choose a Lagrangian grid, which is based relative to the mass itself. Such Lagrangian schemes are commonly used in spherically symmetric simulations, which simplify the differential equations. The Lagrangian scheme is not without its shortcomings as it quickly becomes tangled in the multi-dimensional, hydrodynamic flow. For this reason, Eulerian schemes are generally used in multi-D simulations. To recover the advantages of a Lagrangian scheme of matter, computational physicists have introduced the *tracer (or test) particle method* (TPM)*.

*There are other Lagrangian schemes that use particles to evolve state of the fluid, for example smooth particle hydrodynamics (SPH). Lagrangian tracers passively advect with the fluid while recording environmental conditions.

Other computational groups have used tracer particles for post-processing nucleosynthesis calculations in core-collapse supernovae (see Nagataki et al., 1998a; Pruet et al., 2005), in simulations of Type-Ia SN (Travaglio et al., 2004), to study Hypernova and Gamma ray bursts (Nagataki et al., 2006), to study the mixing in core-collapse SN (Nagataki, 1999), and to investigate turbulent mixing in the interstellar medium (Federrath et al., 2008).

By using massless tracer particles, we can perform a bounding study of the evolution of the nucleosyntheis in a model by comparing the outcome of the particles post-processed results (from an alpha-network run) to that of a run with a large network in-situ (see Chapter 4.1). By the nature of their implementation, tracer particles underestimate small-scale diffusive fluid mixing whereas CHIMERA tends to over-estimate this property by mixing at the scale of the grid. Additionally, only by comparing the results of the tracer analysis to that of a large network can we determine their true accuracy and usefulness with respect to the cost of their implementation in limited network simulation.

5.1 Tracer Particle Analysis

To obtain a representative picture of our simulations, we initially distribute tracer particles uniformly in mass within the outer iron-core and the silicon and oxygen layers of the model, which are regions expected to be ejected. Our tracer particles record time dependent thermodynamic, hydrodynamic, gravitational energy, nuclear binding energy, and neutrino energy deposition rates and neutrino flux quantities for the parcels of matter throughout the evolution of our supernovae simulations. Depending on the size of the progenitor and the dimensionality of the simulation, we distribute several thousand tracer particles in 2D and hundreds of thousands in 3D.

If we were to record the tracer particle data for each cycle, this would produce a data density far exceeding our ability to store on the supercomputer file systems as well our requirements for analysis. I have determined a representative picture can be built by limiting the output tracer data to whenever there is a 1% change in either density or neutrino flux or a 0.1% change in temperature for a given tracer. Even at these rates, a run containing 8,000 tracers, evolved for 1284 ms from the start of collapse, produces approximately 400 GB of pre-processed data (consisting of neutrino fluxes, spectral energies values, and thermodynamic properties) in binary format. After down-sampling the data to a useful resolution in time and calculating characteristic neutrino temperatures from the recorded spectra, we are left with approximately 47 GB that will be used for post-processing nucleosynthesis. Since the tracer's physical movement causes it to move from processor to processor during the simulation decomposition of each tracer particle must be represented by an individual file. For these reasons, careful and proper data management, efficient processing, and long-term storage must be considered.

5.2 The Tracer Particle Reader

The thermodynamic profiles are generated by CHIMERA with one binary data file per tracer, which contains undigested temporal data from an individual run. To handle the tracer particle processing and data management, I have developed a *tracer particle reader* (TPR) to (1) read in the binary tracer files generated by CHIMERA; (2) digest and pre-process the data – including handling CHIMERA restarts, which may include "rewinding" the data; (3) perform the automated analysis of CHIMERA data not necessarily associated with nucleosynthesis; and (4) organize the particle information into suitable formats for post-processing nucleosynthesis by the general purpose nuclear kinetic solver XNet. These profiles are then fed into a stand-alone version of XNet that then calculates the nuclear kinetics, using roughly one thousand of nuclear species, from the thermodynamic tracer profiles. This provides detailed abundance histories and more accurate nuclear burning energies than what CHIMERA is capable of producing with a limited alpha-network. Results can be tested against CHIMERA's alpha-network to gauge the level of importance of this energy generation.

As development on CHIMERA has progressed, the tracer reader was required to handle a large number of particles (between 4000 and 8000 individual files), spread across many folders, whose data needed to be accepted or rejecting based on CHIMERA's run time and restarts epochs.

Although our tracer particles were primarily developed to perform post-processing nucleosynthesis calculations, they have been useful tools to search for possible code problems manifested in physical quantities during code development and throughout production runs. We use the tracer particles to explore multi-dimensional effects that stem from anisotropies, instabilities, and fluid mixing. We have also found them invaluable in checking the consistency of our models throughout code development. The tracer particle reader performs many service tasks such as finding bad tracers (tracers whose data may have become corrupt due to I/O or file system issues), and hunting down tracers of particular interest. Without an effective data management tool, attempting to sort through more than 4000 (in 2D), much less the 100,000 or more we anticipate in 3D, individual files in search of a particular set of physical conditions would be a daunting task.

5.3 A Lagrangian Perspective

I will highlight some of the many ways of utilizing tracer particles as a tool to understand and interpret different models. Figure 5.1 provides a different perspective on multi-dimensionality and mixing issues. Here, seven tracer particles are shown from the same initial radius (approximately 2800 km), but different latitudes, having vastly different trajectories due to hydrodynamic flows; although none of the tracers are captured in this particular figure, three of these tracers are brought to within approximately within 60 km of the center of our grid near the PNS, while the others are deflected shortly after hitting the shock from above. This scenario would not be possible in one-dimensional models, which can not capture the complex, multi-dimensional behavior of the inner most supernova ejecta. As discussed in Chapter 3, multi-dimensional simulations are required for models to explode via the neutrino reheating mechanism and to explore the nucleosynthesis that results.

Figure 5.2 shows tracers superimposed on a colored entropy map in a simulation of a 15 $M_{\odot}$ progenitor at approximately 300 ms after core bounce. The tracers are shown with their color code indicating the amount of neutrino heating or cooling. The pattern of the tracers illustrates how in-falling matter is concentrated into low entropy down-flows towards the proto-neutron star. The neutrino heating occurs predominately in the inner 100 km, but the heated matter, with entrapped tracers, rises to form low density, high entropy, plumes which push the stalled shock outward. This layering of data illustrates how the correlation between two sets of information can be better understood. Though more poorly sampled than the Eulerian grid, the Lagrangian nature of the tracers provides a unique perspective, for example, in this case, highlighting convection (and neutrino-heating) of mass in the down-flows. This

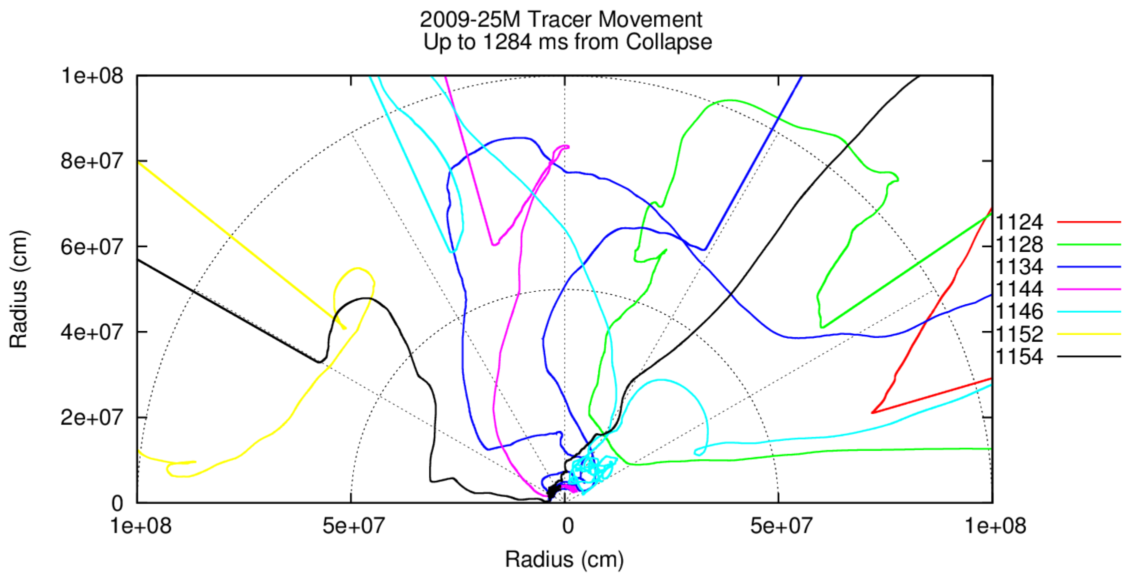

Figure 5.1: The time history of seven example tracers from an initial spherically symmetric distribution within our 25 $M_{\odot}$ run from 2009. Three of these tracers are brought to within 60 km of the center of our grid near the PNS, while the others are deflected shortly after hitting the shock from above.

type of display can also be an invaluable diagnostic tool, to obtain a more global picture of supernovae evolutions.

Prior to 2D models, simulations of the nucleosynthesis prescribed a “mass-cut” to differentiate matter destined to become part of the PNS from ejecta. Non-spherical models, by definition, are not defined by a single radial-ray between the inner core and outer envelope. Thus, the parameterized nature of 1D models limit the scope with which the physical realism of simulations could be analyzed. The tracer particles enable the exploration of issues pertinent to multi-dimensional models. For example, Figure 5.3 shows the location of tracers at $\sim$ 1000 ms post-bounce for the 25 $M_{\odot}$ simulation. The color coding of the tracers indicates the layer in the progenitor from which that tracer originated. The presence of several red-colored tracers, which originated in the inner part of the silicon layer, illustrates that the “mass-cut” of spherically symmetric models is really a misnomer. This figure also

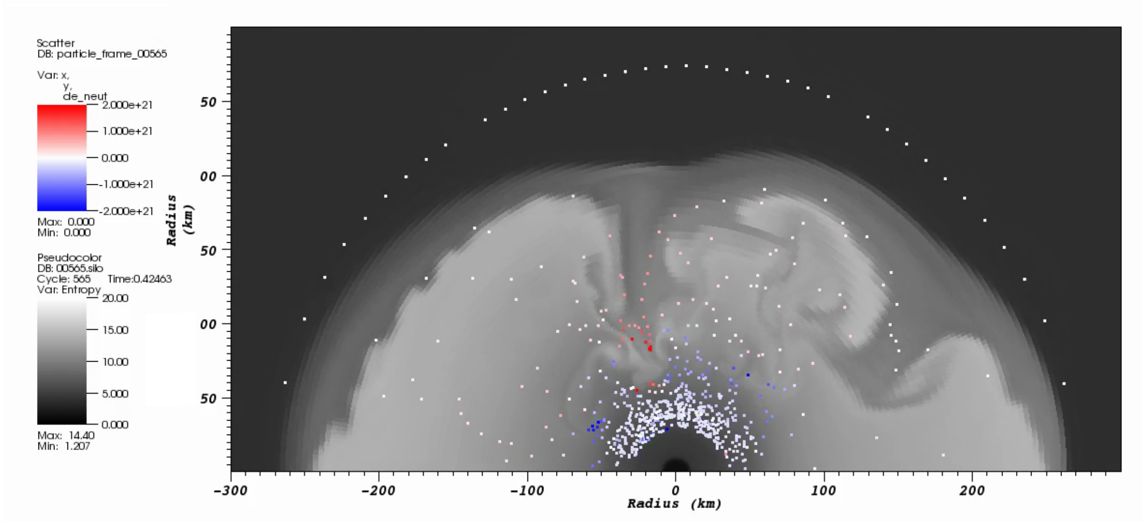

Figure 5.2: Tracer particles plotted over an entropy grey-map. Here, the tracers are colored to represent the superposition of neutrino-heating. The pattern of the tracers illustrates how infalling matter is concentrated into the low entropy down-flows as it flows towards the proto-neutron star at 300 ms after bounce.

indicates the complexity of mixing in the ejecta relative to the initial composition distributions. While both CHIMERA's Eulerian grid and the tracer's movement can capture macroscopic mixing, CHIMERA overestimates microscopic mixing due to zone interpolation, while the tracers underestimate microscopic mixing because of their Lagrangian nature. Taking these limitations into consideration we can create bounds on the amount of mixing within a simulation. We hope to provide this as a tuning parameter, along with explosion energies and delay times, for future 1D parametrized runs.

In the context of tracer particle analysis and nucleosyntheis studies, I describe two suites of iron-core simulations that we, the CHIMERA team, have produced in the last several years; one was begun in 2009, and the other in 2012. The latter suite contains significant improvements in both code development and physical fidelity, which will be described in Section 5.5.

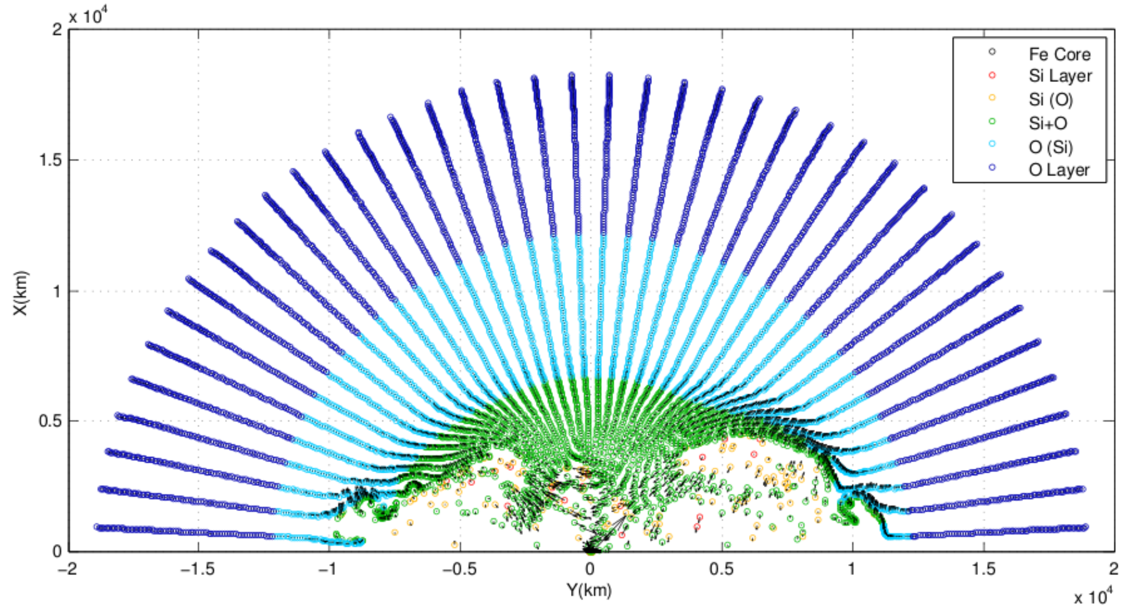

Figure 5.3: Tracer particles from a $25M_\odot$ model at $\sim$ 1000 ms post-bounce have diverged from initial spherical symmetry illustrating that the definition of a "mass-cut" is not well defined in multi-dimensions. This figure also indicates the complexity of mixing issues relative to the initial composition distributions.

5.4 CHIMERA's 2009 Simulations

To prepare for, and help expedite, the post-processing of the latest 2012 CHIMERA simulations (see Chapter 5.5), we have developed an analysis pipeline using the tracers from the CHIMERA-2009 models as a trial set. In early 2009, we had initiated from collapse a suite of four models based on the 12, 15, 20, and 25 $M_\odot$ progenitors of Woosley & Heger (2007). These simulations used a moving grid with 256 radial zones (covering 0 to 18000 km) $\times$ 256 latitudinal zones (representing 0 to 180°).

Unfortunately, due to issues with CHIMERA's development, these models exhibited various problems at later times such as issues at the shock boundary, spurious entropy generation in the inner most part of the core, and advection discontinuities between the NSE & non-NSE boundary. The most troubling of these issues was the mis-application of the "carbuncle" suppression algorithm in the shock.

The carbuncle, or odd-even decoupling instability, is unphysical systematic change in a hydrodynamic flow when shocks align with the dimensionally split numerical solutions (Quirk, 1994). The remedy for this is an application of diffusion along grid-aligned shocks. In CHIMERA-2009, over-zealous application of this diffusion distorted lateral shocks.

With the accumulation of so many uncertainties, the 2009 models were suspended in October of 2009 prior to completion, although we used their data to build the tools to be used later, these results were not published. We did publish results from a GW analysis of the first few hundred milliseconds after core bounce (see Section 5.6).

Nominally, a run can not be considered "complete" until there is a converged combination of explosion energy (approaching 1 Bethe†), and ejected mass. Although an explosion can not be definitely quantified, of these earlier models, the 25 $M_{\odot}$ (hereafter "2009-25M") was the most physically complete, having evolved the furthest – out to 1283.9 ms from the start of collapse with an explosion energy of just over 0.7 Bethe (B) (see Figure 5.4). Here, I present the results evolution of 2009-25M and the results of the post-processing nucleosynthesis for this model.

Of the CHIMERA-2009 suite of simulations, only the 25 $M_{\odot}$ model reached a post-bounce time of beyond 1000 ms. We distribute tracer particles uniformly in mass throughout the model in 200 rows of 40 tracers each down to the outer edges of the iron core. For the 25 $M_{\odot}$, this means the 8000 tracers, each consisting of $\sim$ 0.00034 $M_{\odot}$, make up $\sim$ 2.7480 $M_{\odot}$ of the total progenitor. I separated the tracers at the final epoch of the model's evolution into four categories: (1) "bound" (or to be bound), (2) "unbound" (projected to become ejecta), (3) "unknown" (primarily tracers in the low entropy downflows), and (4) "still in-falling" (i.e. material that is still above the maximum shock radius). I have determined that for 2009-25M at

† $1\,\mathrm{B} = 10^{51}$ ergs

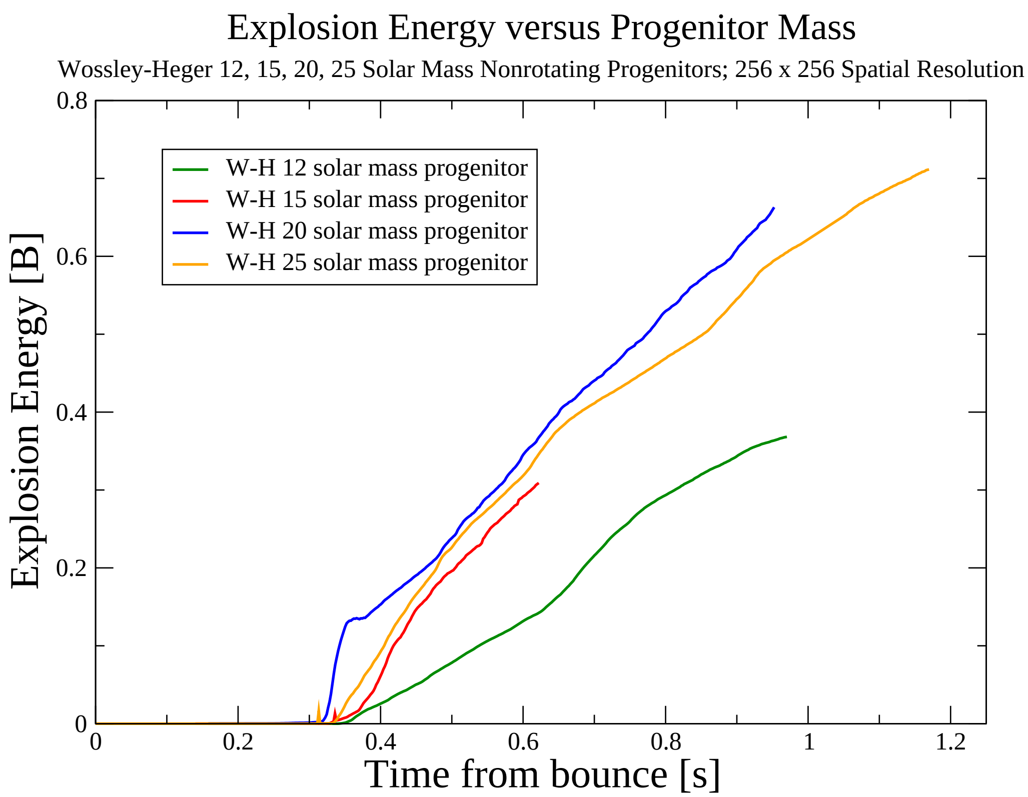

Figure 5.4: The explosion energy of the 2009 Chimera models at post-bounce times. Since the 25 $M_{\odot}$ was the most evolved, I used its data set as a test bed for building preliminary analysis tools. Completed SNe simulations are expected to have an explosion energy several hundred Bethes.

1283.9 ms elapsed-time out of the total 2.7480 $M_{\odot}$ that makes the total mass of the tracer particles, $\sim$0.8412 $M_{\odot}$ is explicitly bound, $\sim$1.6011 $M_{\odot}$ is still above the radius of the maximum shock, and $\sim$0.1999 $M_{\odot}$ has an undetermined fate as part of the low entropy down-flow, and $\sim$0.1055 $M_{\odot}$ is unbound. Clearly, the shock has not reached a radius suitable to perform complete ejected nucleosynthesis studies. This is a strong indication that the current 2012 runs will probably have to be evolved beyond the canonical epoch of 1000 ms if meaningful post-processed nucleosynthesis is to be produced.

Projections on whether a tracer will become ejecta or not can be inferred based on the final position, velocity, and environmental conditions of the 2009-25M data set. These projections will become increasing reliable as models proceed beyond 1000 ms. However, without fully completed explosions, predicting the precise final arrangement and heating condition for uncompleted models is difficult because the hydrodynamic flow is non-linear.

Although the rate of cooling (see Figure 5.7) is one means of determining which particles might become ejecta, the primary means is to calculate the ratio of a tracer's kinetic energy to gravitational binding energy (taking into consideration the vector of its velocity). This quantity is called "boundedness", which is given by, $x = \frac{v_r}{|v_r|}\frac{KE}{E_{Grav}}$. For this simple case, we ignore the later hydrodynamic behavior for the tracers that are unbound by the end of our simulation.

Using the criteria in Table 5.1, we have calculated the total mass contribution from each particle in 2009-25M to determine how much of the matter might become become part of the PNS ("bound") and the ejecta ("unbound"). At this stage in the CCSN simulation it is difficult to predict accurately the fate of the particles in the cold, low entropy down-flows, but these tracers can still be isolated by their total mass and labeled as "downflow". Finally, there are particles that have yet to cross the outward traveling shock ("Still in-falling"). Although many of these particles at this stage in 2009-25M will most likely become ejecta, and thus included in our calculation of nucleosynthesis, these particles have been separately identified for further analysis. The mass quantities and grouping of tracers can be seen in Figure 5.5. This analysis will be very useful after the completed explosion of the 2012 run. Figure 5.6 shows the distribution of tracer within the inner portion of 2009-25M differentiating which particles have become bound and which ones are believed would most likely become ejecta based on the criteria from Table 5.1. The simulations downflow and upflows can clearly be seen.

Table 5.1: Boundedness criterion for tracers particles

State	Bound Criterion $x = \frac{v_r}{\lvert v_r \rvert} \frac{KE}{E_{Grav}}$	Criterion Index
Bound	$\lvert x \rvert < 1$	1
Un-bound	$x > 1$	2
Downflow	$r < r_{shock-max}$ & $v_r < 0$	3
Still in-falling	$r > r_{shock-max}$	3

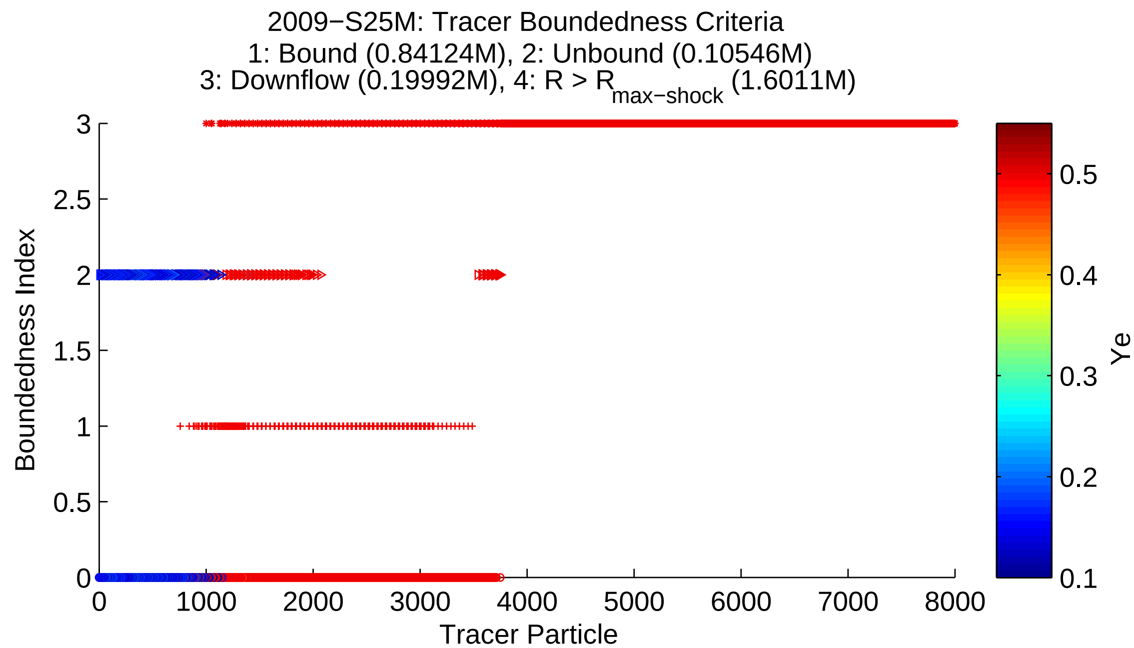

Figure 5.5: Using the data 2009-25M, the tracers are binned by their boundedness criteria, from Table 5.1, to obtain estimates of their distribution within the PNS, as ejecta, and the tracers whose fate cannot yet be determined.

As expected with the 2009-25M data set, the fate of much of the material (bound to the PNS or ejecta) is indeterminate at this stage in the simulation. The spacial distribution of species at this time is a proof-of-principle that will become extremely useful once the 2012 models are well into the ejecta phase of their explosions.

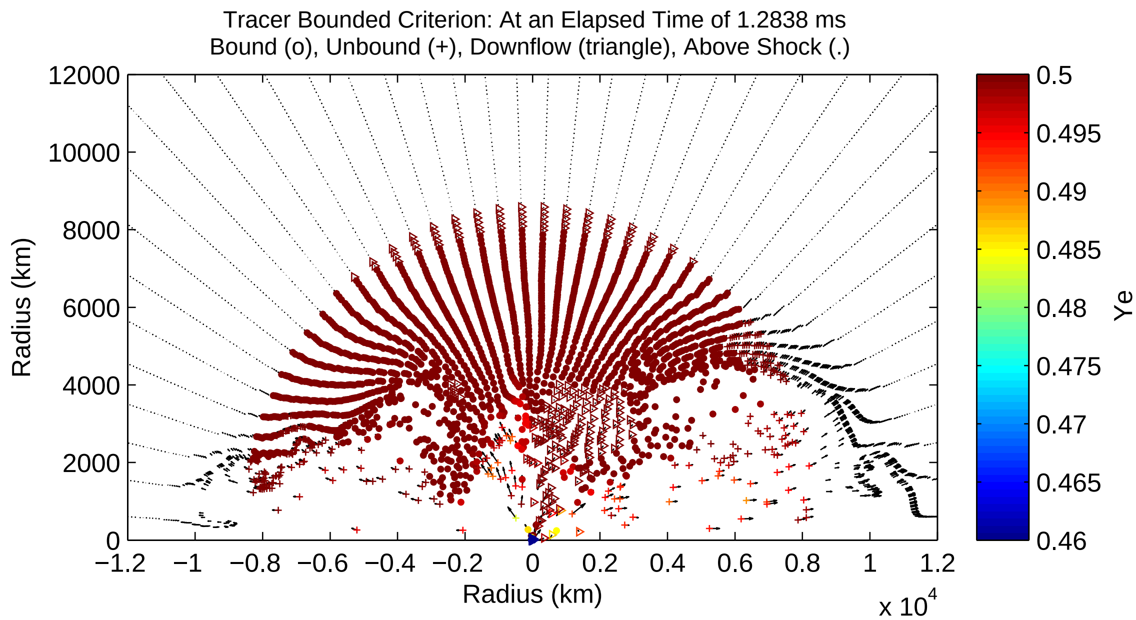

Figure 5.6: The final distribution of the tracers from 2009-25M binned by their boundedness criteria from Table 5.1. The velocity represented by arrows from each tracer to show the direction of their individual motion at 1.28 seconds. The tracers are also color coded by their Y_e values (see the color bar) to show we can use the neutronization levels for ejecta abundance calculations once the model is complete.

If accurate nuclesynthesis of supernovae is to be modeled, we must follow the evolution of the matter until it produces ejecta whose abundances patterns are no longer driven by the shock, but by freely expanding until freeze-out temperatures (generally around ~ 1 GK) are reached. Since the data from 2009-25M did not evolve to this epoch, I was required to extrapolate the data using expansion timescales calculated from the tracer's final trajectory. For tracers which are freely expanding, the resultant adiabatic expansion can be reliably extrapolated. I deemed the tracers that show no sign of such cooling patterns (a peak in temperature followed by a steady decline that was continuous at the end of the simulation) to be bound, but found a handful of examples of tracers whose temperature patterns could be reasonable extrapolated but were later determined to be bound. For these tracers, I built an iterative algorithm to smoothly extrapolate their cooling. Figure 5.7 is an example of a thermodynamic profile we used to performe post-processing nucleosynthesis with 1160 species. For this profile, Figure 5.8 displays the species with mass fractions above 10^{-4}. By mimicking adiabatic cooling through extrapolating the temperature to 1 GK, the abundance of ^{4}He is allowed to change by way of captures onto the iron-group isotopes, specifically, in this case, ^{58}Ni, ^{56}Ni, and ^{62}Zn.

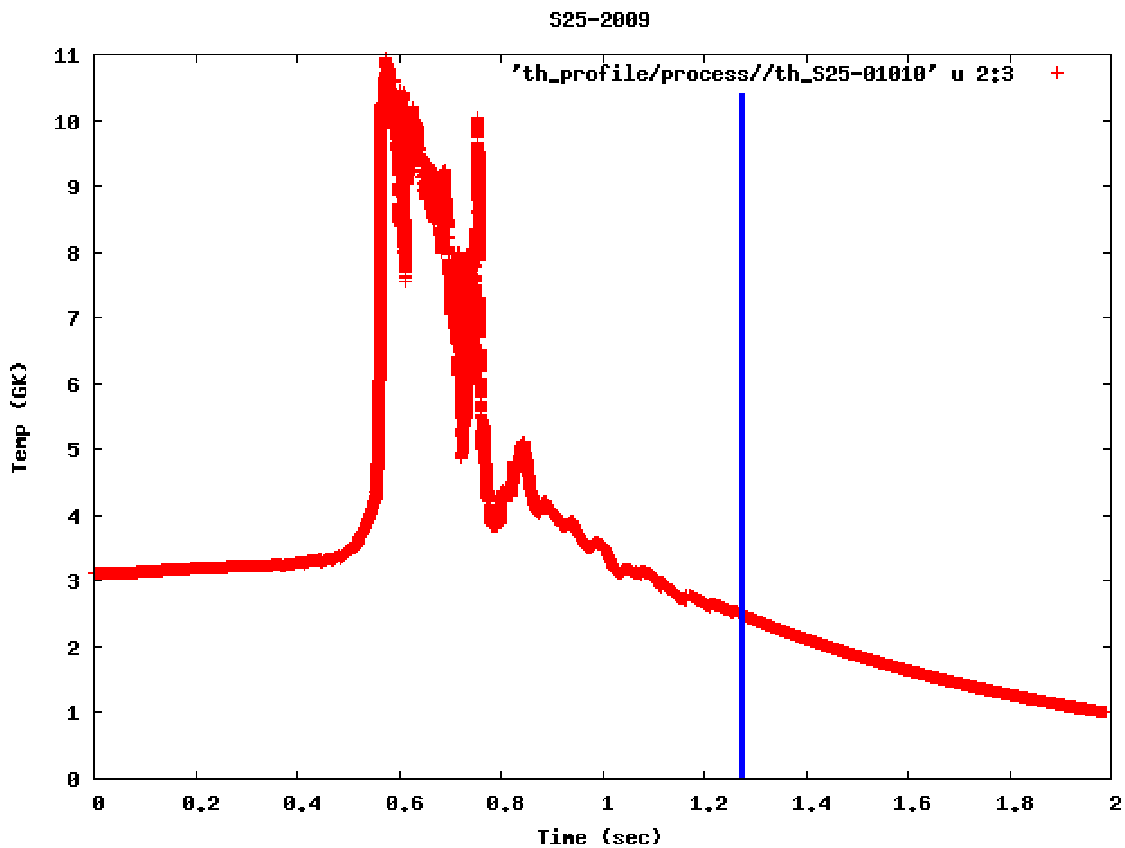

Figure 5.7: An example thermodynamic profile from tracer data as generated by CHIMERA from the 2009-25 $M_{\odot}$ model. Since the simulation did not evolve to completion, it was necessary to extrapolated the data to a temperature of 1 GK to simulate the adiabatic cooling towards freeze-out temperatures. The extrapolated data begins at the vertical blue line beyond ~ 1.28 sec. My algorithm does a fairy robust job of completing these profiles which enable the calculation of proper freeze-out conditions.

As an first attempt to use graphical processor units (GPUs) for improving the speed of nuclear calculations within a CHIMERA run, the nuclear kinetics calculation

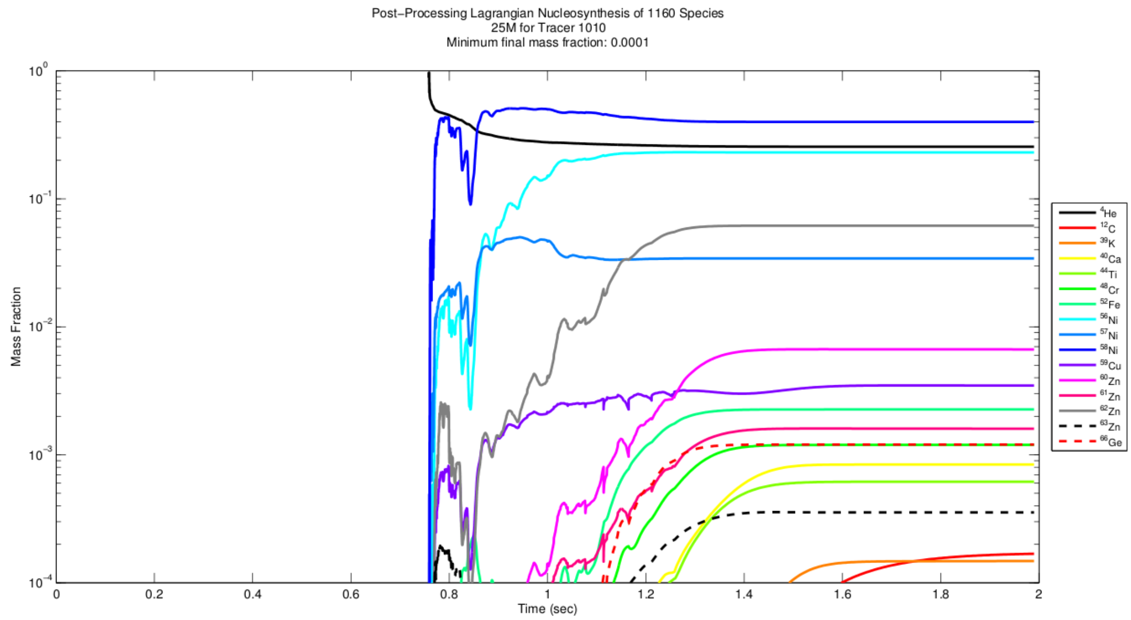

Figure 5.8: Detailed nucleosynthesis calculation for the thermodynamic profile of tracer particle 1010 from 2009-25M of species above a final mass fraction of 10^{-4}. The abundances only exist past $\sim 0.75\,\mathrm{sec}$ to match the extrapolated profile from Figure 5.7, where the tracer drops out of NSE and nucleosynthesis calculations with XNet begin.

was executed completely on an accelerator device with the intention of leaving the host CPU free to process hydrodynamics. The networks matrix inversion must be solved thousands of times, in the course of the iterative Backward Euler integration, to evolve the nuclear composition of each zone or particle. The matrix is of the same size as of the number of nuclear species. We garner science results from this effort by conducting this study as a means to also post process data from CHIMERA with a large nuclear reaction network designed to study the νp-process (Fröhlich et al., 2006). The resulting data was processed in a nuclear reaction network with 1160 species. Previous work indicated that networks with greater than 1000 species benefit from APIs, such as CULA and MAGMA, developed for enabling easy device accelerated matrix algebra. MPI was used to run hundreds of instances of the network simultaneously; each instance using the conditions given by one tracer particle. The networks central matrix was built on the host and but solved on the GPU device.

Here, I highlight our work investigating if the νp-process exists within my post-processing results from the 2009-25M data set. I have used the extrapolated thermodynamic profile of tracer particle number 759 as an example of a post-processing nucleosynthesis result (using 1160 species) to show the difference between considering and ignoring neutrino-nucleon reactions. Figure 5.9 shows these results, where the solid lines are from a calculation with neutrino-nucleon reactions included and the dashed lines are with these reactions ignored. The primary advantage of post-processing particle data with CHIMERA is the ability to use larger and more complete nuclear networks to determine compositional evolution. Upon the completion of the CHIMERA-2012 simulations, this analysis will be performed in detail for the early ejecta to determine the true impact of the νp-process at late times.

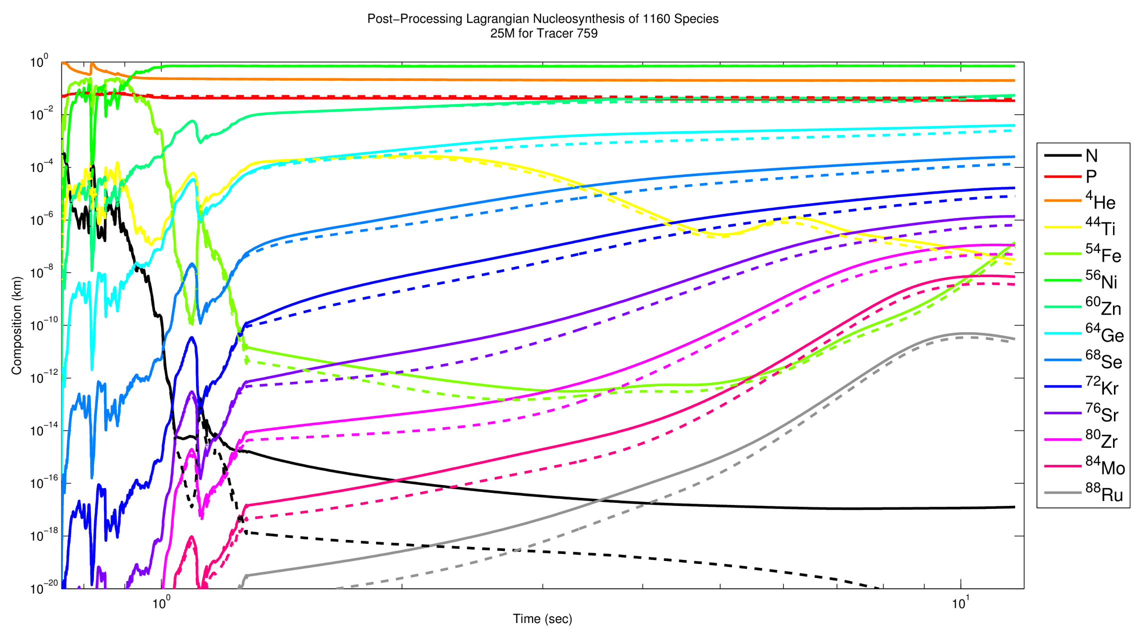

Figure 5.9: νp-process nucleosynthesis calculation for a tracer particle trajectory from an explosion simulation using the 25 $M_{\odot}$ progenitor of Woosley & Heger (2007). Shown are evolutions with neutrino-nucleus reactions included (solid) and ignored (dashed).

Using the many ways I have shown of looking at the tracer particles through temporal and spacial distributions, and most notably, my proof of principle results on advanced nucleosynthesis processing techniques, including my νp-process analysis, the CHIMERA team is well situated to produce unprecedented nucleosynthesis results from future CCSNe simulations.

5.5 CHIMERA's 2012 Simulations

In March of 2012, we re-initiated the 2D collapse of the 12, 15, 20, and 25 $M_{\odot}$ iron-core models based on the "WH07" progenitors of Woosley & Heger (2007). Figure 5.10 shows the density profile for each mass model, as well as two other models used by other groups. Using the latest version of CHIMERA, these simulations use a moving grid with 512 radial (covering 20000 km) by 256 angular, or latitudinal, zones (representing 0 to 180°). The runs also contain 4 neutrino flavors with 20 energy zones from 4 to 250 MeV. We use the Lattimer-Swesty EoS (Lattimer & Swesty, 1991) at high densities (K = 220 MeV) and highly modified BCK EoS (Baron et al., 1985) at lower densities. One significant improvement of CHIMERA-2012 over CHIMERA-2009 is the development of an additional simplified 17-species NSE network that operates for moderately neutronized material ($Y_e \geq 0.46$) to ease the transition of abundances between NSE and the thermonuclear nuclear network.

These models are presently running on Hopper, a supercomputer at the National Energy Research Scientific Computing Center (NERSC), and Kraken, a supercomputer at the National Institute of Computational Science (NICS). Hopper is currently processing the 12 $M_{\odot}$ and 25 $M_{\odot}$ models; and Kraken is currently processing the 15 $M_{\odot}$ and 20 $M_{\odot}$ models. These runs have taken 4-5 months of wall-clock time to evolve through core bounce to 300-500 ms post-bounce. Table 5.2 shows the current

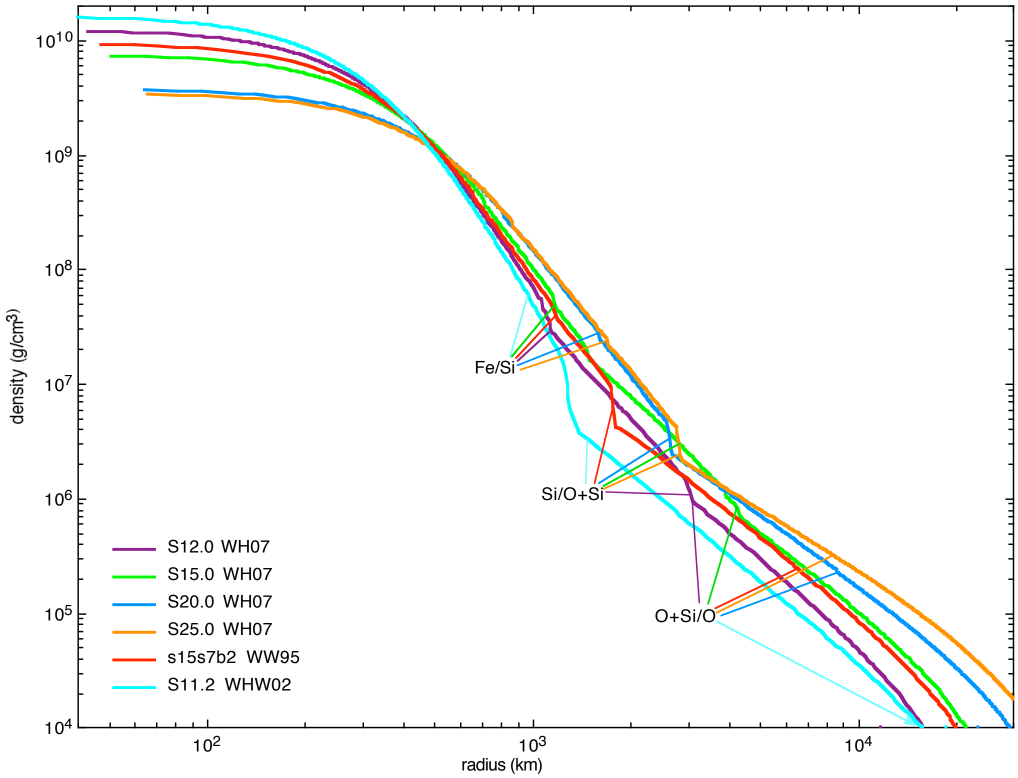

Figure 5.10: Density profile of iron-core progenitors of Woosley & Heger (2007). The CHIMERA team evolves the "WH07" progenitors.

post-bounce time and explosion energies for each mass model. Hopper is a Cray XE6 with a peak performance of 1.28 petaflops/sec, containing 153,216 processor cores, 212 TB of memory, and 2 petabytes of online disk storage. Kraken is a 1,030-teraflops Cray XT5 system containing 18,816 compute sockets (each with six cores), 147 terabytes of memory, and 3.3 petabytes of raw disk space.

As can be seen in the shock radii of each model in Figure 5.11 and in the entropy plots of Figures 5.12, 5.13, 5.14, and 5.15, these simulations have already broken spherical symmetry and progressed to post-bounce times between 271.6 and 533.0 ms as of July 27 2012. The 12 $M_{\odot}$ run (hereafter "2012-12M"), has evolved the furthest and is now showing signs of a growing explosion energy, starting somewhere

Table 5.2: Progenitor evolution data for the 2012 full-physics production runs. The 20, and 25 $M_\odot$ models have yet to have appreciable explosion energies, whereas the 12 and 15 $M_\odot$ are just beginning to produce an outward explosions.

Progenitor Mass ($M_\odot$)	**Post-Bounce Time (ms)**	**Explosion Energy (Bethe)**
12	533.0	0.03-0.16
15	338.6	0.01-0.04
20	277.6	N/A
25	350.4	N/A

between 280 ms and 310 ms post bounce (see Figure 5.16). The minimum explosion energy estimate is calculated using the sum of the gravitational, internal, and kinetic energies of the exploding zones, but with nuclear binding energy excluded. The larger explosion energy estimate includes the nuclear binding energy that might be released as the material expands and the nuclei recombine. To obtain the second estimate, all alpha particle nuclei are assumed to burn to ^{56}Ni, as would neutron and proton pairs, and the excess neutrons or protons being left over (though this is not accurate for left over neutrons), and the auxiliary nucleus would burn to ^{56}Fe.

As can be seen in Figure 5.11 (for the shock) and Figure 5.17 (for the composition), the shock of 2012-12M has progressed beyond a radius of 2000 km pushing through the silicon layer (green) and into the oxygen layer (light blue) where oxygen burning has ensued, at 3000 km, to create a mean nuclear mass of ~31 (possibly composed of light nuclei and isotopes of silicon, phosphorus, and sulfur). The 2D color plots used to show status of the 2012 models have been generated with the model plotting tool, Bellerophon[‡]. In Figure 5.12, large lobes of high-entropy neutrino heated gas are pushing the shock outwards in the polar regions, while two accretion funnels have developed in the equatorial region channeling lower-entropy newly-shocked material down into the gain layer to be heated via neutrino-nucleon reactions. The 15 $M_\odot$

[‡]Developed in-house by the CHIMERA team

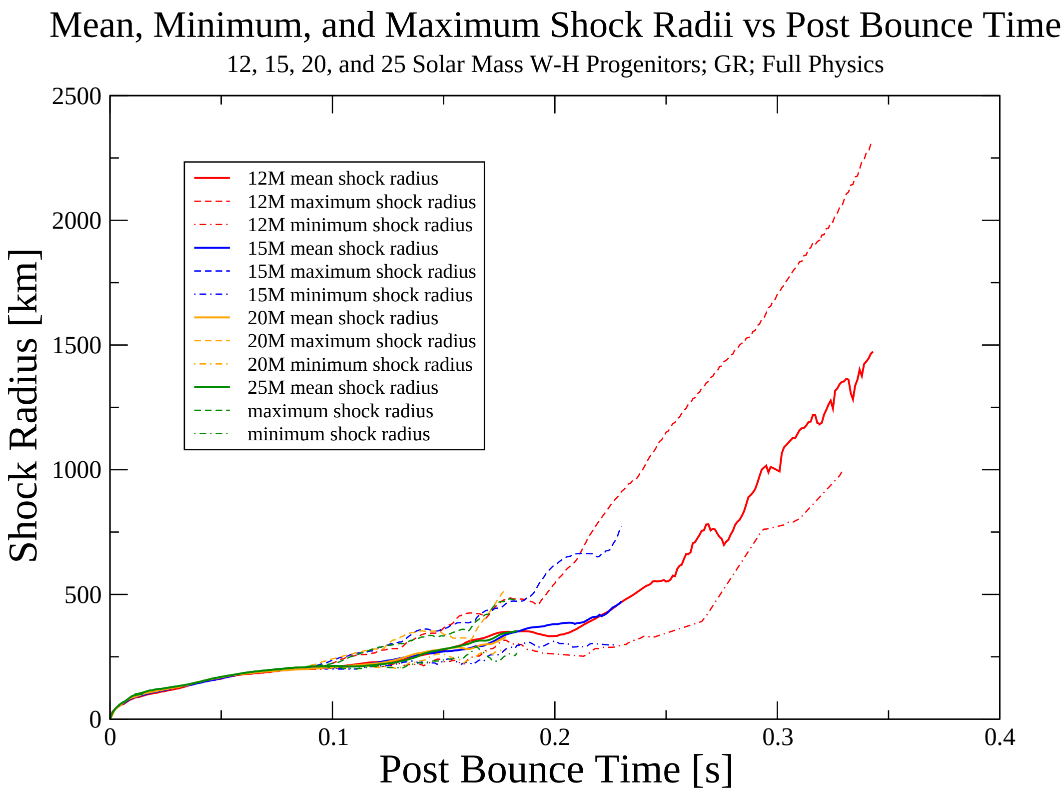

Figure 5.11: Shock radius vs post-bounce time for a suite of 2012 CHIMERA runs. The 12 $M_{\odot}$ has evolved the furthest whereas the 15, 20, and 25 $M_{\odot}$ lag behind. The shock, being non-spherical has minimum and maximum values.

model is just beginning to exhibit positive explosion energies. The other models, although progressing, have yet to show signs of explosions. They are still exhibiting non-spherical, post-bounce perturbations such as growing SASI features.

For insight into how the runs are progressing, Figure 5.18 shows the radial velocity of matter, where, interestingly, the down-flows appear to have been choked off at the surface of the shock – a feature we have not observed the 2009 runs. We will have to wait to see how the hydrodynamics respond as the run progresses. Upon processing the tracer files, this feature can be investigated using the tracer particles (i.e. their change in neutrino heating, entropies, and compositions) as they flow within this section of matter.

At their present evolution rates, the models will complete in the fall or winter (see Figure 5.19). Since the post-processing nucleosynthesis cannot be calculated until these models complete, the final analysis of our most recent models must wait until the end of 2012.

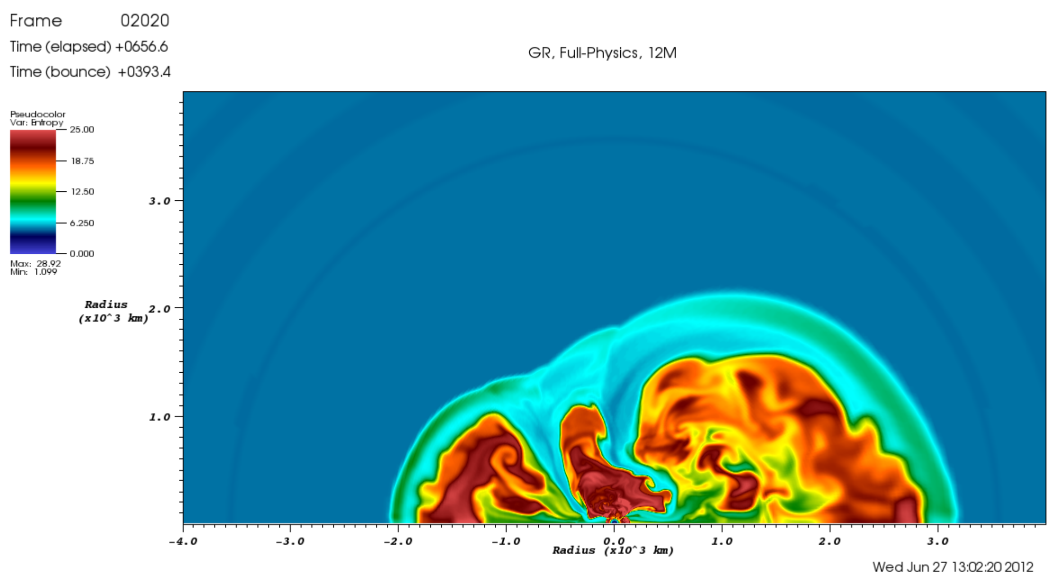

Figure 5.12: Snapshot of the entropy distribution for the 12 $M_{\odot}$ 2012 CHIMERA run.

5.6 Gravitational Waves From Tracer Data

This section describes a use of our tracer particles that goes far beyond their original intent as tools for post-processing nucleosynthesis. By following the Lagrangian trajectories, the tracer particles provide information on the movement of macroscopic quantities of matter. This allows us to use the tracer particle method to explore multi-dimensional effects, in general, that stem from anisotropies, instabilities, and

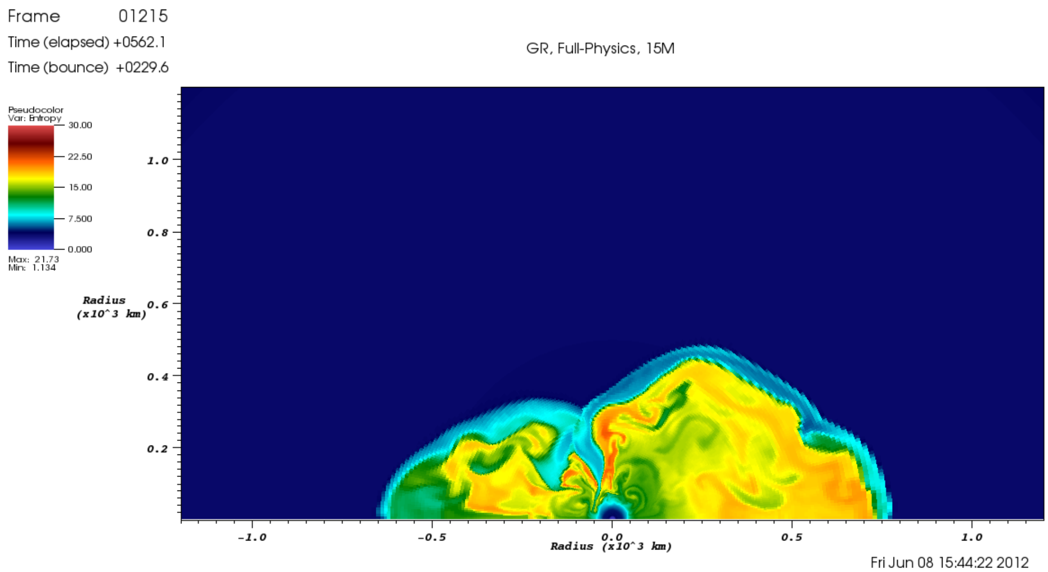

Figure 5.13: Snapshot of the entropy distribution for the 15 $M_{\odot}$ 2012 CHIMERA run.

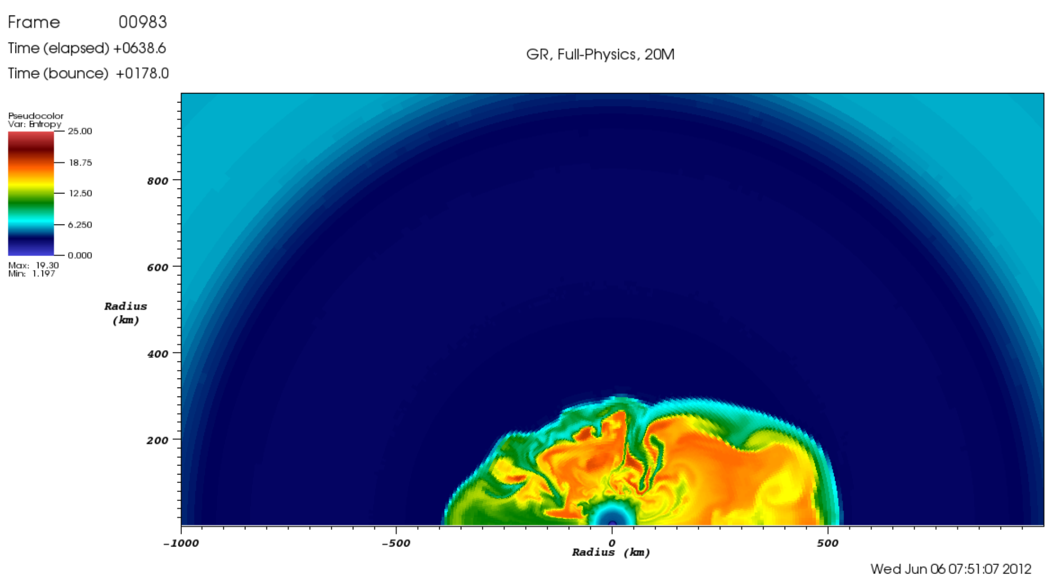

Figure 5.14: Snapshot of the entropy distribution for the 20 $M_{\odot}$ 2012 CHIMERA run.

fluid mixing. We have taken this concept further by using them to aid in the analysis of gravitational wave (GW) signatures from the 2009 2D iron-core supernovae models.

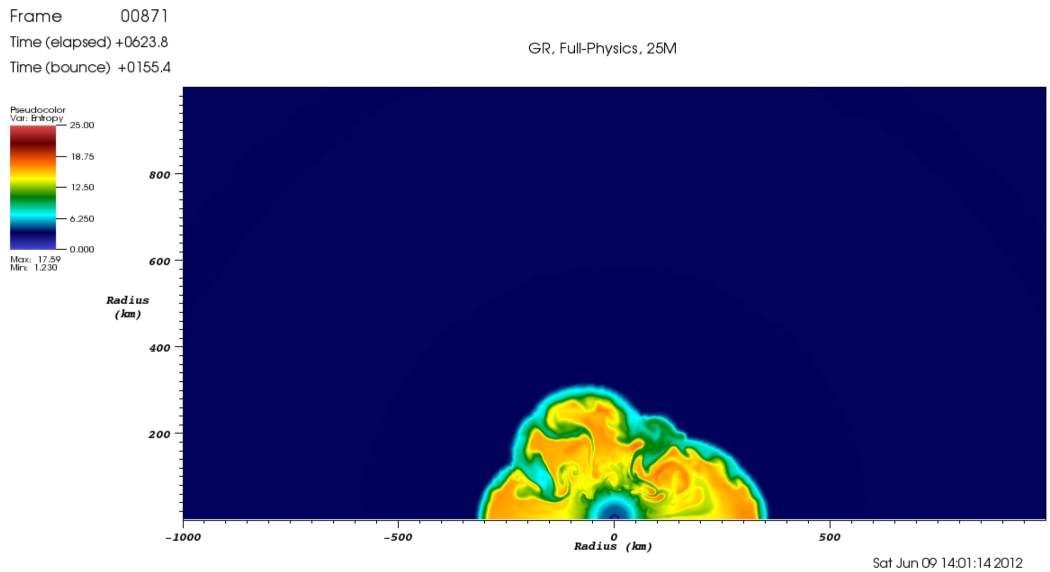

Figure 5.15: Snapshot of the entropy distribution for the 25 $M_{\odot}$ 2012 CHIMERA run.

In these models, each particle is assigned a constant mass spread evenly within the outer core and through the oxygen layer.

Comparing the GW signal corresponding to a given group of tracers with the signal produced by the bulk-matter motion (captured on the Eulerian grid) has allowed us to isolate a specific GW feature. By decomposing gravitational wave signal calculations we have identified an additional source of the prompt signal (previously attributed solely to prompt convection) due to the deflection of in-falling matter through the shock as can be seen in Figure 5.20 (left) (Yakunin et al., 2010a). The signal for our 15 $M_{\odot}$ run has been split into the contributions from the inner-core ($r < 30$ km) and outer-core ($r > 30$ km) regions (see Figure 5.21), but it is in the tracer analysis, shown in Figure 5.20 (right), where this becomes most evident. The matter-generated GW (solid red) is closely tracked by the GW generated by the infalling tracer particles deflected by the shock (dashed blue), some of which are shown in the left panel. Although the hydrodynamic resolution (256 radial and 256 angular zones) for this

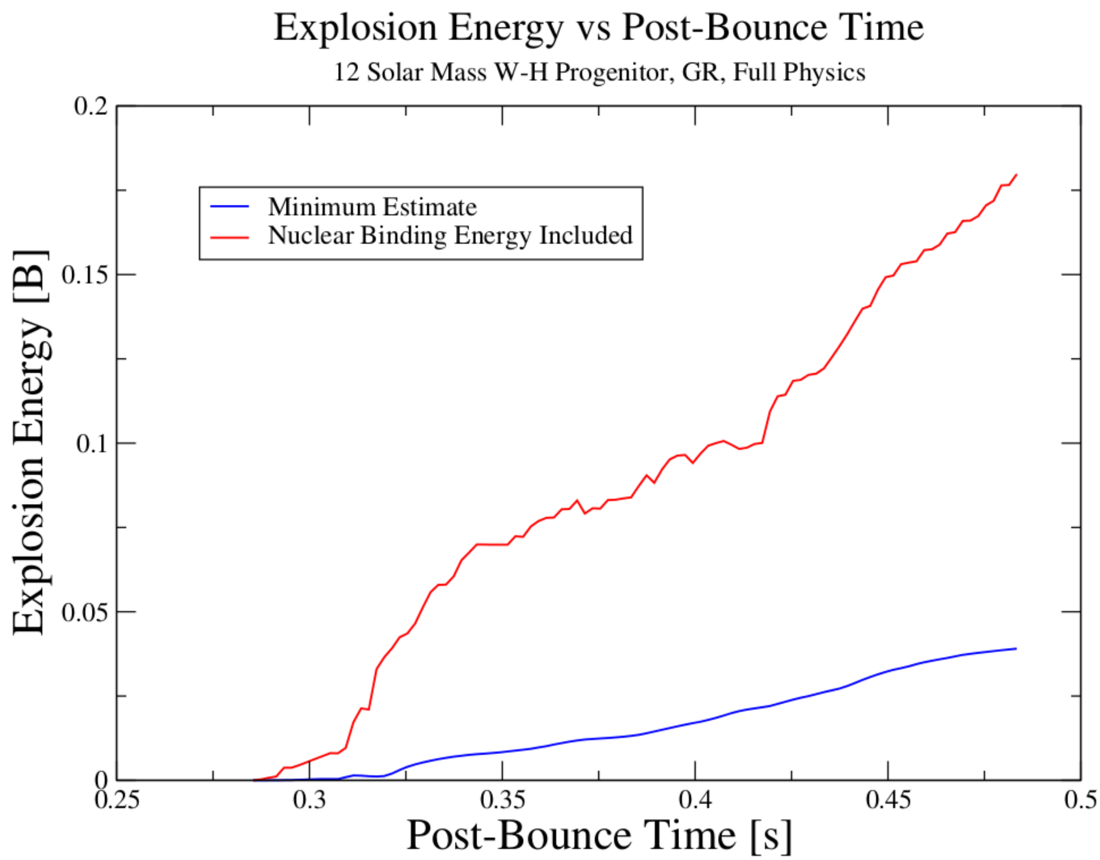

Figure 5.16: Explosion energy of 2012 CHIMERA runs. The 12 $M_\odot$ model is the only model which has begun to show positive explosion energies.

suite of runs was significantly finer than the tracer-matter resolution (40×125 tracers), we identified a low-frequency signal from 20 to 60 ms after bounce originating at the shock radius, which is at approximately 100 km at this time and well outside the PNS.

We have calculated the contribution to the signals produced by both baryonic matter motion and anisotropic neutrino emissions up to 530 ms after bounce for all four progenitors from the 2009 models. This analysis matches the predictions based on the parameterized models by Murphy et al. (2009). Given the development of non-parameterized explosions in these models, we were able to compute the waveforms

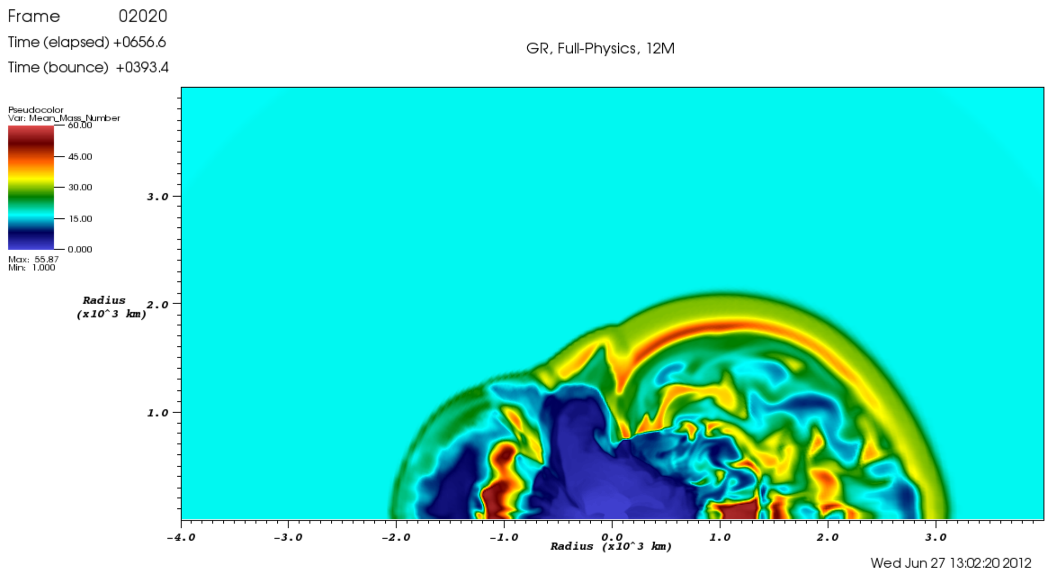

Figure 5.17: Snapshot of the $\bar{A}$ distribution for the 12 $M_{\odot}$ 2012 CHIMERA run. For example, in the oxygen burning region around 3000 km the mean nuclear mass is about 31, where it is possibly composed of light nuclei and isotopes of silicon, phosphorus, and sulfur.

through explosion and determine, with greater fidelity, the per-explosion amplitudes and timescales.

The results presented here are significant, but preliminary. As a more advanced "follow-up" study to our original gravitational waves investigation in Yakunin et al. (2010a), we are performing the GW analysis of the 2012 models, using both the hydrodynamic results and tracer particle data to investigate the GW signal at lower frequencies within post-bounce dynamics.

5.7 Conclusion on Tracer Particles

With their ability to help diagnose the physical fidelity of CHIMERA results such as hydrodynamic flows, their ability to investigate computational prescriptions such as mass mixing and the transcription of values between lateral zone crossings,

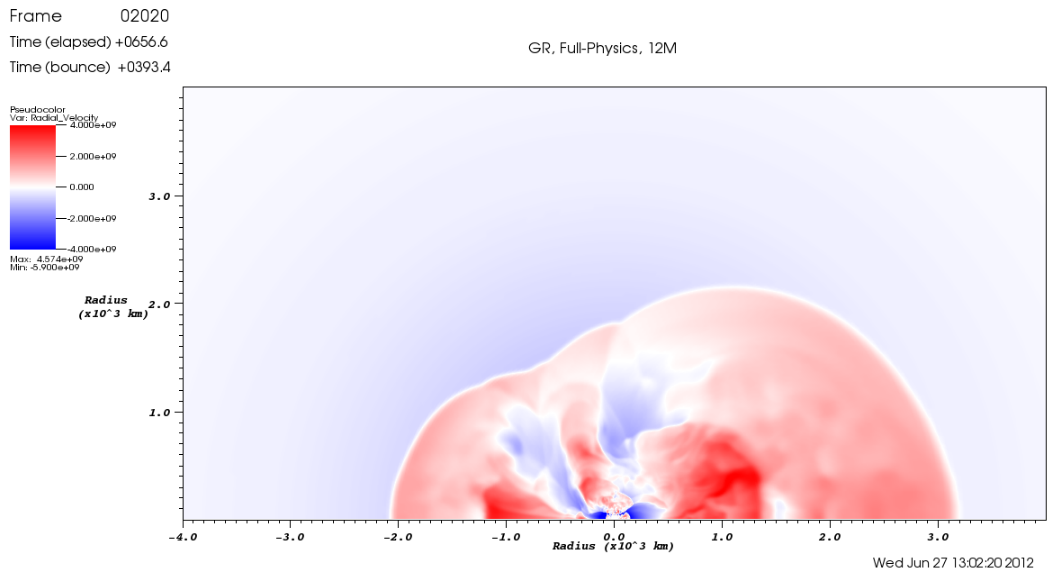

Figure 5.18: Snapshot of the radial velocity distribution for the 12 $M_\odot$ 2012 CHIMERA run. Red is positive radial velocity and blue is negative radial velocity. We have not previously observed the cool (low entropy) down-flows to be cut-off from above as they are at approximately 1300 km.

through their resourcefulness in helping us define discrete parcels of ejecta, and finally in their ability to make scientific contributions to gravitational wave studies, the tracer particles have proven to be an invaluable resource beyond their original intent of allowing post-processing nucleosynthesis results. It must be stressed that nucleosynthesis remains their primary function, and much effort has gone into their continued development in both their deployment within the CHIMERA code and their analysis by way of the tracer reader.

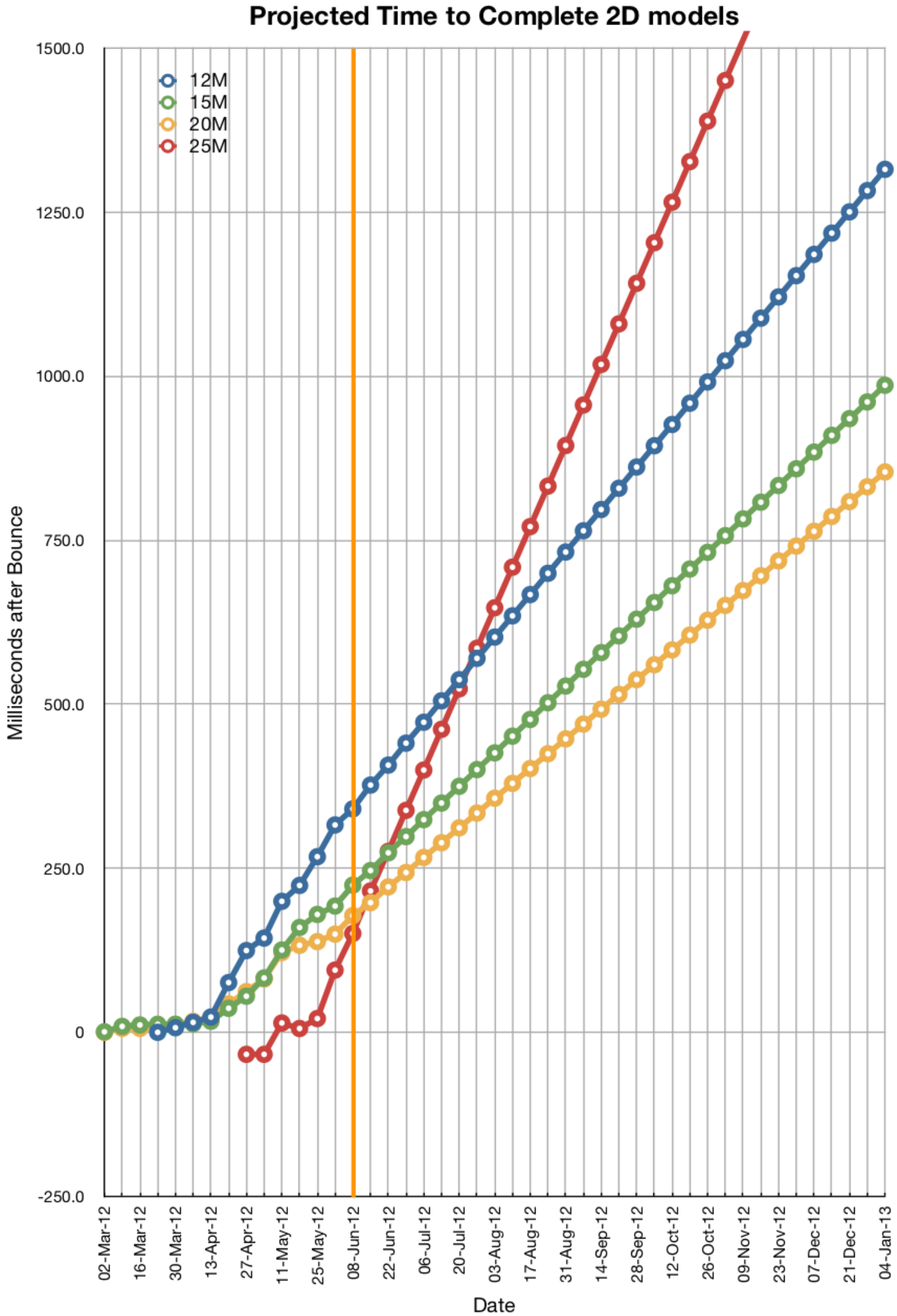

Figure 5.19: Projected progress for our suite of 2012 CHIMERA runs as of June 8, 2012.

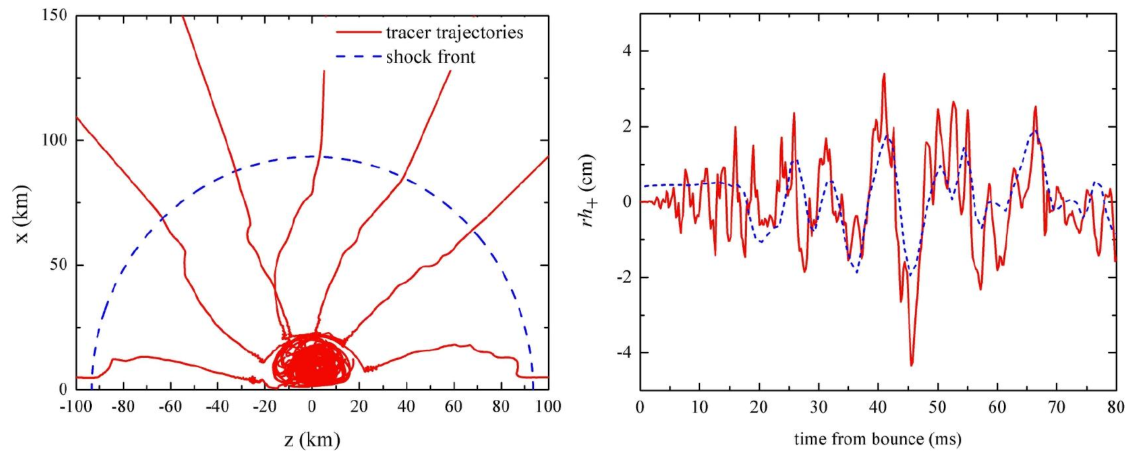

Figure 5.20: Left: Deflection of infalling tracer particles passing through the shock at 60 ms post-bounce in the 2009-15 $M_\odot$ Woosley & Heger (2007) simulation. These tracers collectively produce a low-frequency high-amplitude component of the GW signal shown on the right panel. Right: Comparison between the matter signal (solid red) and signal calculated using the tracers (dashed blue). Yakunin et al. (2010b).

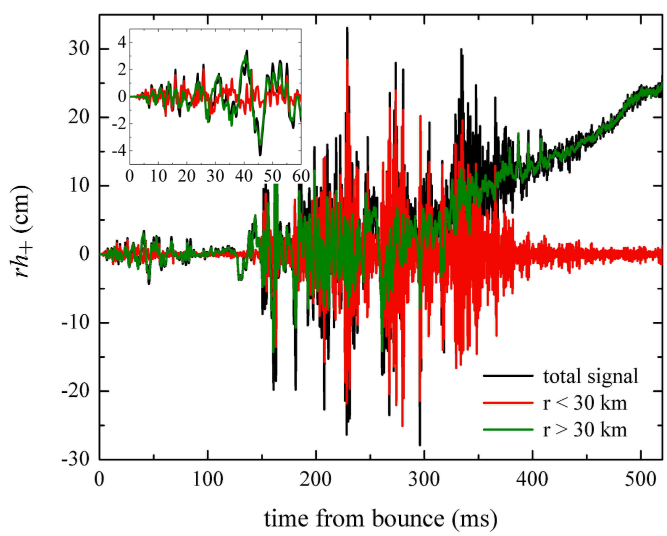

Figure 5.21: Contributions to the matter-generated GW signal from two different regions for the 15 $M_\odot$ model: the PNS ($r < 30$ km) and the region above the PNS ($r > 30$ km). The latter includes the region of neutrino-driven convection, the SASI, and the shock. Yakunin et al. (2010b).

Chapter 6

Electron Capture Supernovae from ONeMg-Core Progenitors

With our self-consistent, multi-dimensional, tracer-laden CHIMERA code, and a network extended beyond 14-species, we can expand the scope of CCSN models by investigating progenitors of various masses, metallicities*, and core compositions. With this is mind, we have begun an exploration into the lower mass range of CCSN progenitors between $8 \lesssim M_\odot \lesssim 10$. Within this range, stars lack the necessary mass for gravitational contraction to drive nuclear production beyond magnesium. At this stage, the core, composed of strongly degenerate oxygen, neon, and magnesium (ONeMg), becomes physically inert, but hydrogen and helium-burning shells continue to deposit carbon and oxygen from above. Collapse is finally induced when the degenerate electrons become relativistic and capture onto ^{24}Mg, ^{24}Na, ^{20}Ne, and ^{20}F (Miyaji et al., 1980; Nomoto, 1987) — thus giving these special CCSNe the name *electron capture supernovae* (ECSNe). Upon the rapid decrease in Y_e, the core rapidly

*Metalicity is the total mass fraction of elements heavier than helium.

contracts igniting an oxygen deflagration at a central density of $p_c > 10^{10}\,\mathrm{g/cm^3}$, which increases the size of the NSE region within the core.

Relative to their iron-core counterparts, the explosion associated with ECSNe are expected to be relatively weak ($\sim 10^{50}$ ergs), and since they eject little carbon and oxygen and very little ^{56}Ni ($\sim 10^{-3}\ M_\odot$) they are expected to be relatively dim (Pumo et al., 2009; Nomoto, 1987). Due to the steep decline in density near the surface of the oxygen-core (see Figure 6.1), the rebounding shock wave propagates faster than it would in the iron-core models, leading ECSNe to have lower mass accretion rates and smaller ram pressures from the in-falling shell (Janka, 2012). For this reason, it is "easier" to explode oxygen-cores than more massive iron-cores. Though the explosion mechanism is still under some debate, recent studies point towards a requirement for neutrino energy deposition behind a stalled shock (Kitaura et al., 2006; Wanajo et al., 2009), aided by the continuously increasing radius of the accretion shock (Janka, 2012). There is a large interest in resolving the specific mechanism of ECSNe as they have been suggested as a potential source of r-process elements (Ning et al., 2007), though more recent models suggest ECSNe produce at most a light r-process, producing elements heavier than Zn up to, potentially, Cd (Wanajo et al., 2009). Although ECSNe have not been definitively observed, there is a growing list of possible candidates showing these expected characteristic features, including SN 1054 (The Crab remnant), 1997D, 1999br, 2005cs, 2008S (Janka, 2012).

Kitaura et al. (2006) have created spherically symmetric ECSN models up to one second after bounce, finding a delayed neutrino-driven explosion instead of the prompt-shock mechanism as described by Hillebrandt et al. (1984). Although Kitaura et al. carefully considered a description of weak interactions, they were still limited by a seven species alpha-chain network, meaning that even though they project ECSNe to produce neutron-rich ejecta with Y_e as low as ~ 0.2 (and entropies down to $\sim$

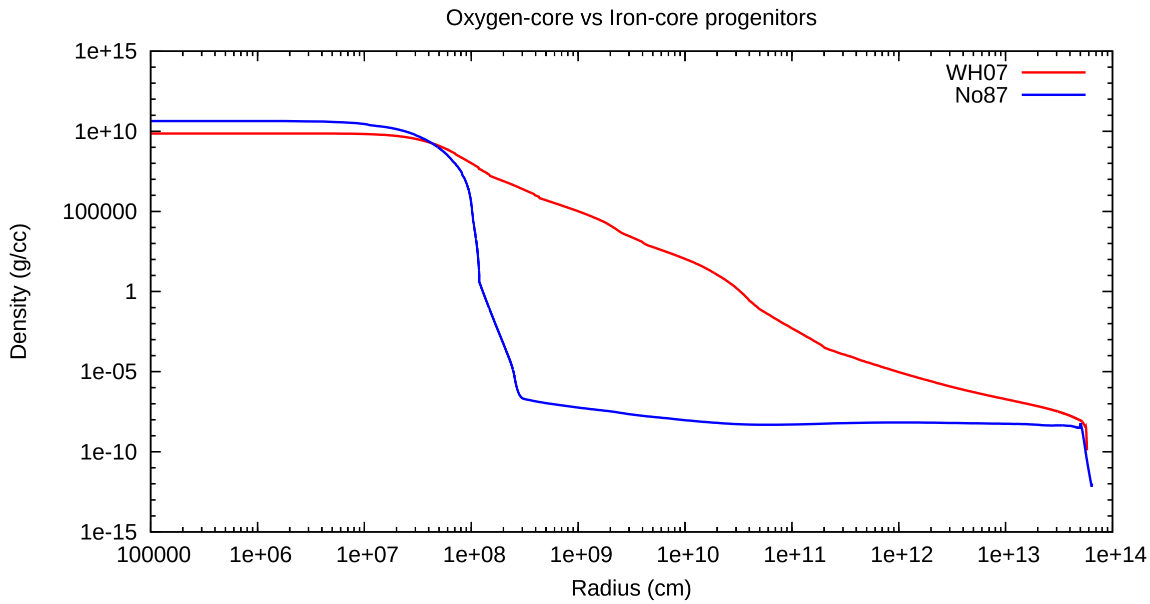

Figure 6.1: Density profiles of an 8.8 $M_\odot$ (No87) and 15 $M_\odot$ (WH07) progenitor before the onset of core collapse. Due to the steep density decline in the outer part of No87, these stars are expected to explode more easily as the shock propogates into less dense material.

$10\,\mathrm{k_B}$), they cannot accurately follow the nucleosynthesis that occurs under such neutronization.

Using the same nuclear network as Kitaura et al., the 2D model of Janka et al. (2008) was modestly more energetic than previous studies due to convective overturn in the gain layer. Although Janka et al. determine that neutrino energy deposition within the gain region is the primary source for accelerating a slowing shock, their model fails to create conditions to support the r-process scenario of Ning et al. (2007) by having too modest entropies and insufficient temperatures. Janka et al. point out that their thermonuclear energy production is approximate and a full reaction network is desired in order to take electron capture rates into consideration.

Using models similar to Kitaura et al. and Janka et al. , Wanajo et al. (2009) found that a multi-dimensional model produces neutron-rich ejecta due to convective overturn that could otherwise not be seen in 1D cases. Aside from finding that the explosion energy was enhanced by approximately 10% in their 2D case, they also performed the first nucleosynthesis study using tracer particles (for post-processing), where they found neutron-rich lumps with electron fractions down to 0.40, which can lead to nuclei up to $A \sim 80$. Wanajo et al. hypothesize that 3D models may eject a tiny amount of matter with a Y_e as low as $\sim 0.35 - 0.30$, leading to the creation of Cd. Unfortunately, they were limited by resolution and dimensionality constraints, as well as a small network, and could not exclude weak r-process elements beyond $N = 50$ up to Pd, Ag, and Cd.

Theoretical and observational studies of ECSNe are still subject to many uncertainties (Hillebrandt et al. 1984; Janka et al. 2008; Kitaura et al. 2006; Wanajo et al. 2009 (the Garching group) and Pumo et al. (2009)). We are presently working on initial trials to evolve the ONeMg core of Nomoto (1987) (henceforth "No87") using CHIMERA. No87 is the same pre-collapse core used in the Prometheus-Vertex models of the Garching Group (Kitaura et al., 2006; Janka et al., 2008; Wanajo et al., 2009). My initial attempts at evolving No87 are in 1D with a radial grid resolution of 1024 zones encompassing a radius of 1.376×10^9 cm, which are described in Section 6.2. It is the intention of the CHIMERA team to evolve this models beyond 1000 ms post-bounce. Moving beyond 1D, we believe we can extend our ECSNe resolution to match our previous 2D iron-core models of 512 radial $\times$ 256 lateral zones.

Were it not for my work on generalizing the nuclear network within CHIMERA (as described in Chapter 4.1), it would not be possible to construct an appropriate network needed to evolve ONeMg-cores and investigate the ECSNe mechanism. Since a naive implementation of a large network would greatly increase the cost of a run in

2D, my initial study uses a slight modification of our nominal alpha-network where I have included four extra species (^{20}O, ^{20}F, ^{24}Ne, ^{24}Na) to allow for electron capture reactions. This network, referred hereafter to as "alpha+6" (including neutrons and protons), will serve as a baseline for comparison to a forthcoming large free network implementation we are currently developing. Using our latest version of CHIMERA, the alpha+6 network will allow the ONeMg core to collapse and produce physically meaningful results in both the evolution and in nucleosynthesis studies at a level of sophistication similar to the Garching group's efforts. With a large network tuned to reactions within ECSNe our results will be unparalleled for quite some time — as we know of no developments of this kind throughout the SNe community.

6.1 Nomoto's 1987 8.8 $M_\odot$ Progenitor

At the onset of this thesis project, we had four different Progenitor Generator (PG) programs, each customized to build a specific iron-core progenitor. Rather than construct a fifth PG program for the ONeMg-core progenitor, I combined the original four into a single program based around a dynamic "*heger-read*" and "*nomoto-read*" scheme that uses an input file to tune the generalized PG for the various parameters of each model. Nominally, a progenitor, for use in CHIMERA, should only be construct once per model, but because the ONeMg-core has very different physical characteristics than what CHIMERA's architecture was designed to handle, choosing how to modify the ONeMg progenitor required an iterative testing process. Furthermore, as we make progress on simulations, we occasionally find that the gridding of a progenitor needs to be modified to enhance its physical fidelity. By working on, and generalizing, the PG, I have helped lay the groundwork for future progenitor mass studies. Here, I describe my initial investigation of No87.

As previously stated, the core of Nomoto (1987) consists of ONeMg which is surrounded by a large C+O layer, followed by a very thin pure He layer at approximately 1.20×10^9 cm, atop which is a hydrostatic H-rich envelope that extends to 6.41×10^{13} cm, making up the remaining 83% of the star. The star is assumed to have lost much of its envelope mass during the AGB phase, so that the total stellar mass has been reduced from 8.8 $M_\odot$ to 2.626 $M_\odot$. My initial trial run only evolves the inner 1.376 $M_\odot$, which is still sufficient to produce an ECSN.

Ken'ichi Nomoto of the University of Tokyo provided us with three separate files containing sometimes conflicting data about the No87 model. Figure 6.2 shows the characteristic profiles for temperature, pressure, Y_e, and velocity from the most extended of these files (N3). At approximately 10 GK, the inner $\sim10^7$ cm has already entered NSE, but only a small window between $\sim4\times10^7$ cm and $\sim1\times10^8$ cm has a $Y_e = 0.5$, which suitable for an alpha-network.

Unfortunately, we found this model to be incomplete in that it had missing abundances, inconsistencies in the radial zoning profile, and it lacked sufficient precision in the mass shell of each zone to be considered a Lagrangian model. I will discuss each of these deficiencies, my work towards correcting No87, and the trial runs that have aided us towards producing a viable ONeMg progenitor for CHIMERA.

The composition, as given in the file N1, was insufficient to match the constraints given by Y_e, the mean nuclear mass ($\bar{A}$), and a requirement that each zone has a mass fraction that sums to unity. Incomplete mass fractions of ^{4}He, ^{12}C, ^{16}O, ^{20}Ne, ^{24}Mg, were provided inside of $\sim10^8$ cm with no composition available for the envelope. To satisfy these constraints, we were required to add four additional species to the initial network. From Nomoto (1987), there must have been significant conversion of ^{20}Ne into ^{20}O and ^{24}Mg into ^{24}Ne, which were used to reconstruct the composition. By trial and error, we found that ^{32}S provided positive mass fractions and accurately

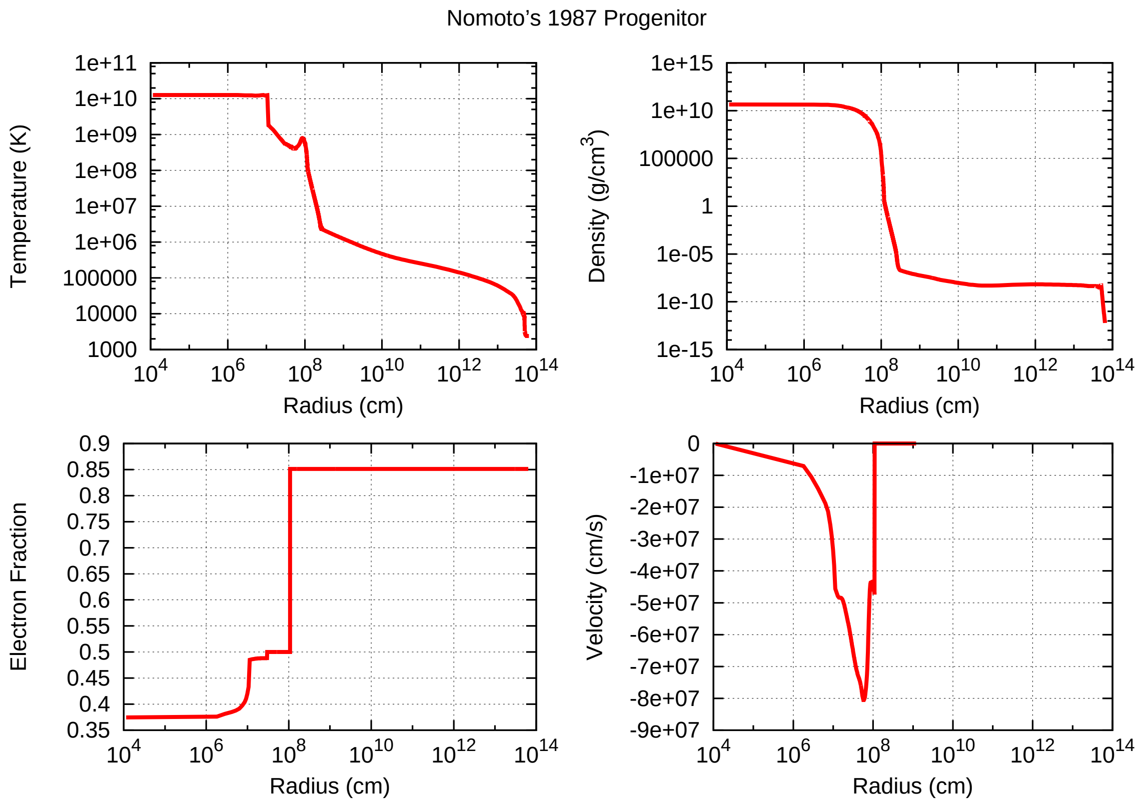

Figure 6.2: Original Nomoto progenitor's state variables (from N3) as a function of mass. The high temperatures in the core indicate that the core has begun to collapse and significant nuclear burning has initiated in NSE conditions.

reconstructed the constraint conditions mentioned above in the inner regions while ^{1}H is required in the outer envelope. This revised composition is illustrated in Figure 6.3. At the time of this writing, we have received a more complete composition profile from Nomoto and will include it in our forthcoming investigations.

With a complete initial composition, we extended our nuclear network to include these new species to satisfy the nuclear kinetics required for the electron capture reaction of ^{24}Mg$(e^{-}, \nu)^{24}$Na$(e^{-}, \nu)^{24}$Ne and ^{20}Ne$(e^{-}, \nu)^{20}$F$(e^{-}, \nu)^{20}$O expected to take place in the core, which help drive the collapse through the loss of the electron degeneracy pressure (Nomoto, 1987).

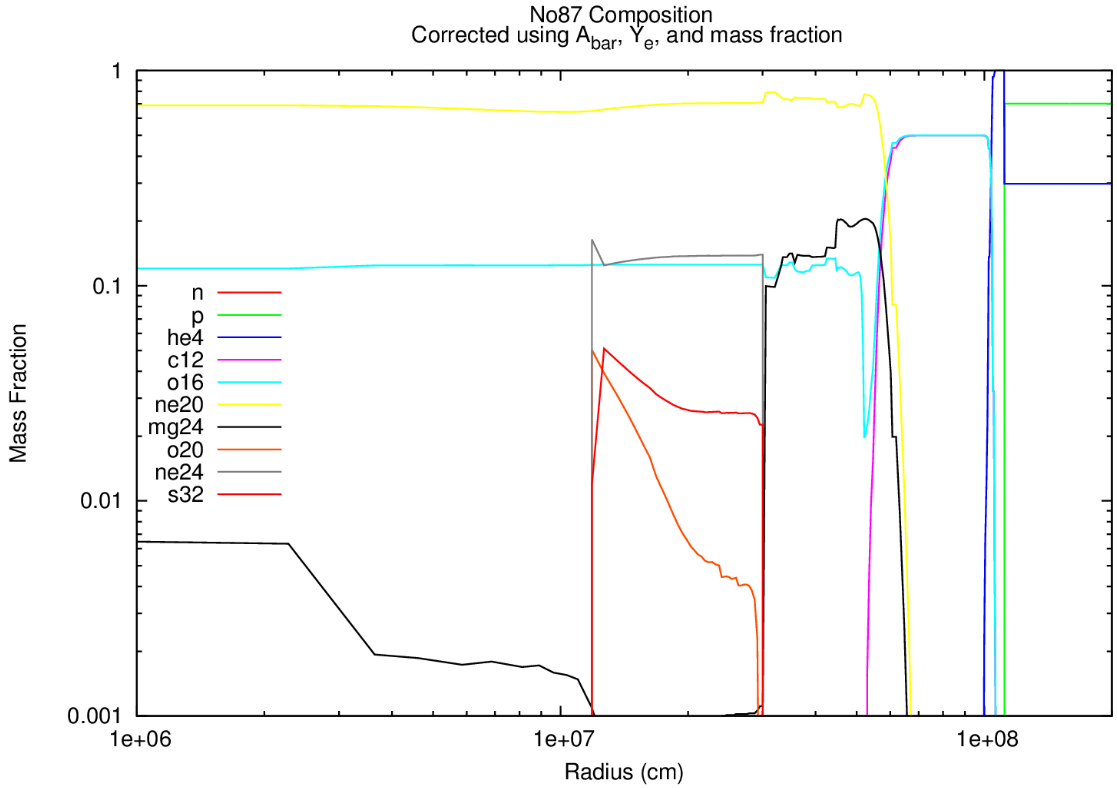

Figure 6.3: The initial composition required to satisfy Ye, $\bar{A}$, and a mass fraction which sums to 1.0. From Nomoto (1987), we see there must have been significant conversion of ^{20}Ne into ^{20}O and ^{24}Mg into ^{24}Ne

Based on the initial conditions in No87, and a simplistic approximation of collapse, we built a cartoon model of the conditions in the collapsing core to serve as a basis for an exploration in a post-processing calculation (using 1160 nuclear species) shown in Figure 6.4. This provides a hint at the fascinating nucleosynthesis to come. In the cartoon thermodynamic profile of the subplot of Figure 6.4), based on an iron-core collapse but scaled to a lower initial temperature and higher initial density to match No87's progenitor, it can be seen that 4 GK occurs at approximately $1\times10^{13}\,\mathrm{g/cm^3}$ and 5 GK at $2\times10^{13}\,\mathrm{g/cm^3}$. This deep in the ONeMg core, the ^{24}Mg has already captured electrons to form ^{24}Ne, so the first burning stage is the electron capture of $^{20}\mathrm{Ne}(e^-,\nu)^{20}\mathrm{F}(e^-,\nu)^{20}\mathrm{O}$. ^{16}O burning happens at the same time, but not to ^{28}Si/^{32}S as it would under less neutron-rich conditions. Silicon does not appear until about 2 ms before the end of the calculation (roughly 2 ms before bounce), where a sequence of reactions ^{20}O→^{24}Ne→^{28}Mg→^{34}Si finally burns oxygen and neon at a temperature of 4GK. The "silicon" then burns around 5GK, with flux passing through species like ^{50}Ca and ^{53}Sc on its way to a very neutron-rich NSE, dominated by species like astatine and selenium. Importantly, we are using this analysis to isolate the significant nuclear species (and reactions) for a larger species nuclear reaction network for future studies by considering the analysis like that in Figure 6.5, which shows the maximum mass fraction of the species included in our cartoon post-processing nucleosynthesis study. Building a network which can accommodate such neutron-rich burning as well as the less neutron-rich conditions of the surface may require a minimum of 300 species.

6.2 Evolving ECSNe with CHIMERA

After improving the composition and building a suitable alpha+6 nuclear network, the initial trial run of the progenitor failed to collapse; where instead of maintaining hydrostatic equilibrium (at the very least!), the core rapidly exploded at the initiation of the simulation, as shown in Figure 6.6.

Upon deeper investigation, it was discovered that the radii provided from Nomoto were not consistent with the masses and densities for each given zone. Since Nomoto (1987) evolved a Lagrangian grid to produce this model (and CHIMERA uses an Eulerian grid), I used the mass and density as independent variables to calculate corrected radii in an attempt to reproduce hydrostatic equilibrium. Using the mass

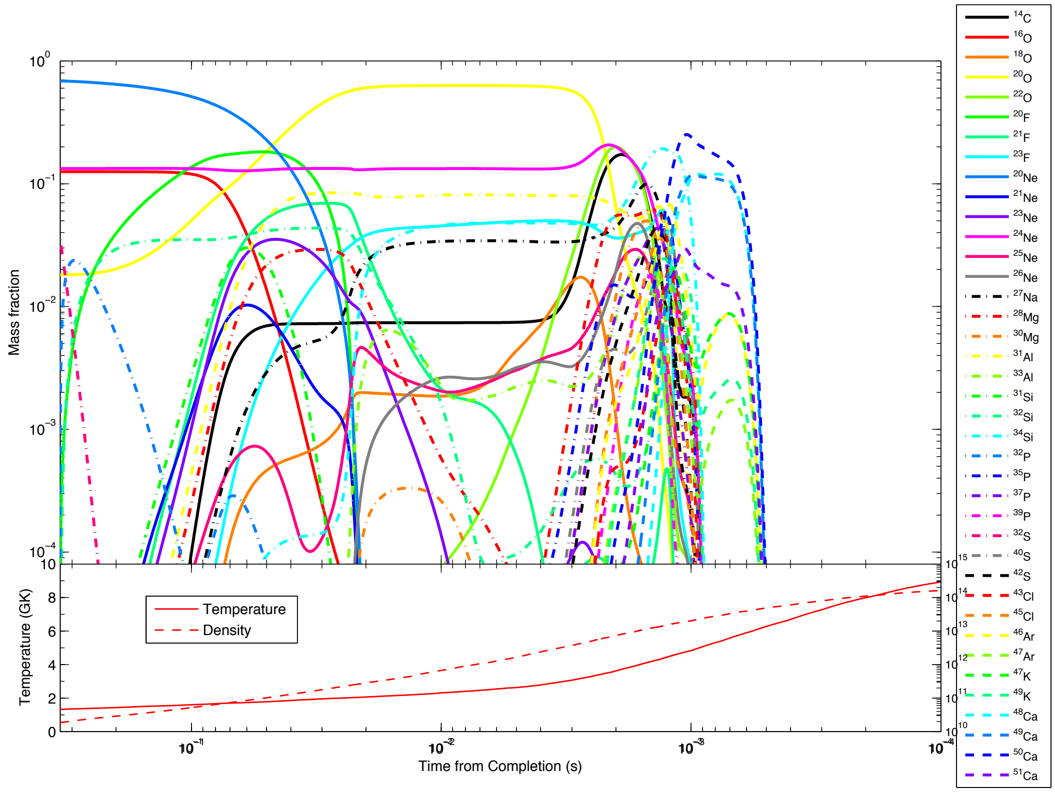

Figure 6.4: Approximation of collapse nucleosynthesis and condition for 1D ECSN based on an appropriately scaled Lagrangian coordinate from an iron-core model. Since ^{24}Mg has already electron captured to form ^{24}Ne, initial electron captures producing ^{20}Ne→^{20}F→^{20}O are now already evident.

shell relation in Equation 6.1,

$$r^3{}_i = \frac{3(M_i - M_{i-1})}{4\pi\rho_i} + r^3{}_{i-1}, \tag{6.1}$$

we found that the calculated radii values deviated from the original values by as much as 400 km as the radius approached the outer C+O layer near the H+He envelope. In attempting to reconstruct the radii, I was prohibited from using Equation 6.1 at the C+O→He+H boundary (between 1.00429×10^8 cm and 5.39471×10^8 cm) because the differences in mass (provided in the initial model files) as a function of zone

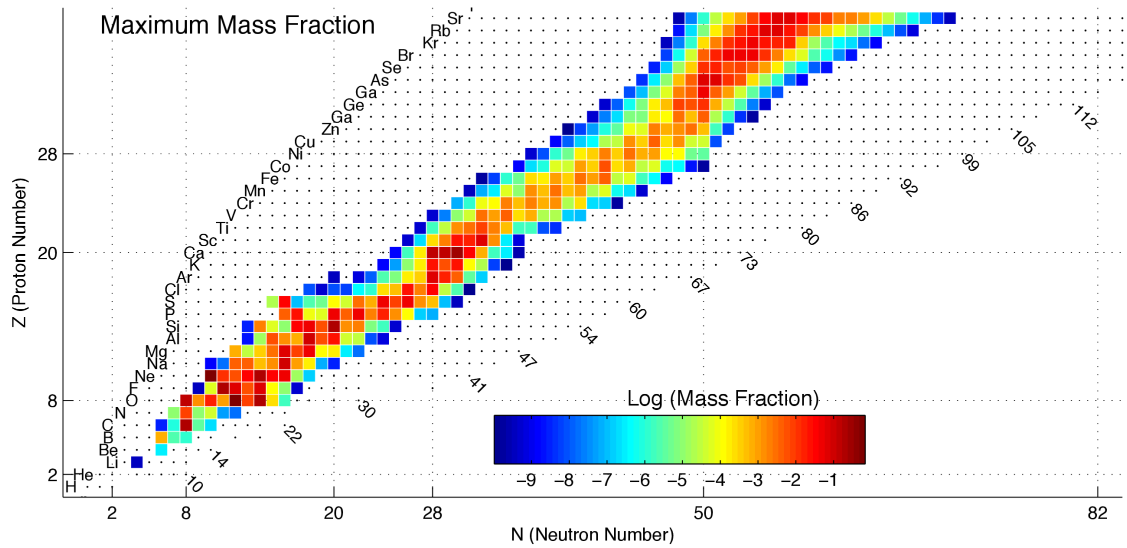

Figure 6.5: Z-N plane depicting the maximum mass at any point throughout our 1D ECSN nucleosynthesis approximation in Figure 6.4. We can see the corresponding abundances of ^{20}Ne, ^{20}O, and ^{50}Ca, and importantly, other species that play a potentially prominent role, but who may have reaction rates that prohibit the significant abundances for long periods of time.

in this region approached zero ($M_i - M_{i-1} \to 0$). The mass values provided by Nomoto contained only six significant figures and thus lacked sufficient precision. Using an empirically determined scaling factor of 1.033, I was able to re-constructed the "missing" radii between the region where $dM = 0$ ($1.00429{\times}10^8\,\mathrm{cm} \leq r \leq 9.16166{\times}10^{11}\,\mathrm{cm}$).

The lack of precision in the provided mass prohibited us from using the mass zoning scheme in our Progenitor Generator as discussed in Chapter 3.2. For this reason I had to modify our PG to use a re-gridding technique based on a constant change in $d\rho/\rho$ for each neighboring zone in order to capture the steep density gradient of the oxygen-core model with sufficient resolution. This is more consistent with the algorithm used to dynamically adjust the grid in CHIMERA, so we have also adopted this scheme for future iron-core models. With these improvements, I constructed a progenitor for CHIMERA with the resolution shown in Figure 6.7 — the bottom

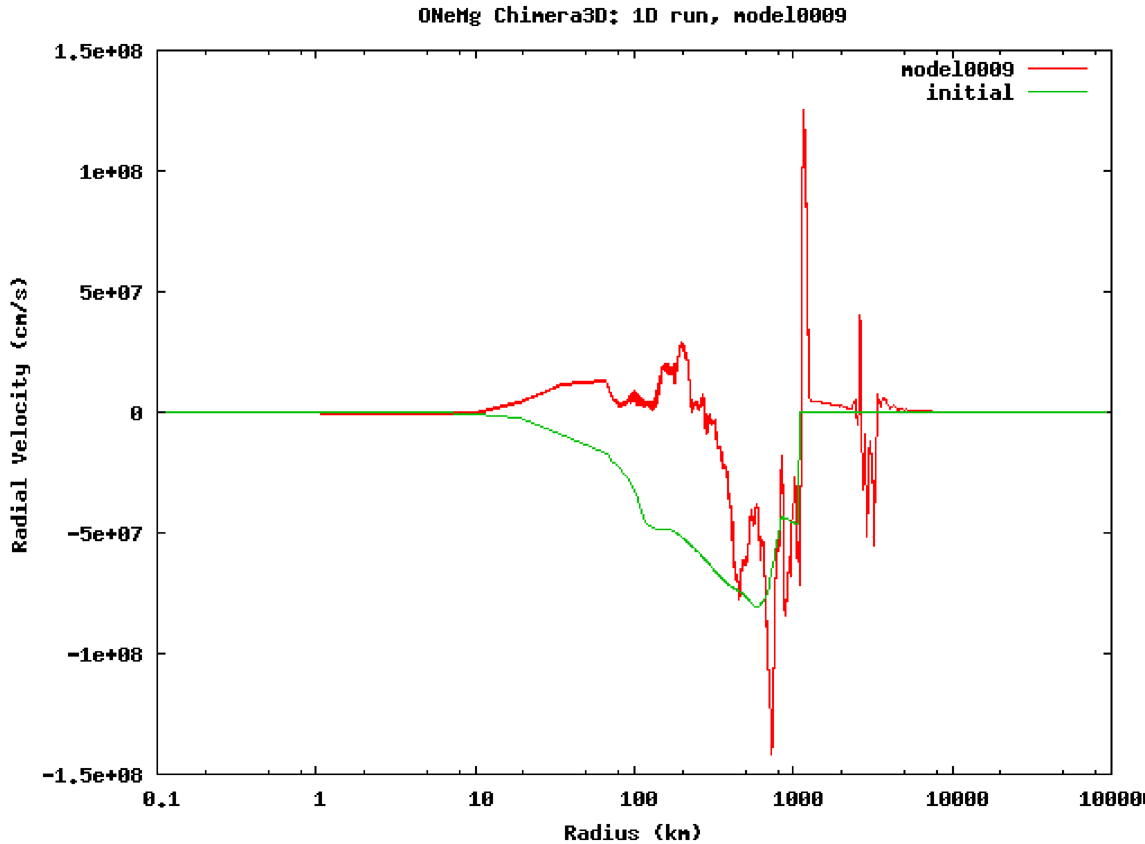

Figure 6.6: No87 trian run set number 1: Unphysical swelling at approximately 8.3 ms (red) of the ONeMg-core in the first set of initial trial runs. The swelling was determined to be due to an inconsistency in the provided radial profile of the Lagrangian run of Nomoto (1987). The initial velocity profile (green) is included for comparison.

radial plot relates the zone indexing to the progenitors radius. This progenitor has a relative radial resolution better than 0.05% and a relative density change less than 10% in the region of the steep density gradient (see Figure 6.1).

Despite my best attempts at correcting the radii at the surface of the white dwarf, my trial runs show expansion of the surface layers, as shown in Figure 6.8 and Figure 6.9 at 1 ms and 48 ms, respectively, from the start of our run. As can be seen in Figure 6.8, the initial evolution has many, small velocity perturbations — most likely from the various pressure gradients of the model settling into a local

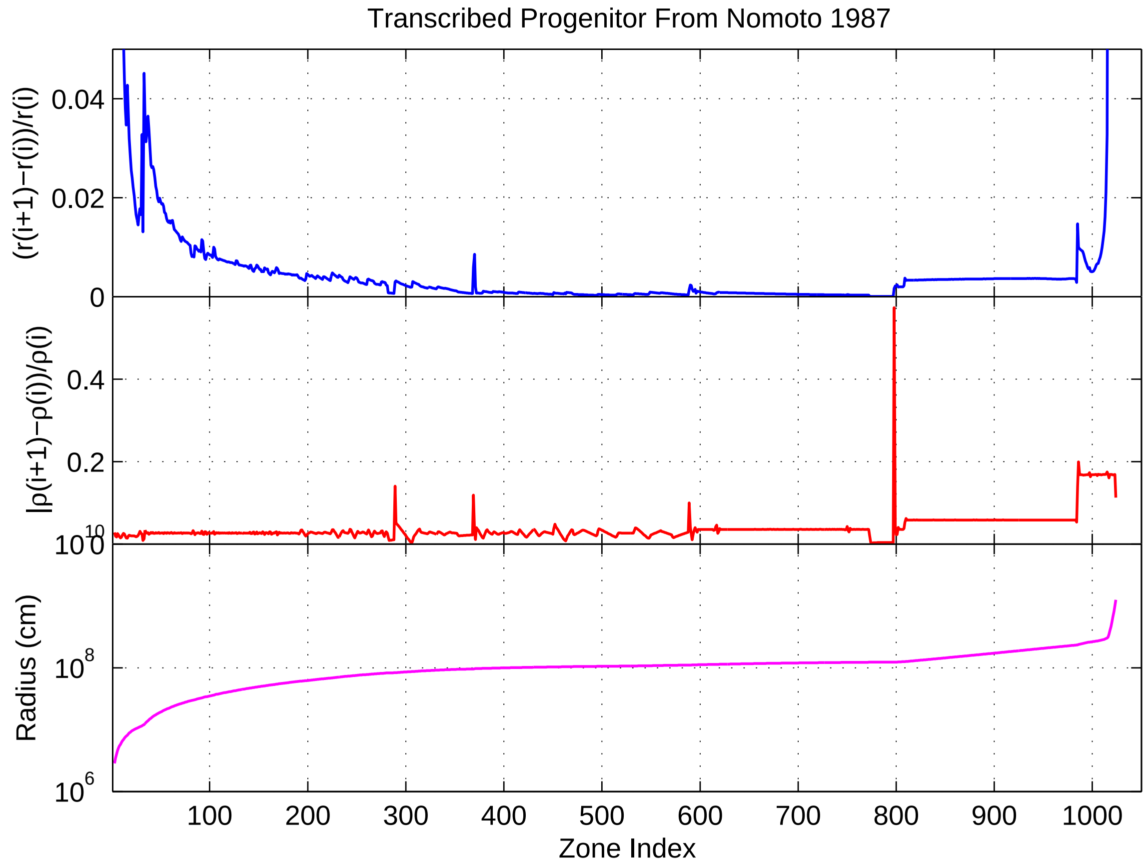

Figure 6.7: In these resolution plots one can see that the radial spacing is better than 0.05% and the density change less than 10% in the region of the density gradient between zones 250 and 700 ($\sim 7\times10^7$ cm $\leq r \leq 1.2\times10^8$ cm).

equilibrium. As Figure 6.9 shows, these largely settle out, allowing the star to collapse, except for surface velocity features at approximately 1000 km. Not only does the surface of the progenitor completely blow-off as the run progresses, but the run's initial velocity shows us that the model does not begin in hydrostatic equilibrium as is expected in this part of the star (Nomoto, 1987; Janka et al., 2008; Janka, 2012). As it is the pressure that drives the velocity in the hydrodynamics, a closer look at the initial pressure of the original No87 files and the initial values of the pressure components calculated by CHIMERA was warranted. These pressures (by components) are shown in Figure 6.10. The original pressure from N3 (solid thick blue) has a "glitch" at a radius of 1.07841×10^8 cm (where the Y_e transitions from 0.500 to 8.512), whereas CHIMERA calculates an overpressure at radius of $\sim1.09\times10^8$ cm to $\sim1.19\times10^8$ cm. CHIMERA's total pressure (thick black) is dominated by the electron pressure (magenta) below $\sim1.17\times10^8$ cm and is dominated by radiation pressure above $\sim1.17\times10^8$ cm.

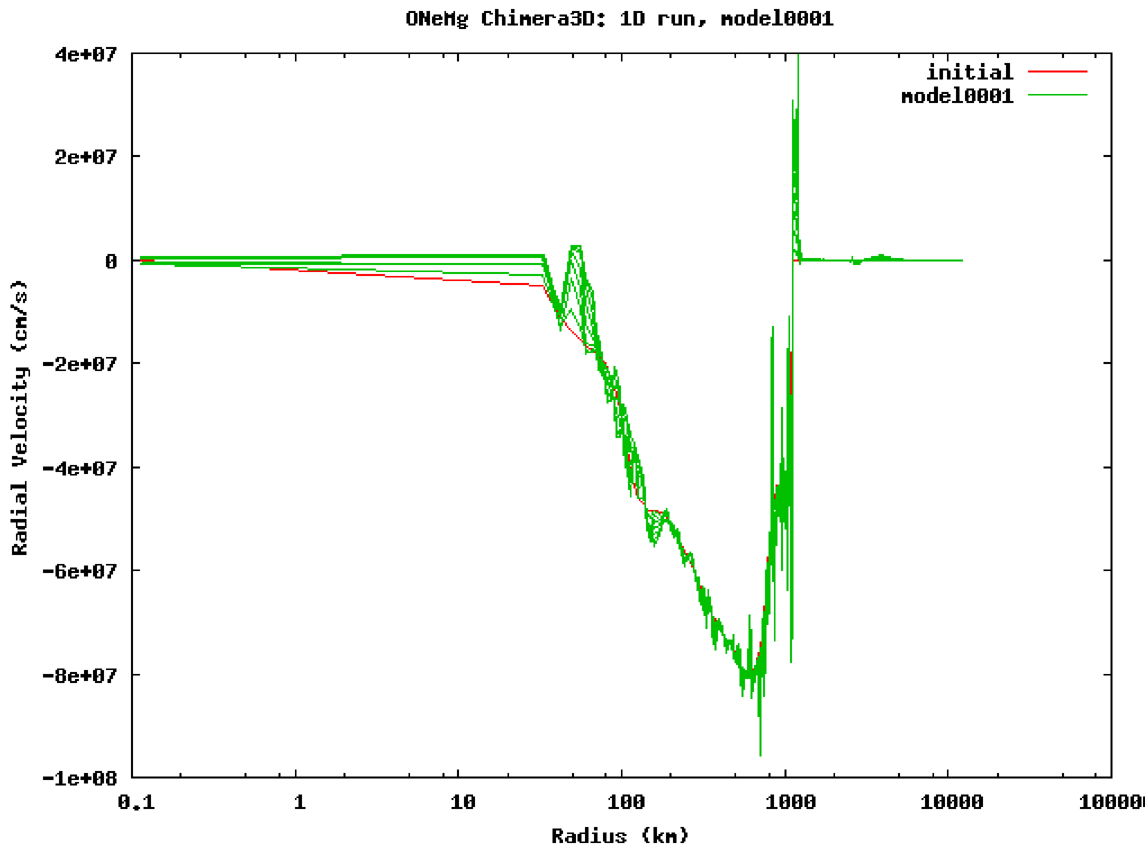

Figure 6.8: No87 trial run set number 2: velocity profiles leading up to an elapsed time of 1.0 ms from collapse (green). Extreme over-pressure around 1000 km leads to an unrealistic swelling of the white dwarf surface. The initial velocity (red) is included for comparison.

In investigating this pressure discontinuity, the transition from the 100% helium envelope to the 30% He plus 70% H envelope occurs essentially at constant density and temperature. Since the number of particles (nucleons/nuclei + electrons) per volume almost doubles when crossing through this interface, the pressure must also

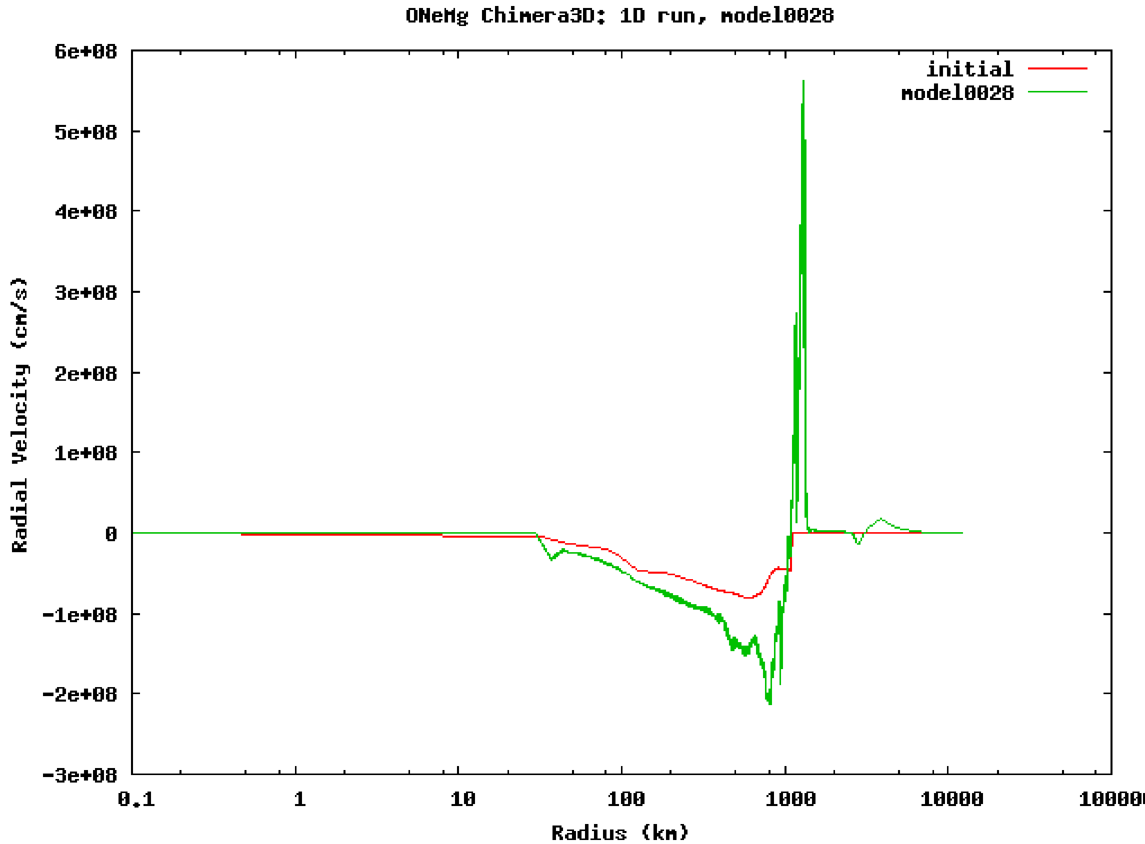

Figure 6.9: No87 trial run set number 2: velocity profile at an elapsed time of 48 ms from the start of the run. The core has not collapsed nor has hydrostatic been maintained as expected. Rather, the surface of the WD has simply blown off due to an overpressure at the surface of the C+O layer in the WD.

double — as shown in Figure 6.10. This is potentially the cause of the unexpected (and unwanted) hydrodynamics in the envelope from Figures 6.8 and 6.9.

Although it is not desirable to change the state variables of the original No87, it appears we are required modify the progenitor to obtain a model that is more realistic. By properly lowering the temperature (or density) in the appropriate regions, we seek to reconstruct hydrostatic equilibrium at the surface. Figure 6.11 shows my initial modification of the temperature profile where we remove the temperature "hump" across the outer C+O surface in an attempt to alleviate the heating of the H+He envelope. As can be seen in Figure 6.12, the run associated with the modified

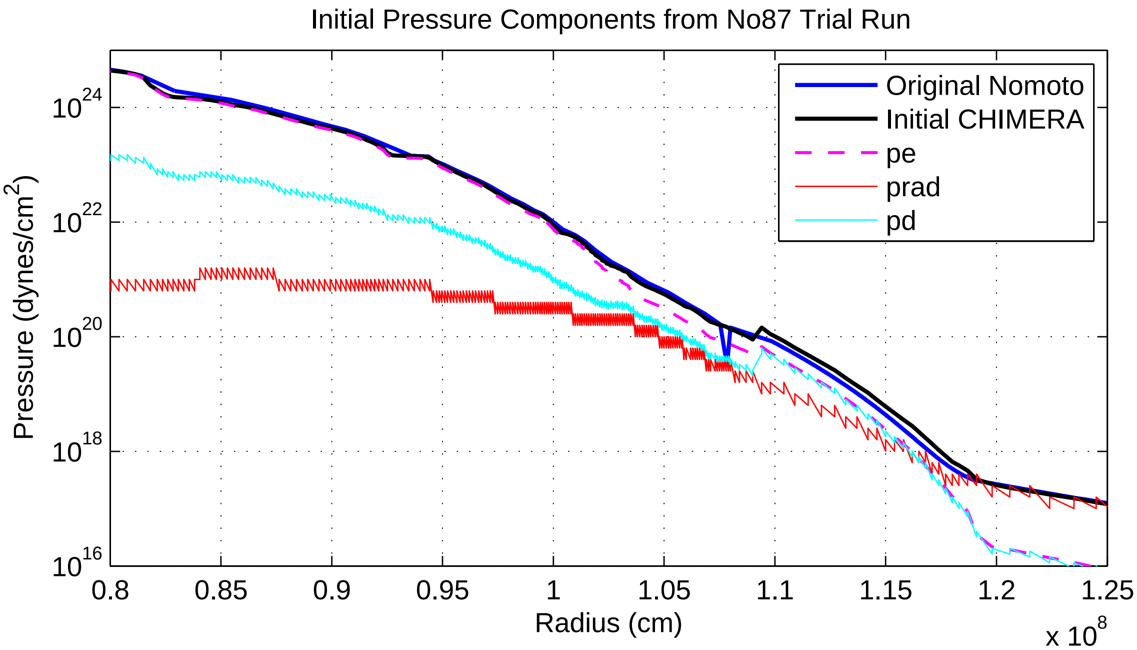

Figure 6.10: No87 initial pressure components: the original total pressure as provided by Nomoto (thick blue), Chimera's total pressure (thick black), and how the various components (electron pressure (dashed magenta), radiation pressure (red), nuclear pressure (cyan)) sum to equate CHIMERA's pressure. Interestingly, at approximately $1.07{\times}10^8$ cm we can see the transition from the region dominated by electron pressure to a region dominated by radiation pressure.

temperature has a weaker "explosive" feature than our earliest trials (see Figure 6.8) — although positive features in the envelope between roughly 1200 and 1500 km still exist. More importantly, Figure 6.13 shows that at an elapsed time of 48 ms, the surface layers of the core join the inner core in its collapse despite minor pressure perturbations that drive fluctuations in the inner H+He envelope.

Unfortunately, this run still failed due to a strong discontinuity forming at a radius of just above 1000 km in Figure 6.13, which stems from a growing discontinuity in temperature (see Figure 6.14) and density (see Figure 6.15). This new discontinuity is most likely seeded from issues that persist in our initial progenitor. Rather than simply removing the temperature hump from Figure 6.11, we have a plan to use CHIMERA's EoS to iterate over these problematic regions to manually reconstruct

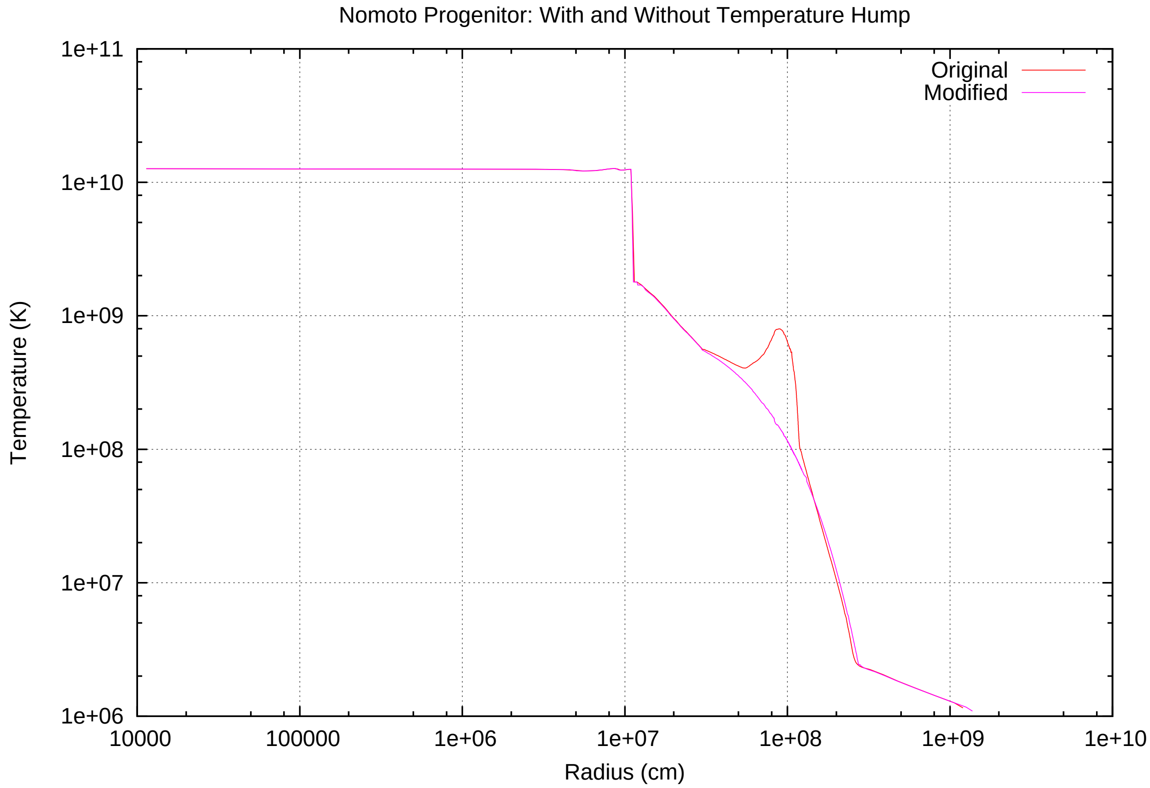

Figure 6.11: Original Nomoto temperature profile (with hump) versus modified temperature profile (without hump). This profile was modified in an attempt to alleviate the heating discontinuity of the H+He envelope across the surface of the WD.

hydrostatic equilibrium zone by zone. We hope this new attempt will remove many of pressure and hydrodynamic the problems that persist in this model.

6.3 ECSN Conclusions

Once we have a viable progenitor that proceeds through collapse and explosion in 1D, we plan to produce 2D ECSNe simulations to perform nucleosynthesis comparison studies between a large network (under development) and the alpha+6 network (using tracer particles for post-processing). Since nuclear burning plays such a crucial role in ECSN models, we would also like to perform a detailed study on how

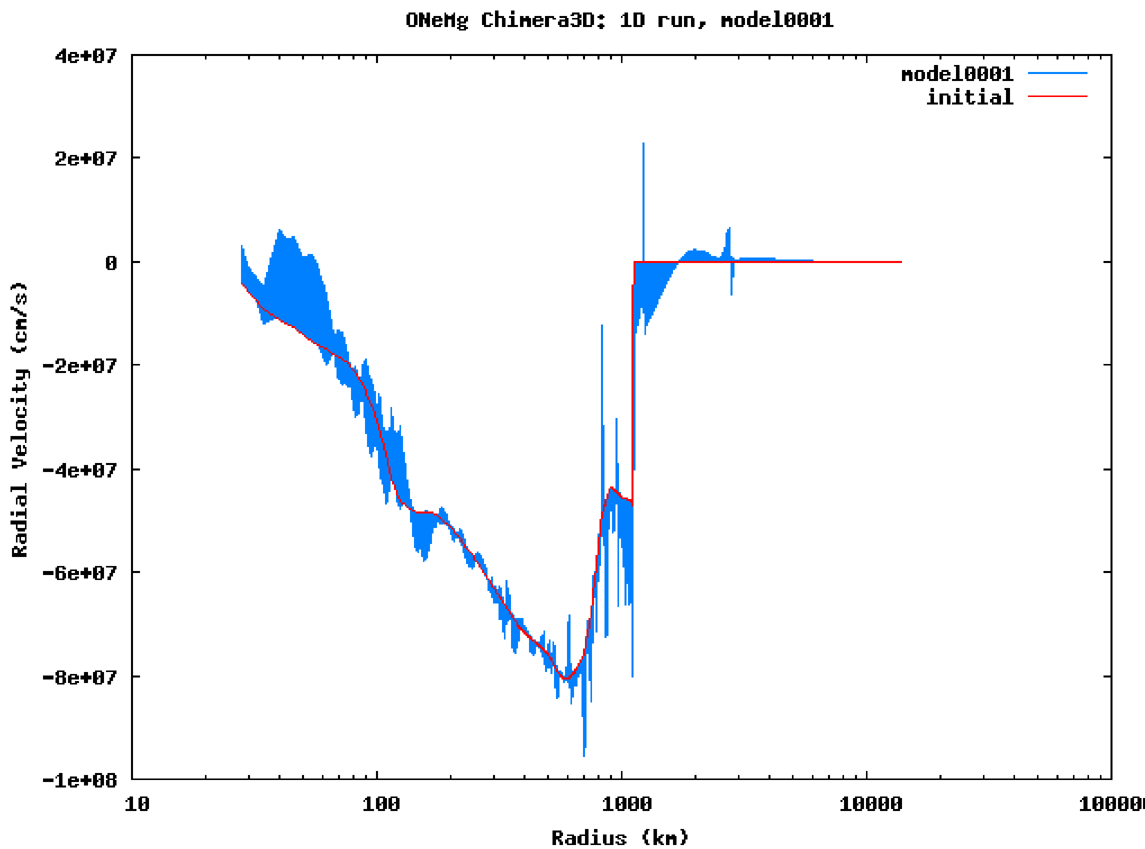

Figure 6.12: No87 trial run set number 3 (without temperature hump): Initial velocity (red) and final velocity (blue) profiles at an elapsed time of 48 ms. Comparing to the velocity profile of the run that included the Figure 6.8, the initial profile is much more well behaved at the surface of the white dwarf, with a few, small, exceptions between 1000 km and 2000 km.

the thermonuclear energy generation rates feed back into the hydrodynamics. This will help us understand the effect thermonuclear energy release has on the outward propagating shock and supernova evolution, in general.

Moving beyond 2D ECSNe models (which, with alpha+6 will provide verification of, and with a large network represent a notable improvement over, the Garching group's studies), we would like to evolve ECSNe with a "Yin-Yang" grid, which is a modern method of creating pole-free 3D grids that avoid the small Courant limited time-steps found near the pole of typical spherical-polar grids (Kageyama & Sato

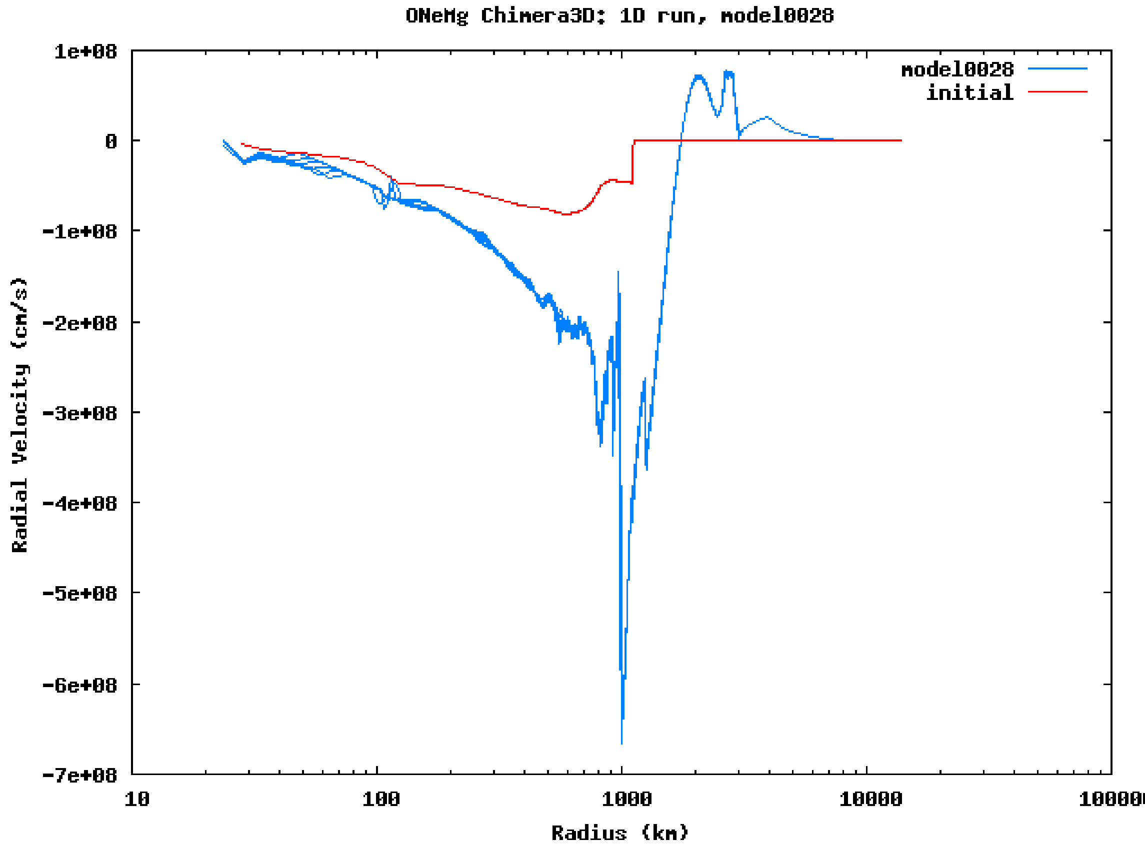

Figure 6.13: No87 trial run set number 3 (no temperature hump): Initial velocity (red) and final velocity (blue) profiles at an elapse time of 48 ms. Comparing to the velocity profile of the run that included the Figure 6.9, the surface layers of the core join the inner core in its collapse despite minor pressure perturbations.

(2004), and Lentz et al. (2013)). As with any realistic hydrodynamic model, a self-consistent 3D model would provide a verification of 2D results, but most importantly, as stated by Wanajo et al. (2009) and Pumo et al. (2009), a 3D run is required to not only study the creation of nuclei within ECSNe, but to understand the composition of the ejecta due to a more realistic determination of convective processes afforded by the move to 3D.

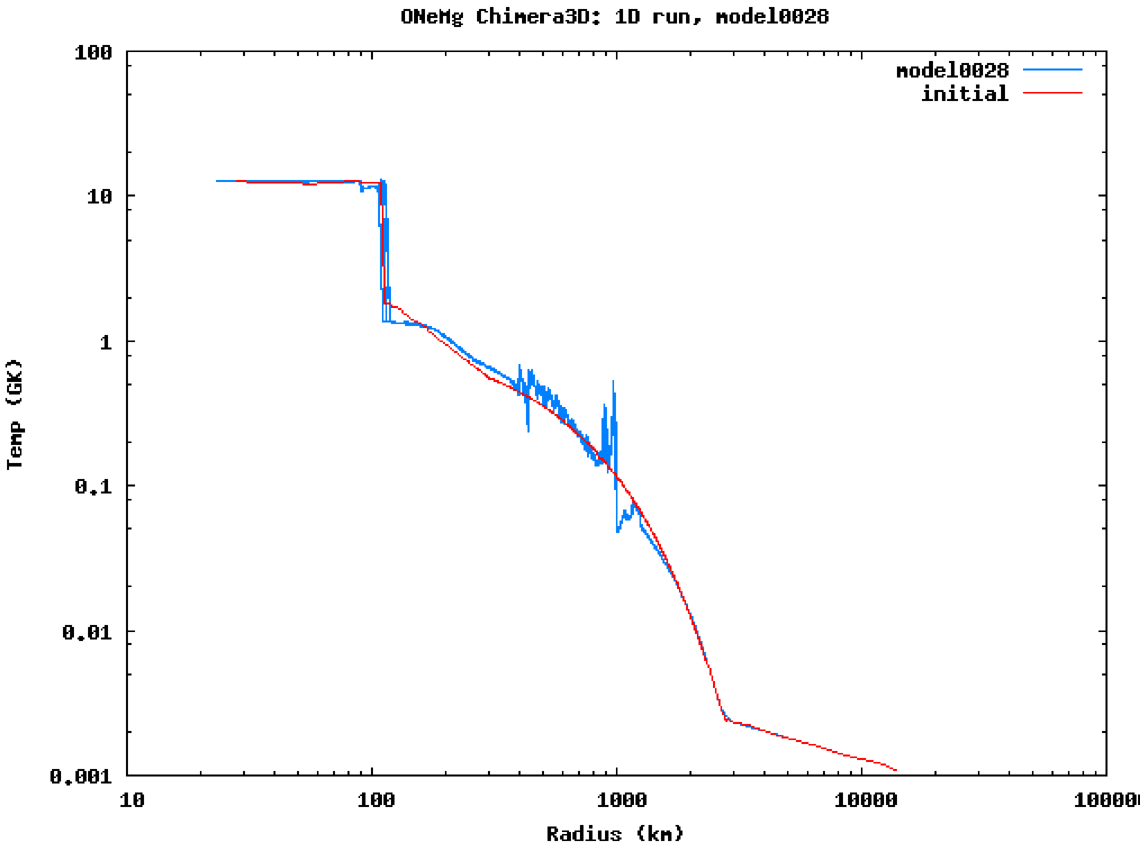

Figure 6.14: No87 trial run set number 3 (no temperature hump): Final temperature profile at an elapsed time of 48 ms. A discontinuity from an unknown source can be seen at a radius of ∼1000 km.

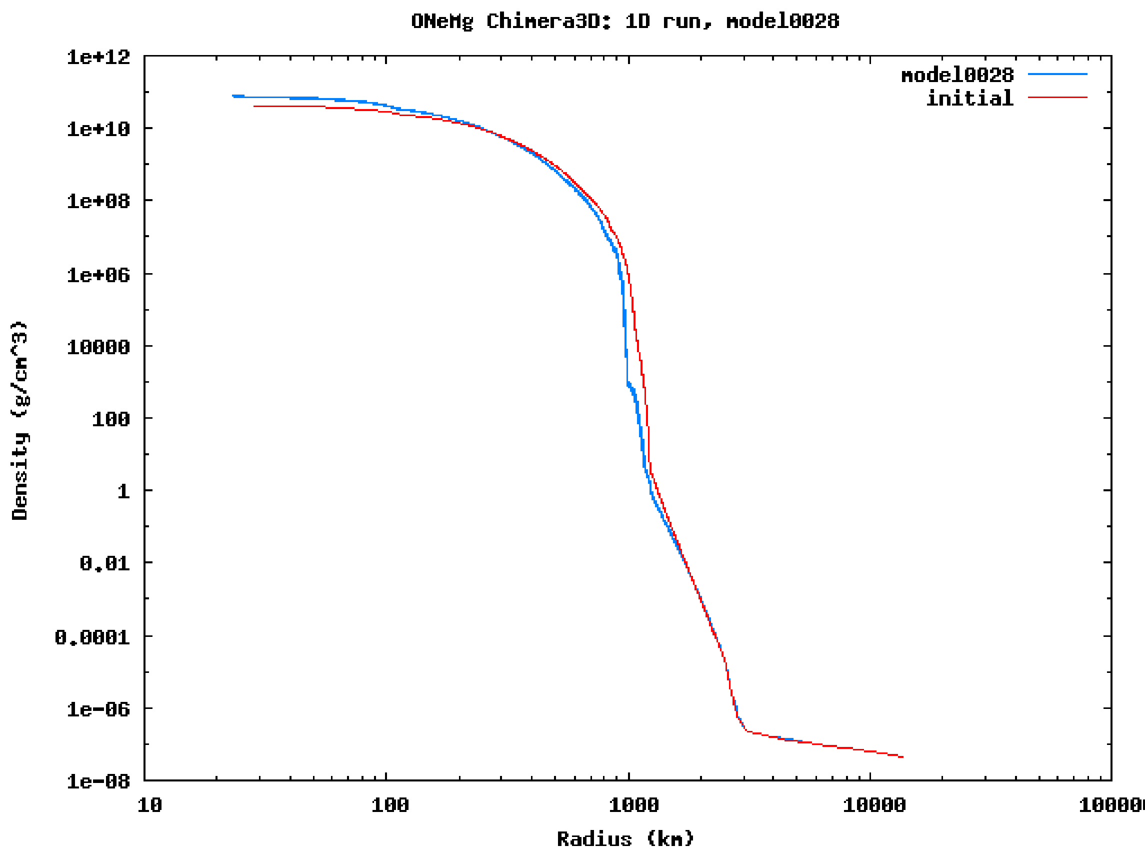

Figure 6.15: No87 trial run set number 3 (no temperature hump): Final density profile at an elapsed time of 48 ms. A discontinuity from an unknown source can be seen at a radius of ∼1000 km. At this time, the core has not reached nuclear densities ($> 10^{14}$ g/cm^3) meaning core-bounce has yet to be achieved.

Chapter 7

Conclusion

The CHIMERA group seeks to extend existing core-collapse supernova models to examine nucleosynthesis in a self-consistent fashion. Self-consistency requires, among other things, a code that evolves explosions, from a collapse phase, without parameterized methods to obtain neutrino-heated shock revival and ejecta that match CCSNe morphologies and galactic abundance contributions.

Through my work, CHIMERA's architecture had been improved to handle a generalized network from XNet, and I have run the first spherically symmetric supernova simulations with a realistic nuclear network coupled to the simulation in order to test my implementation. We have learned much from these 1D models despite the inability of symmetric models to produce explosions. This work brings the CHIMERA team several steps closer to an ambitious agenda of running many 2D and 3D models with realistic thermonuclear networks to examine the effects of progenitor mass, metallicities, core compositions, rotation rates, and micro-physics input on the evolution and the explosion mechanism of CCSNe. Most importantly, since computational investigations must be constrained by observations, the more realistic calculations of nucleosynthesis products (specifically in the ejecta) that our improvements will afford will play a vital role in determining the physical fidelity of our models.

The first step in modeling core-collapse supernovae entails taking a "finished" model from stellar evolution codes and transcribing them into a pre-collapsed progenitor to be run with a radiation hydrodynamic code, CHIMERA. Up until the work within this thesis, CHIMERA had been developed to run only the iron-core progenitors of Woosley & Heger (2007). I have extended this progenitor generator to include more realistic compositions and alternative progenitor masses.

With this generalized network and generalized progenitor generator, we are currently making steady progress on our attempts to model ECSNe. Our team has now crossed the initial hurdles of creating a network that will allow an ONeMg-core to collapse via electron captures. We believe once we are successful in building a viable progenitor that exhibits hydrostatic equilibrium at the transition from the surface of the C+O core to the He+H envelope, CHIMERA should be able to produce explosions in 1D and 2D models.

The tracer particles have been (and continue to be) a vital tool in our efforts to investigate the physical and numerical reliability of our models. But most essentially, the work I have performed on the tracers, in preparing the tools to use them in post-processing nucleosynthesis of the ongoing 2012 CHIMERA models, will provide unprecedented scientific results, as no CCSNe models to date has achieved the level of physical realism developed within CHIMERA. The trial analysis of early models has taught us much about the practical needs of this analysis and provided hints of interesting outcomes from future studies.

Looking towards the future, beyond our 2012 2D runs, we have initiated a full-physics pilot run in 3D using our latest development of a 2-grid ("Yin-Yang") architecture in CHIMERA. This simulation uses 4800 rays with a resolution in longitude and latitude of approximately 3.3°. After a successful pilot run, we will run with an alpha-network and populate our grid with several hundred thousand tracer particles. Our hope is that this model may one day produce ejecta giving us an unparalleled, advanced, self-consistent model with realistic nucleosyntheis results.

List of References

References

Arnett, W. D. 1969, ApJ, 157, 1369 18

Arnett, W. D. 1977, ApJ, 218, 815 15

Arnett, W. D. 1996, Supernovae and nucleosynthesis : an investigation of the history of matter, from the big bang to the present (Princeton: Princeton University Press) 13

Arnett, W. D., Bahcall, J. N., Kirshner, R. P., & Woosley, S. E. 1987, ARA&A, 27, 701 21

Baade, W. & Zwicky, F. 1934, Proceedings of the National Academy of Science, 20, 254 10

Baron, E., Cooperstein, J., & Kahana, S. 1985, Phys. Rev. Lett., 55, 126 26, 60

Bethe, H. 1996, Nuc. Phys. A 14, 15

Bethe, H. A. & Wilson, J. R. 1985, ApJ, 295, 14 2, 16

Blondin, J., Mezzacappa, A., & DeMarino, C. 2003, ApJ, 584, 971 16

Blondin, J. M. & Mezzacappa, A. 2006, ApJ, 642, 401 23

—. 2007, Nature, 445, 58 17

Bodansky, D., Clayton, D., & Fowler, W. 1968, ApJS, 16, 299 4, 13

Bruenn, S. W. 1985, ApJS, 58, 771 15, 16

Bruenn, S. W., De Nisco, K. R., & Mezzacappa, A. 2001, ApJ, 560, 326 16

Bruenn, S. W., Dirk, C. J., Mezzacappa, A., Hayes, J. C., Blondin, J. M., Hix, W. R., & Messer, O. E. B. 2006, J. Phys.: Conf. Ser., 46, 393 16, 22, 23

Bruenn, S. W., Mezzacappa, A., Hix, W. R., Blondin, J. M., Marronetti, P., Messer, O. E. B., Dirk, C. J., & Yoshida, S. 2010, Atomic Data and Nuclear Data Tables, 5 4, 17, 24

Buras, R., Rampp, M., Janka, H.-T., & Kifonidis, K. 2003, Phys. Rev. Lett., 90, 241101 17

—. 2006, A&A, 447, 1049 22, 23

Burrows, A. & Goshy, J. 1993, ApJ, 416, L75 16

Burrows, A., Hayes, J., & Fryxell, B. A. 1995, ApJ, 450, 830 16

Burrows, A. & Lattimer, J. M. 1985, ApJ, 299, L19 15

Burrows, A., Livne, E., Dessart, L., Ott, C. D., & Murohy, J. 2004, Apj 29

Cayrel, R., Depagne, E., Spite, M., Hill, V., Spite, F., François, P., Plez, B., Beers, T., Primas, F., Andersen, J., Barbuy, B., Bonifacio, P., Molaro, P., & Nordström, B. 2004, A&A, 416, 1117 30

Chertkow, M., Hix, W. R., Bruenn, S., Lentz, E., Blondin, J., Bronson Messer, O. E., Lee, C.-T., Mezzacappa, A., Marronetti, P., & Yakunin, K. 2011, in APS Southeastern Section Meeting Abstracts, L6 4, 24

Colgate, S. A. & White, R. H. 1966, ApJ, 143, 626 2

Federrath, C., Glover, S., Klessen, R., & Schmidt, W. 2008, arXiv.org:0805.0196v1 45

Fröhlich, C., Hauser, P., Liebendörfer, M., Martínez-Pinedo, G., Thielemann, F.-K., Bravo, E., Zinner, N. T., Hix, W. R., Langanke, K., Mezzacappa, A., & Nomoto, K. 2006a, ApJ, 637, 415 30

Fröhlich, C., Hix, W. R., Martínez-Pinedo, G., Liebendörfer, M., Thielemann, F.-K., Bravo, E., Langanke, K., & Zinner, N. T. 2006b, New Astronomy Review, 50, 496 19, 31, 32

Fröhlich, C., Liebendörfer, M., Thielemann, F.-K., Martínez-Pinedo, G., Langanke, K., Zinner, N., Hix, W., & Bravo, E. 2006, in Proceedings of Nuclei in the Cosmos –IX, ed. e. a. A. Mengoni (SISSA Proceedings of Science), 33 4

Fröhlich, C., Martínez-Pinedo, G., Liebendörfer, M., Thielemann, F. K., Bravo, E., Hix, W. R., Langanke, K., & Zinner, N. T. 2006, Phys. Rev. Lett., 96, 142502 58

G. Audi, O. Bersillon, J. B. & Wapstra, A. H. 2003, Nuclear Physics, 337 27

Galama, T. J., Vreeswijk, P. M., van Paradijs, J., Kouveliotou, C., Augusteijn, T., Bohnhardt, H., Brewer, J. P., Doublier, V., Gonzalez, J.-F., Leibundgut, B., Lidman, C., Hainaut, O. R., Patat, F., Heise, J., in 't Zand, J., Hurley, K., Groot, P. J., Strom, R. G., Mazzali, P. A., Iwamoto, K., Nomoto, K., Umeda, H., Nakamura, T., Young, T. R., Suzuki, T., Shigeyama, T., Koshut, T., Kippen, M., Robinson, C., de Wildt, P., Wijers, R. A. M. J., Tanvir, N., Greiner, J., Pian, E., Palazzi, E., Frontera, F., Masetti, N., Nicastro, L., Feroci, M., Costa, E., Piro, L., Peterson, B. A., Tinney, C., Boyle, B., Cannon, R., Stathakis, R., Sadler, E., Begam, M. C., & Ianna, P. 1998, Nature, 395, 670 3

Gratton, R. G. & Sneden, C. 1991, A&A, 241, 501 30

Hachisu, I., Matsuda, T., Nomoto, K., & Shigeyama, T. 1990, ApJ, 358, L57 29

Hammer, D., Hornschemeier, A. E., Mobasher, B., Miller, N., Smith, R., Arnouts, S., Milliard, B., & Jenkins, L. 2010, VizieR Online Data Catalog, 219, 43 29

Herant, M. & Benz, W. 1991, ApJ, 370, L81 29

Herant, M., Benz, W., Hix, W. R., Fryer, C. L., & Colgate, S. A. 1994, ApJ, 435, 339 16, 30

Hillebrandt, W. 1986, Highlights of Astronomy, 7, 629 14

Hillebrandt, W., Nomoto, K., & Wolff, R. 1984, Astronomy and Astrophysics, 133, 175 73, 75

Hix, W. R., Parete-Koon, S. T., Freiburghaus, C., & Thielemann, F.-K. 2007, ApJ, 667, 476 4

Hix, W. R. & Thielemann, F. 1995, BAAS, 27, 1423 26, 31

Hix, W. R. & Thielemann, F.-K. 1996, ApJ, 460, 869 13, 31, 42

Hix, W. R. & Thielemann, F.-K. 1999, ApJ, 511, 862 5, 8, 19

Hoyle, F. & Fowler, W. 1960, ApJ, 132, 565 11

Janka, H.-T. 2001, A&A, 368, 527 16

Janka, H. T. 2012, 35 21, 73, 84

Janka, H. T., Buras, R., Kifonidis, K., Marek, A., & Rampp, M. 2004, arXiv.org/astro-ph/040161v1 16

Janka, H.-T., Müller, B., Kitaura, F. S., & Buras, R. 2008, Astronomy & Astrophysics, 485, 199 74, 75, 84

Janka, H.-T. & Müller, E. 1996, A&A, 306, 167 16, 30

Kageyama, A. & Sato, T. 2004, Geochemistry, Geophysics, Geosystems, 5, 9 89

Kasen, D., Woosley, S. E., & Heger, A. 2011, The Astrophysical Journal, 734, 102 11

Keil, W., Janka, H.-T., & Müller, E. 1996, ApJ, 473, L111 16

Kifonidis, K., Plewa, T., Janka, H.-T., & Müller, E. 2003, A&A, 408, 621 29

Kitaura, F. S., Janka, H.-T., & Hillebrandt, W. 2006, Astronomy & Astrophysics, 450, 345 73, 74, 75

Lattimer, J. & Swesty, F. D. 1991, Nucl. Phys. A, 535, 331 24, 26, 60

Lee, T. C. 2008, PhD thesis, University of Tennessee Knoxville 44

Liebendörfer, M., Messer, O. E. B., Mezzacappa, A., Hix, W. R., Thielemann, F.-K., & Langanke, K. 2002, in Proceedings of the 11th Workshop on Nuclear Astrophysics, Ringberg Castle, Tegernsee, Germany, February 11-16, 2002, ed. W. Hillebrandt & E. Müller, 126 29

Limongi, M. & Chieffi, A. 2003, ApJ, 592, 404 18, 28

Lingerfelt, E. 2007 34

Lund, T., Marek, A., Lunardini, C., Janka, H.-T., & Raffelt, G. 2010, Physical Review D: Particles, Fields, Gravitation and Cosmology, 82, 063007 3

Maeda, K., Nakamura, T., Nomoto, K., Mazzali, P. A., Patat, F., & Hachisu, I. 2002, ApJ, 565, 405 29

Marek, A., Janka, H., & Muller, E. 2008, A and A 17, 23, 31

Matheson, T., Garnavich, P. M., Stanek, K. Z., Bersier, D., Holland, S. T., Krisciunas, K., Caldwell, N., Berlind, P., Bloom, J. S., Bolte, M., Bonanos, A. Z., Brown, M. J. I., Brown, W. R., Calkins, M. L., Challis, P., Chornock, R., Echevarria, L., Eisenstein, D. J., Everett, M. E., Filippenko, A. V., Flint, K., Foley, R. J., Freedman, D. L., Hamuy, M., Harding, P., Hathi, N. P., Hicken, M., Hoopes, C., Impey, C., Jannuzi, B. T., Jansen, R. A., Jha, S., Kaluzny, J., Kannappan, S., Kirshner, R. P., Latham, D. W., Lee, J. C., Leonard, D. C., Li, W., Luhman, K. L., Martini, P., Mathis, H., Maza, J., Megeath, S. T., Miller, L. R., Minniti, D., Olszewski, E. W., Papenkova, M., Phillips, M. M., Pindor, B., Sasselov, D. D., Schild, R., Schweiker, H., Spahr, T., Thomas-Osip, J., Thompson, I., Weisz, D., Windhorst, R., & Zaritsky, D. 2003, ApJ, 599, 394 3

McCray, R. 1993, ARA&A, 31, 175 21

Messer, O., Bruenn, S., Blondin, J., Hix, W., Mezzacappa, A., & Dirk, C. 2007, Journal of Physics 22

Messer, O. E. B., Bruenn, S. W., Blondin, J. M., Chertkow, M. A., Hix, W. R., Lee, C., Lentz, E. J., Marronetti, P., & Yakunin, K. N. 2010, in Proceedings of Nuclei in the Cosmos XI, ed. G. Martínez-Pinedo & et al. (SISSA Proceedings of Science) 24

Messer, O. E. B., Bruenn, S. W., Blondin, J. M., Hix, W. R., Mezzacappa, A., & Dirk, C. J. 2007, 78, 1 4, 24

Messer, O. E. B., Mezzacappa, A., Bruenn, S. W., & Guidry, M. W. 1998, ApJ, 507, 353 16

Mezzacappa, A., Calder, A. C., Bruenn, S. W., Blondin, J. M., Guidry, M. W., Strayer, M. R., & Umar, A. S. 1998, ApJ, 495, 911 16

Mezzacappa, A., Liebendörfer, M., Messer, O., Hix, W., Thielemann, F.-K., & Bruenn, S. 2001, Phys. Rev. Lett., 86, 1935 16

Mezzacappa, T. 2004, arXiv.org 17

Miyaji, S., Nomoto, K., Yokoi, K., & Sugimoto, D. 1980, Publications of the Astronomical Society of Japan, 32, 303 72

Müller, E., Fryxell, B., & Arnett, D. 1991, A&A, 251, 505 29

Murphy, J. W., Ott, C. D., & Burrows, A. 2009, The Astrophysical Journal, 707, 1173 67

Nagataki, S. 1999, ApJ, 511, 341 45

Nagataki, S., Mizuta, A., & Sato, K. 2006, ApJ, 647, 1255 45

Nagataki, S., Shimizu, T., & Katsuhiko, S. 1998a, ApJ 45

Nagataki, S., Shimizu, T. M., & Sato, K. 1998b, ApJ, 495, 413 28, 29

Ning, H., Qian, Y.-Z., & Meyer, B. S. 2007, The Astrophysical Journal, 667, L159 73, 74

Nomoto, K. 1987, ApJ, 322, 206 27, 72, 73, 75, 77, 78, 79, 80, 83, 84

Parete-Koon, S., Hix, W., & Thielemann, F. 2008, BAAS, 39, 162.10 41

Pruet, J., Hoffman, R. D., Woosley, S. E., Janka, H.-T., & Buras, R. 2006, ApJ, 644, 1028 32

Pruet, J., Woosley, S. E., Buras, R., Janka, H.-T., & Hoffman, R. D. 2005, ApJ, 623, 325 30, 32, 45

Pumo, M. L., Turatto, M., Botticella, M. T., Pastorello, A., Valenti, S., Zampieri, L., Benetti, S., & Patat, F. 2009, October 73, 75, 90

Quirk, J. J. 1994, International Journal for Numerical Methods in Fluids, 18, 555 52

Rampp, M. & Janka, H.-T. 2002, A&A, 396, 361 29

Rauscher, T., Heger, A., Hoffman, R. D., & Woosley, S. E. 2002, ApJ, 576, 323 28

Rauscher, T. & Thielemann, F. K. 2000, 22 26

Scheck, L., Kifonidis, K., Janka, H.-T., & Müller, E. 2006, A&A, 457, 963 15

Sumiyoshi, K., Suzuki, H., Yamada, S., & Toki, H. 2004, Nucl. Phys. A, 730, 227 26

Sumiyoshi, K. & Yamada, S. 2012, The Astrophysical Journal, 199, 17 22

Thielemann, F.-K., Nomoto, K., & Hashimoto, M. 1996, ApJ, 460, 408 18, 28, 30

Timmes, F. X., Hoffman, R. D., & Woosley, S. E. 2000, ApJS, 129, 377 31

Timmes, F. X. & Woosley, S. E. 2000, Astronomy, 377 33

Travaglio, C., Hillebrandt, W., Reinecke, M., & Thielemann, F.-K. 2004, A&A, 425, 1029 45

Trimble, V. 1991, A&AR, 3, 1 30

Wanajo, S., Nomoto, K., Janka, H.-T., Kitaura, F. S., & Müller, B. 2009, The Astrophysical Journal, 695, 208 73, 75, 90

Wilson, J. R. 1985, in Numerical Astrophysics, ed. J. M. Centrella, J. M. LeBlanc, & R. L. Bowers (Boston: Jones and Bartlett), 422–434 2, 16

Wilson, J. R. & Mayle, R. W. 1993, Phys. Rep., 227, 97 16

Woosley, S. E., Arnett, W. D., & Clayton, D. D. 1973, ApJS, 26, 231 13, 18

Woosley, S. E. & Heger, A. 2007, Physics Reports, 442, 269 27, 35, 51, 59, 60, 61, 71, 94

Woosley, S. E. & Weaver, T. A. 1995, ApJS, 101, 181 18, 28, 30

Yahil, A. 1983, ApJ, 265, 1047 14

Yakunin, K. N., Marronetti, P., Mezzacappa, A., Bruenn, S. W., Lee, C., Chertkow, M. A., Hix, W., Blondin, J. M., Lentz, E. J., Bronson Messer, O., & Yoshida, S. 2010, Classical Quantum Gravity, 27, 194005 2, 5

Yakunin, K. N., Marronetti, P., Mezzacappa, A., Bruenn, S. W., Lee, C.-T., Chertkow, M. a., Hix, W. R., Blondin, J. M., Lentz, E. J., Messer, O. E. B., & Yoshida, S. 2010a, Classical and Quantum Gravity, 27, 194005 66, 68

Yakunin, K. N., Marronetti, P., Mezzacappa, A., Bruenn, S. W., Lee, C.-T., Chertkow, M. A., Hix, W. R., Blondin, J. M., Lentz, E. J., Messer, O. E. B., & Yoshida, S. 2010b, Classical and Quantum Gravity, 27, 194005 71

Appendix

Appendix

Abbreviations

- CCSN(e) - core-collapse supernova(e)
- CNO - Carbon Nitrogen Oxygen
- ECSN(e) - electron capture supernova(e)
- EOS (also EoS) - Equation of State
- FAU - Florida Atlantic University
- GW - Gravitational Waves
- GPU - Graphical Processor Unit
- MGFLD - Multigroup Flux Limited Diffusion
- MGBT - Multi Group Boltzmann Transport
- MHD - Magnetohydrodynamics
- MPI - Message Passing Interface
- NCSU - North Carolina State University
- NERSC - National Energy Research Scientific Computing Center
- NSE - Nuclear Statistical Equilibrium
- OMP - OpenMP
- ONeMg - Oxygen Neon Magnesium
- ORNL - Oak Ridge National Lab
- PNS - proto-neutron star
- QSE - Quasi-Statistical Equilibrium
- TPM - Tracer Particle Method
- TPR - Tracer Particle Reader
- UTK - University of Tennessee, Knoxville
- SASI - Standing Accretion Shock Instability
- SN(e) - Supernova(e)
- Ye - Electron Fraction

Cost of Nuclear Burning

The nominal 150-isotope network costs approximately ~ 58 % of the total runtime in CHIMERA. Using the 1-thread run as a reference, the total runtime, by parts, can be expressed as,

$$t_{total_{1-thread}} = t_{CHIMERA} + t_{XNet_{1-thread}} \tag{7.1}$$

where

$$t_{XNet_{1-thread}} = \frac{5.8}{10} \times t_{total_{1-thread}} \tag{7.2}$$

which means,

$$t_{CHIMERA} = \frac{4.2}{10} \times t_{total_{1-thread}} \tag{7.3}$$

And thus,

$$t_{total_{1-thread}} = (\frac{4.2}{10} + \frac{5.8}{10}) \times t_{total_{1-thread}} = \frac{10}{10} \times t_{total_{1-thread}} \tag{7.4}$$

As shown in Figure 4.6, utilizing 4 or 8 threads across 2 NUMA domains pushes the cost of the nuclear burning down to ~ 9.75 % of the total runtime. Note that the rest of CHIMERA does not change with respect to threading in XNet, and therefore

$$t_{total_{4-thread}} = t_{CHIMERA} + t_{XNet_{4-thread}}. \tag{7.5}$$

becomes,

$$t_{total_{4-thread}} = \frac{4.2}{10} \times t_{total_{1-thread}} + \frac{0.975}{10} \times t_{total_{1-thread}} \tag{7.6}$$

which means,

$$t_{total_{4-thread}} = \frac{5.175}{10} \times t_{total_{1-thread}} \tag{7.7}$$

Which means that by utilizing 4-threads, we increase the speed of the total run time by a factor of $\frac{10}{5.175}$ or ~ 1.93

Vita

Merek Austin Chertkow was born in Salt Lake City, Utah, on September 3, 1982 as the son of Merek Chertkow and Rhonda Chertkow.

After graduating in 2001 from Santa Ynez Valley Union High School in California, he attended California State Polytechnic University in Pomona, California where he received his B.S. degree, *magna cum laude*, in 2006 from the department of Physics. During his undergraduate studies, he worked for the Planetary Society in Pasadena, California as part of the Solar Sail (now LightSail) mission operations team, where he worked on spacecraft ground-station tracking as an operations engineer. In the summer of 2005, as an astronomer, he investigated the transiting extra-solar planets Tres-1 and HD209458, and observed the Deep Impact event through the 1-m telescope at Mt. Laguna Observatory at San Diego State University, California for which his work appeared in Sky and Telescope. In 2006, he performed collaborative work with The Jet Propulsion Laboratory's investigative team that has now solve the Pioneer Anomaly.

Now in 2012, Merek expecting to complete his Ph.D in Computational Astrophysics from The University of Tennessee, in Knoxville with a thesis topic on improving the accuracy and self-consistency of core-collapse supernovae simulations through nuclear network and nucleosynthesis studies. He works on some of the world's most powerful supercomputers at The Oak Ridge National Laboratory. He will be starting a new position at Space Exploration Technologies Corporation (SpaceX) in Hawthorne, Calfiornia as an electromagnetic interference engineer, where he will ensure spacecraft survivability in outer-space environments.